CHAPTER 4

RESULTS AND DISCUSSION

4.1 Determination of Cation Exchange Capacity (CEC)

With regards to the determination of CEC values, Figure 4.1 show images of filter papers used in the determination of CEC values for natural kaolin (NK) and metakaolin (N-MK), while Table 4.1 presents the CEC values for (NK) and (N-MK) which were 2.5 meq/100 g and 1.5 meq/100 g, respectively.

The values obtained agreed with those reported in literatures. As reported by Mgbemena et al. (2013) and Adamis and Williams (2005), kaolinite was mentioned to possess CEC values between 2 - 10 meq/100 g. These values of CEC for kaolinite is lower than that of illite (10 - 40 meq/100 g) and montmorillonite (~ 100 meq/100 g). In another research, Ani and Sarapaa (2008) also reported that the CEC of kaolinite lies between 1 - 10 meq/100 g.

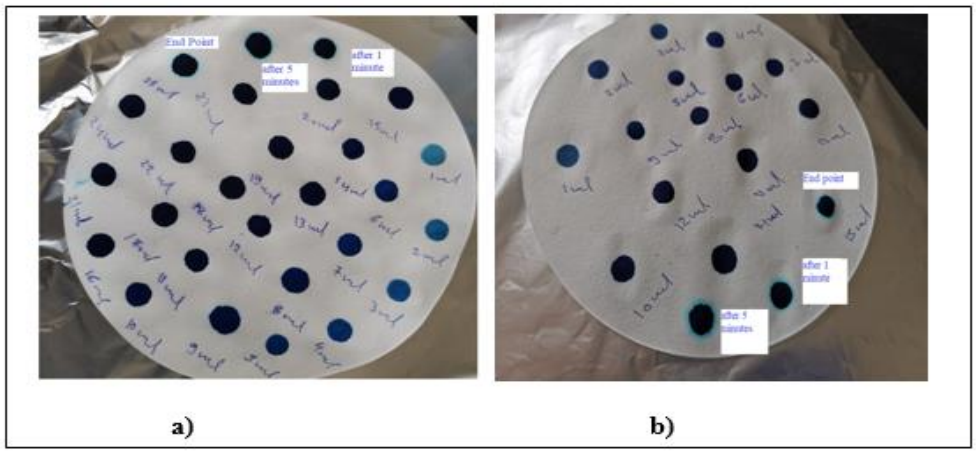

Figure 4.1: Images of Filter Papers Showing End Points in the Determination of CEC Values for (a) NK and (b) N-MK. Determination was done Using Methylene Blue Titration Method where Light Blue Halo around the Drop Indicates an End Point

Table 4.1: Cation Exchange Capacity of Kaolin and Metakaolin

Types of Kaolin	**NK**	**N-MK**
Cation Exchange Capacity (meq/100 g)	2.5	1.5

In this study, the CEC value of NK was higher than N-MK because of the edges of crystal where imperfection necessarily occurs as a result of bond breakage, are electrophilic and are able to trap hydroxyl groups in water (Konan et al., 2007). These phenomena corresponded to the formation of silanol, Si–OH, and aluminol, Al–OH, groups at the edges of the clay platelets, responsible for the fixation of cations available in the solution to which they are added to. Cations can also be trapped by defect, should they be present on the basal planes of the clay materials (Konan et al., 2009).

After thermal treatment, the CEC value showed slight decrease to 1.5 meq/ 100 g. This could be due to the occurrence of dehydroxylation reaction during thermal treatment, where most hydroxyl groups and interlayer cations (H^+ in the case of kaolinite), are eliminated as water molecules. This also leads to a significant decrease in the amount of H^+ in the interlayer space (Boukhemkhem & Rida, 2017). In other words, the decrease in CEC value of N-MK was also due to the decrease in the number of adsorption sites after the thermal treatment (Konan et al., 2009). This suggested that the variation in the CEC values are related and corresponded to the mineralogical modification of clay materials (Calabria et al., 2013). Ma and Eggleton (1999) reported that a high CEC in some kaolinites is found to be due to smectite layers on the surface of the kaolinite crystals.

The value of CEC for clay sample before and after thermal treatment was not very far from the CEC values obtained by Konan and co-authors (2009). Their CEC value for kaolin obtained from Damrec, France was 4.1 meq/100 g, while CEC value for its metakaolin was 2.0 meq/100 g.

In other words, clays of the same type but of different origins may exhibit widely different cation exchange capacity. The pre-treatment procedure, mineralogical composition, the pH, the particle sizes and the presence of impurities may profoundly affect the cation exchange capacity (Liew et al., 1985; Calabria et al., 2013).

4.2 Determination of the Compositions of NK and N-MK

The chemical analysis from EDX for NK and N-MK are shown in Table 4.2. The results reveal the presence of silica and alumina as the main ingredients, with traces of potassium and iron oxides. The percentage contents of Al_2O_3 and SiO_2 for N-MK are 44.83% and 50.79%, respectively, while 36.12% and 36.04 % respectively for NK. This result support the idea that thermal treated kaolin contains 50% to 55% SiO_2 and 40% to 45% of Al_2O_3 (Ramli & Alonge, 2016). Calcination, or heat treatment, degrades the structure of kaolin by causing the loss of structural OH groups and a rearrangement of Si and Al atoms, resulting in reorganisation of the structure of Al–O network while the Si–O network remains largely intact and the appearance of penta- and tetracoordinated (Rashad, 2013).

Table 4.2: Chemical Compositions of Natural Kaolin and Metakaolin

Element	Compound	Compositions (%)	
		NK	N-MK
C	C	24.75	-
O		-	-
Al	Al_2O_3	36.12	44.83
Si	SiO_2	36.04	50.79
K	K_2O	1.68	2.44
Fe	Fe_2O_3	1.41	1.94
	Total	100	100

Fe_2O_3 and K_2O are two other oxide chemicals found in the mixture. Although, they are presented in small percentages, the difference in the chemical composition,

contents show the effect of the heating on the raw kaolin. The increase in the percentage content of SiO_2 and Al_2O_3 in N-MK over NK are 29% and 19%, respectively. This result passes the ASTM C618 "Standard Specification for Coal Fly Ash and Raw or Calcined Natural Pozzolan for Use as a Mineral Admixture in Concrete" because the minimum total expected of SiO_2 and Al_2O_3 compounds is 85% and in this study; the total for both compounds SiO_2 and Al_2O_3 from calcination kaolin (MK) is 95.62%. EDX mapping on chemical composition on selected area show the element content of K and MK as illustrated in Figure 4.2 and Figure 4.3. Which presents the elemental distribution of silicon, aluminum, potassium, oxygen, iron (as identified on the upper side of each picture). A distribution of aluminum, silicon and oxygen is observed, and iron as impurities is reported. On the other hand, the presence of potassium is consistent with detection of muscovite, $KAl_2(AlSi_3O_{10})(OH)_2$, by XRD.

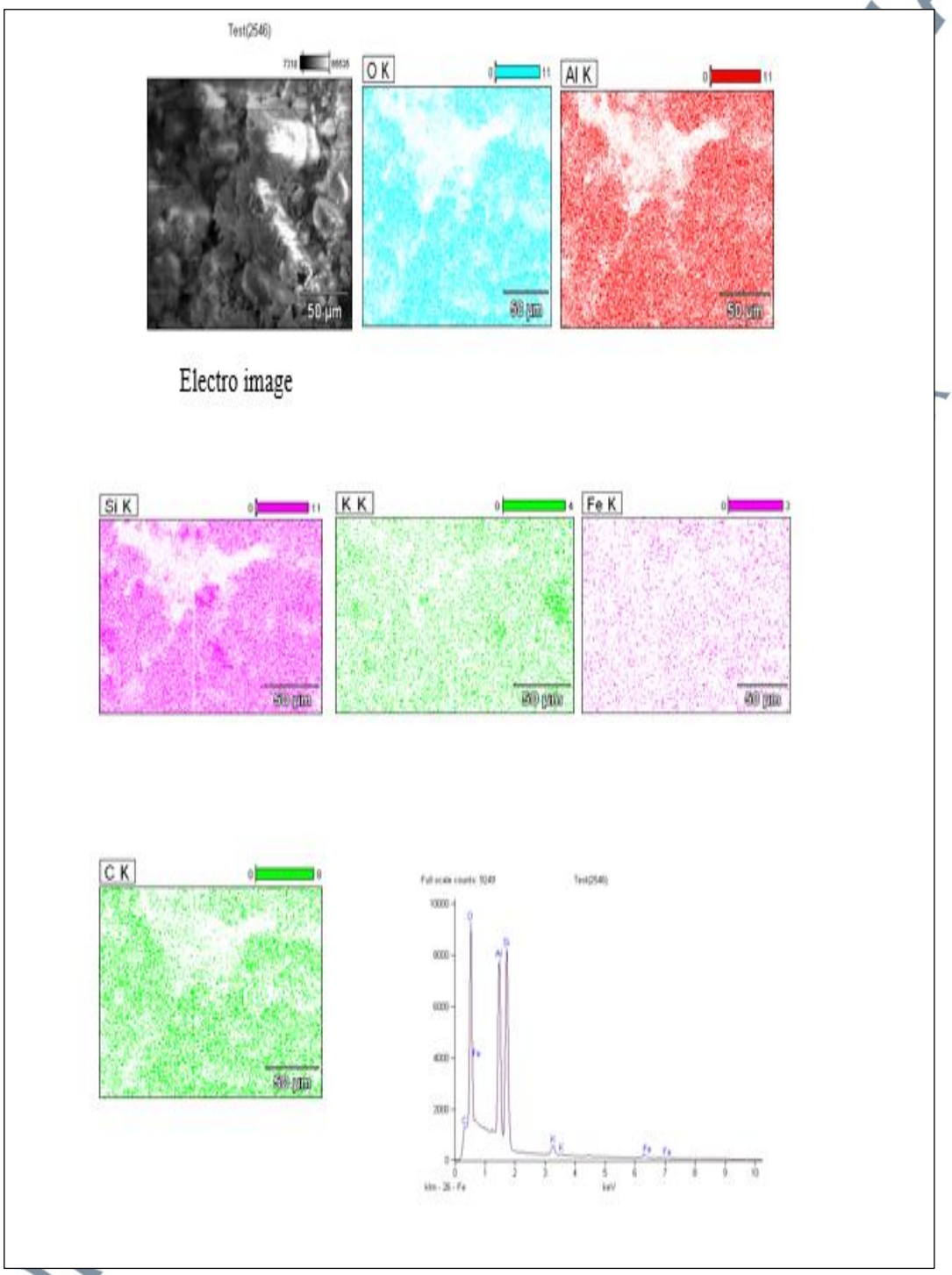

Figure 4.2: Elemental Mapping of the Kaolin Clay Determined Using EDX. The Respective Colour Codes Represent Individual Element

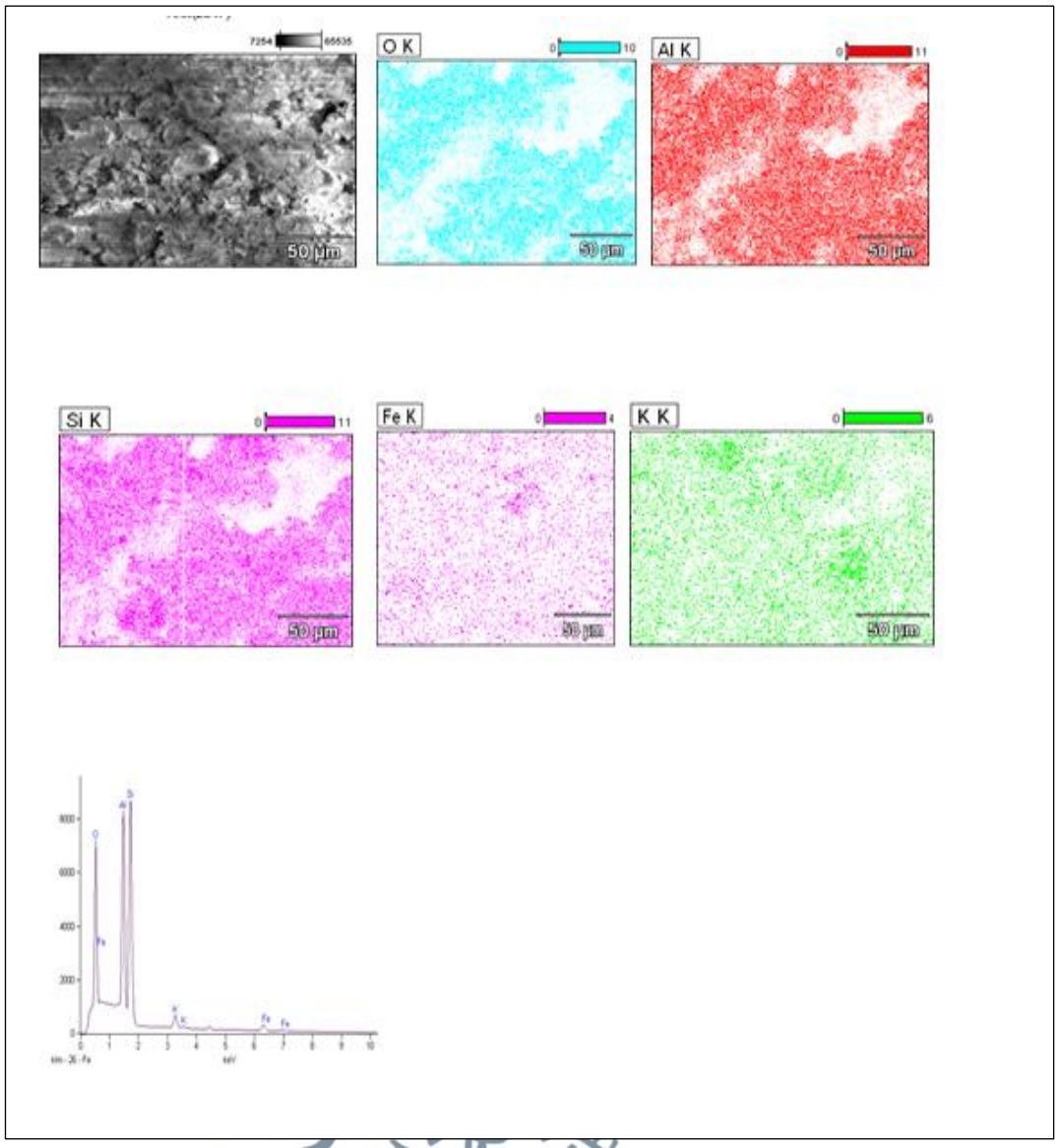

Figure 4.3: Elemental Mapping of the Metakaolin Clay Determined Using EDX. The Respective Colour Codes Represent the Individual Element

4.3 Analysis Using X-ray Diffractometer (XRD)

XRD patterns of NK and organo-modified kaolin samples are shown in Figure 4.4. The patterns detect that the kaolin has a crystalline nature and it also shows that the majority of the kaolin sample is made up of quartz, with a minor quantity of kaolinite thrown in for good measure, muscovite, and anatase. This result is similar to the XRD patterns of kaolin clay observed by (Boukhemkhem and Rida, 2017). The peak intense at $2\theta = 26.7^{\circ}$ is assigned to quartz Q, which consequently appears to be the most

abundant impurity (Liew et al., 2012). Other proportions of quartz mineral (Q) was detected from peaks existing at 2θ values of 21.05°, 36.75°, 39.63° , 42.65° , 50.23°, 60.02°, 68.41°, 73.57°, 75.79° and 77.73°. It can be seen that no significant change in the quartz Q peaks upon modification with $BTEA^+$, which was similar to that obtained by Hashemian and Parsaei (2015), who reported that the main phase of kaolin (quartz) did not change after tetra ethylamoniumiodide (TEAI) loading.

The K_2O content of the samples is used to determine the presence of muscovite because no other mineral containing K has been found. It was clear that the kaolin sample is mainly composed of kaolinite mineral (K). According to Yanguatin et al. (2017) the kaolinite content is distributed between a minimum of 2% and a maximum of 98%, while quartz contents can reach 60%. XRD patterns show the kaolinite mineral at 2θ values 12.46°, 25°, 35.14°, 38.56° and 62.44°. The peak at 2θ = 12.46° which is assigned to the characteristic interlayer basal spacing $d_{(001)}$ of the kaolin clay from Gopeng, Perak, Malaysia at 7.12 A°. A closer value of 7.10 A° was obtained by Mgbemena et al. (2013) for untreated kaolin.

The $d_{(001)}$ for NK and organo-modified kaolin are shown in Table 4.3. The basal spacing which calculated based on Bragg's equation was found that all samples had the $d_{(001)}$ values of around 7.12 to 7.34 A°. The slight increase in the basal spacing is revealed from the shifting of the peaks to slightly higher values of d-spacing, $d_{(001)}$, and towards lower 2θ values.

The factors influencing the $d_{(001)}$ basal spacing of the organo modified kaolin are the amount of exchanged organic cations, the ammonium packing density, and the orientation of intercalated surfactant cations in the interlayer space (Ogbebor et al., 2015). In this study, the basal spacing of 0.5 NK is slightly higher than other organo kaolin clays. Because of its high hydration energy, it's probable that for 0.5 NK, the

surfactant concentration is low enough that there's still a lot of exchangeable Na^+ that can adsorb water, causing the basal spacing to widen (Xi, 2006).

In general, the increasing $d_{(001)}$ basal spacing of kaolin will enhance the hydrophobic and hydrogen interactions between lipase and the intercalated surfactant, as well as the hydroxyl of kaolin, safeguard the original conformation of lipase, leaving the original conformation of lipase unaltered (Dong et al., 2012; Kooli, 2013).

Table 4.3*: d*-spacing Values of NK Before and After Modification With $BTEA^+$

Sample	2θ (º)	$d_{(001)}$ (A˚)	Intensity
NK	12.46	7.12	341.48
0.5 NK	12.04	7.34	217.44
1.0 NK	12.07	7.33	98.86
1.5 NK	12.18	7.26	108.57
2.0 NK	12.28	7.20	107.97

Looking at the slight difference (0.08 - 0.22 Å) in the $d_{(001)}$ basal spacing of the NK and modified kaolin clays obtained in this study; it can be concluded that not all BTEA-Cl was incorporated in the interlayer space of the kaolin clay. Most of the organic modifier could have been deposited on the surface of the clay as it can be seen in following results. This was due to the interlayer space of kaolin clay is unavailable to most of organic cations as a result to the relatively strong hydrogen bonds (Al-OH..O-Si) present between adjacent sheets which makes difficult to intercalate the surfactant (Benco et al., 2001; Matusik et al., 2013; de Souza Lima et al., 2019).

This was consistent with what had been studied previously by Duarte-Silva et al. (2014). They reported that the basal spacing of kaolin did not increase upon reaction with tert-butyldimethylchlorosilane, indicating lack of expansion of the clay. The same finding was found by Aroke and El-Nafaty (2014), which reported that the presence of the hexadecyltrimethylammonium bromide (HDTMA-Br) in the intercalated layer of kaolin clay increased the $d_{(001)}$ spacing of the original clay slightly (0.0187%).

In comparison with bentonite modified by same surfactant (BTEA-Cl) where d(001) spacing increased from 13.9 Å for original bentonite to 15.1 and 15.9 Å for 1.0 and 2.0 CEC respectively (Ramos et al., 2014). The expansion of the interlayer space is due to the removal of smaller hydrated interlayer sodium by the $BTEA^+$ cations besides attaching to the external surface. The same result was obtained by Ghiaci et al., (2009); who reported that the d-value of bentonite shifts from 1.23 nm to 1.38 nm after organo-modification, indicating that the surfactant ions enter the interlayer space.

The increase of basal spacing could potentially be attributable to the existence of smaller clay particles generated as a result of $BTEA^+$ treatment (Duarte-Silva et al., 2014; Ghosh & Bhattacharyya, 2002), or the leaching of Al from the octahedral layer of the clay (Duarte-Silva et al., 2014; Ghosh & Bhattacharyya, 2002). In addition, Jahan et al. (2012) observed that ammonium salt intercalation causes the interlayer gap in the clay structure to expand.

Figure 4.5 shows the XRD patterns of N-MK and modified metakaolin. It can be seen that quartz (Q) is also present in the metakaolin clay. Chandrasekhar and Ramaswamy (2002) reported that ancillary minerals that present in the kaolin such as quartz and mica remain intact during formation of metakaolin. Gonzales et al. (2007) also reported that quartz is not affected by thermal treatment in calcination condition.

The disappearance of the characteristic diffraction peaks of kaolinite and deterioration of its crystal structure suggest that its transformation into metakaolinite by heating at 650 °C for 5 h leads to less crystallinity compared to kaolin (Konan et al., 2009; Al-Harahsheh et al., 2009). The structure of kaolin is sensitive to thermal treatment, and when heated, Kaolinite undergoes structural rearrangement; calcination of kaolin occurs as a result of kaolin dehydroxylation. According to reports, such transformations occur when structural water is lost, the structure reorganises, and the

original triclinic cell collapses. Weak hydrogen connections between hydroxyl groups on the layers' surface were broken as the dehydroxylation process progressed, and only a small portion of AlO_6 octahedra was preserved, while the rest was changed to tetrahedra (Lambert et al., 1989; Duarte-Silva et al., 2014; Tanaskovic et al., 2017).

XRD pattern for N-MK itself is X-ray amorphous and thus produces a broad amorphous halo in the range between 15-35°. It can be seen from Figure 4.5 that quartz is not affected by organo-modification of metakaolin, and the maximum of the amorphous halo shifts to approximately 30° to 35° after treatment with $BTEA^+$, indicating the change in the chemical structure (Luukkonen et al., 2016). New peaks with low intensity were found, two small peaks for 0.5 MK at 13.81° and 23.19°, which also presents in 1.0 MK and 1.5 MK. It can also be seen new small peaks in XRD patterns for 1.5 MK at 29.24° which also presents in 2.0 MK, other peaks at 35.41° and 46.88° presents in 1.5 MK and 2.0 MK, and another peak at 28.03° presents in XRD pattern for 2.0 MK. This indicated that the most modifier cations were uniformly distributed over the clay surface.

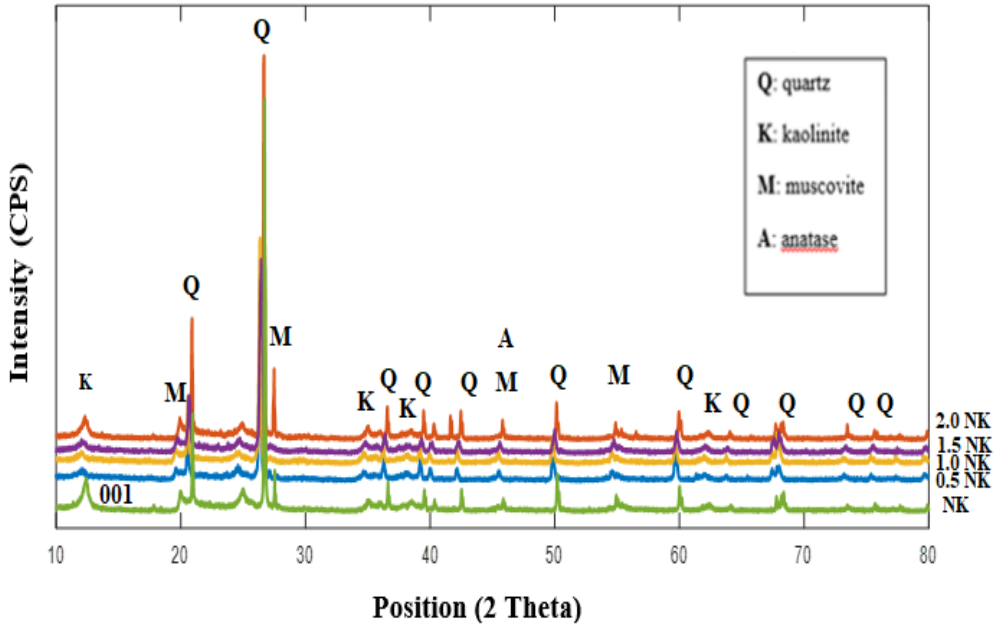

Figure 4.4: XRD Spectrum of NK and Modified Kaolin Samples

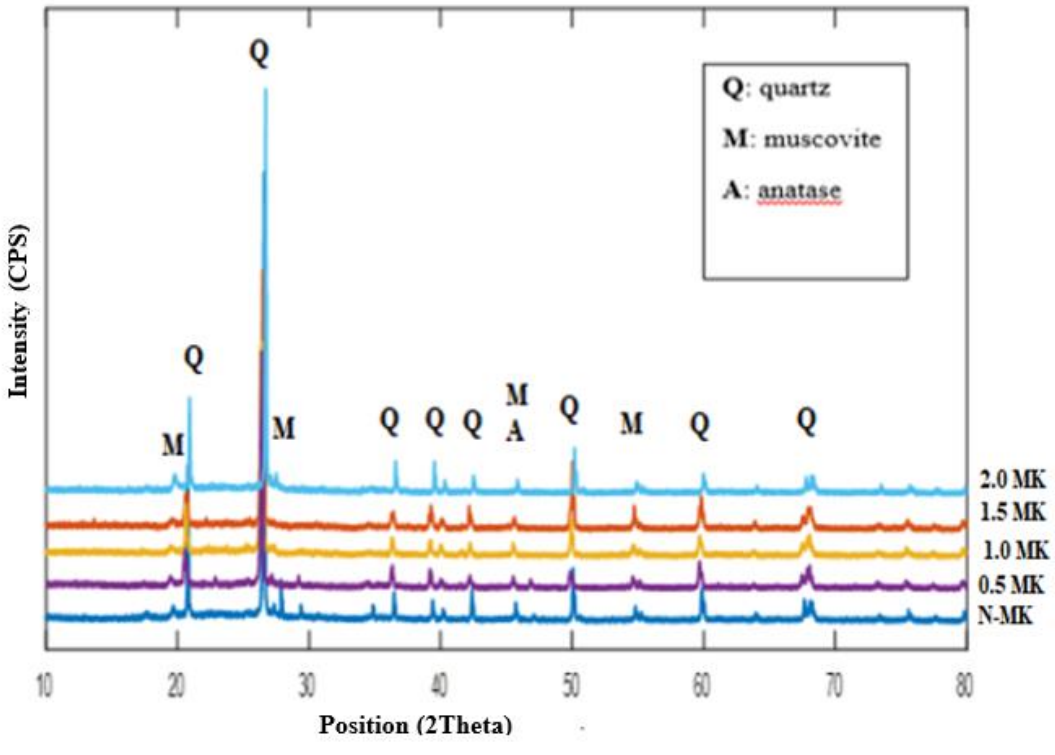

Figure 4.5: XRD Spectrum of N-MK and Modified Metakaolin Samples

4.4 Analysis Using Fourier Transform Infrared (FTIR) Spectrometer

The FTIR spectrum was used to identify some of the characteristic functional groups for organic absorbed. To obtain evidence for the intercalation of quaternary ammonium cation into the silicate lattice; the comparison FTIR spectra before and after modification are included.

4.4.1 FTIR Analysis of BTEA-Cl

The FTIR spectroscopy was used to elucidate the molecular structure of BTEA-Cl chains. It can be seen in Figure 4.6, the bands at 2946 cm^{-1} and 2983 cm^{-1} are attributed to C-H stretching. The most intense absorption bands at 756 and 712 cm^{-1} correspond to the C-H bond in the aromatic mono-substituted benzene ring of BTEA (Park & Kim, 2015). The bands at 1394 cm^{-1} and1484 cm^{-1} are assigned to CH_3 and CH_2 bending, respectively and 1470 cm^{-1} is attributed to CH symmetric bending (Alemdar et al., 2000). The vibrational frequency and assignments for alkylammonium surfactant (BTEA-Cl) is summarized in Table 4.4.

Table 4.4: Vibrational Frequencies and Assignments for BTEA-Cl

Wavenumber (cm^{-1})	Peak Assignment
1323	C-H bending
1236	C-C stretching
1394	CH_3 bending
1484	CH_2 bending
1470	CH symmetric bending
3032	C-H stretch (aromatic)
2920 – 2850	Asymmetric and symmetric stretching vibrations of the -CH_3 and -CH_2 groups of the aliphatic chain of the surfactant
1083	C-H (in plane band)
968 – 1183	C-N stretching
1580 – 1611	C-C stretches in the aromatic ring
907 – 920	=C-H (out of plane)
756 – 712	C-H bond in the aromatic mono-substituted benzene ring

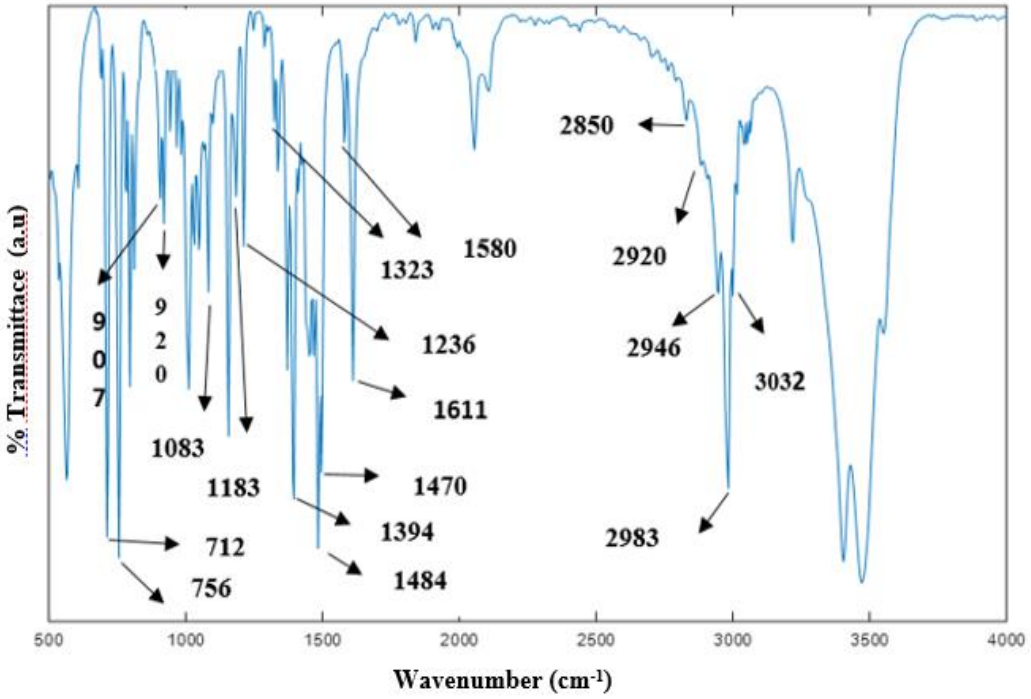

Figure 4.6: FTIR Spectrum of BTEA-Cl

4.4.2 FTIR Analysis of NK and N-MK

Figure 4.7 shows the spectra of NK and N-MK. The spectrum of NK sample was similar to those obtained in the literature and have all of the characteristic bands (Boukhemkhem & Rida, 2017; Castellano et al., 2010; Horvath et al., 2010; Ilić et al., 2010; Vaculíková et al., 2011; Tanaskovic et al., 2017, Menshaz et al., 2017).

The major bands of the NK in the FTIR spectra can be observed at 3697 cm^{-1}, 3626 cm^{-1} and 3654 cm^{-1} which correspond to the different types of hydroxyl groups: i) hydroxyl groups that interact with the oxygen atoms of adjacent layers at the surface of the octahedral layers, and (ii) hydroxyl groups that are positioned in the inner plane of the octahedral sheet and are not exposed at the surface of the kaolin layers. (Frost & Kloprogge, 2015; Vaculíková et al., 2011; Duarte-Silva et al., 2014).

In this case, the bands that appear at 3697 cm^{-1} and 3654 cm^{-1} attributes to the hydroxyl groups at the surface of the clay, while the band at 3626 cm^{-1} is assigned to

the stretching mode of internal hydroxyl groups. The transition of kaolin into metakaolin has been verified through the disappearance of the mention bands because of thermal treatment. In fact, dehydroxylation has eliminated the majority of the hydroxyl groups. (Ahmed et al., 2015; Heah et al., 2012; Lin et al., 2008; Boukhemkhem & Rida, 2017; Konan et al., 2009). The bands of large intensities between 3690 - 3620 cm^{-1} are correspond to well-crystallized kaolinite (Kakali et al., 2001).

On the other hand, bands at 3440 cm^{-1} along with the band at 1636 cm^{-1} originated from stretching and bending vibrations of free water molecules located at the surface of kaolin (hygroscopic moisture). The bands at 937 cm^{-1} and 913 cm^{-1} are assigned to the bending of the inner hydroxyl groups that are connected to Al, while the bands at 795, 754, 696 and 537 cm^{-1} correspond to the vibrations of Si-O-Al groups (Boukhemkhem & Rida, 2017) and to hydroxyl groups perpendicular to the surface. The bands that appeared at 1111 cm^{-1}, 1032 cm^{-1}, and 1007 cm^{-1} correspond to the elongation of Si-O-Si molecule. The band at 1032 cm^{-1} corresponds to quartz impurity (Timofeeva et al., 2017). These bands are all characteristic of the kaolinite clay material. (Daud & Hameed 2010; Boukhemkhem & Rida, 2017).

In the case of the N-MK, the FTIR spectrum shows major changes on the intensity, shape and position of adsorption bands of mentioned above as a result of the thermal treatment which leads not only to a de-hydroxylation of kaolin clay but also to a structural modification. As a result, thermal treatment causes silica tetrahedral deformation (Ahmed et al., 2015). Amorphous silica is assigned to all peaks that correspond to Si–O–Si groups, which are clustered into a single big band at 1051 cm^{-1}. The loss of Al–OH units caused the bands to vanish at 913 cm^{-1} and 937 cm^{-1}, indicating that the structure of the alumina octahedral sheet became chaotic while the structure of

the silica tetrahedral sheet remained constant (Zhang et al., 2017). Furthermore, fading the band at 537 cm^{-1}, as well as an appearance change at band 795 cm^{-1} that shifted to 800 cm^{-1} as a result of change in aluminium coordination, indisputably demonstrated dehydroxylation (Sekuljica et al., 2016).

The results obtained from the FTIR spectra were in agreement with the results obtained from the analysis using XRD, where the disappearance of the characteristic absorption bands of kaolinite at 911 cm^{-1}, 3621 cm^{-1} and 3697 cm^{-1} which means that amorphization by dehydroxylation has occurred (Nmiri et al., 2017).

4.4.3 FTIR Analysis of Organo-Modified NK and N-MK

Figures 4.8 and 4.9 show the spectra of organo-modified kaolin and organo-modified metakaolin clays by $BTEA^+$ cationic surfactant.

After the modification of clay samples with BTEA-Cl, the characteristic bands of the starting clay were still maintained, indicating the retained structure of the natural clay. The bandwidth and peak position of the absorptions corresponding to the clay mineral's hydroxyl stretching (3440 - 3451 cm^{-1}) mode do not change, showing that the hydroxyl groups in kaolin did not react with $BTEA^+$. The same result was obtained by Duarte-Silva et al. (2014) who reported that the hydroxyl group of kaolin did not react with tert-butyldimethylchlorosilane.

As can be seen from Figure 4.8, FTIR spectra for organo-modified kaolin clays showed that the Si-O stretching band moved from 1111 cm^{-1} to 1113 - 1140 cm^{-1}. The intensity of the band at 1032 cm^{-1}, which corresponds to Si-O-Si, significantly decrease for 1.5 NK and 2.0 NK, respectively. However, a band at 1111 cm^{-1} and a doublet with maxima at 1032 cm^{-1} and 1007 cm^{-1} assigned to Si–O stretching modes are very strong

and difficult to get further information about the changes brought on by the interaction with the surfactant. (Bougeard et al., 2000).

The band characteristic of the ammonium salt used is presented in the range of 2991 - 2982 cm^{-1} which was clearly in FTIR spectra of 1.5 NK and 2.0 NK. However, this band typically has a low intensity in the other spectra of organoclay samples in accordance with the result obtained by Romas et al. (2014). The additional two characteristic bands at 1474 cm^{-1} and 1398 cm^{-1} attributed to the torsion of the C-H bonds, which do not present in the spectrum of the starting clay sample. It can be observed from a band at 1457 cm^{-1} that is assigned to CH_3 asymmetric bending (Alemdar et al., 2000). The presence of CH_2, CH_3 groups in the infrared spectra of organoclay as reported by Mota et al. (2015) is a proof that the surfactant's ammonium quaternary cation was intercalated within the interlamellar gaps of the samples.

Band with low intensity at 2851 - 2922 cm^{-1} can be assigned to the symmetric and asymmetric stretching vibrations of the methylene group of the guest molecules. These bands confirm the occurrence of interactions between the ammonium molecules and the clay (Hashmian & Parsaei, 2015; Meziane et al., 2017). Furthermore, FTIR spectra for organokaolin show a band at 1511 cm^{-1} characteristics for C–C ring stretching vibrations (Soliman et al., 2019). Bands at 2954 cm^{-1} and 3135 cm^{-1} which are attributed to symmetric stretch of -CH_3 group, and the aromatic C–H stretching (Saikia & Parthasarathy, 2010; Duarte-Silva et al., 2014) can be observed in the FTIR spectra of 1.5 NK and 2.0 NK. In addition, a band at 646 cm^{-1} is also observed in IR spectra of 0.5 NK and 1.0 NK and a band at about 600 cm^{-1} is presented in IR spectrum of 0.5 MK and 2.0 MK; these bands are attributed to C-H out of plane ring bending. Bands at 850 cm^{-1} and 742 cm^{-1} are corresponding to the amide bonds (C-N) and to C-H bending, respectively, which present in IR spectrum of 0.5 NK.

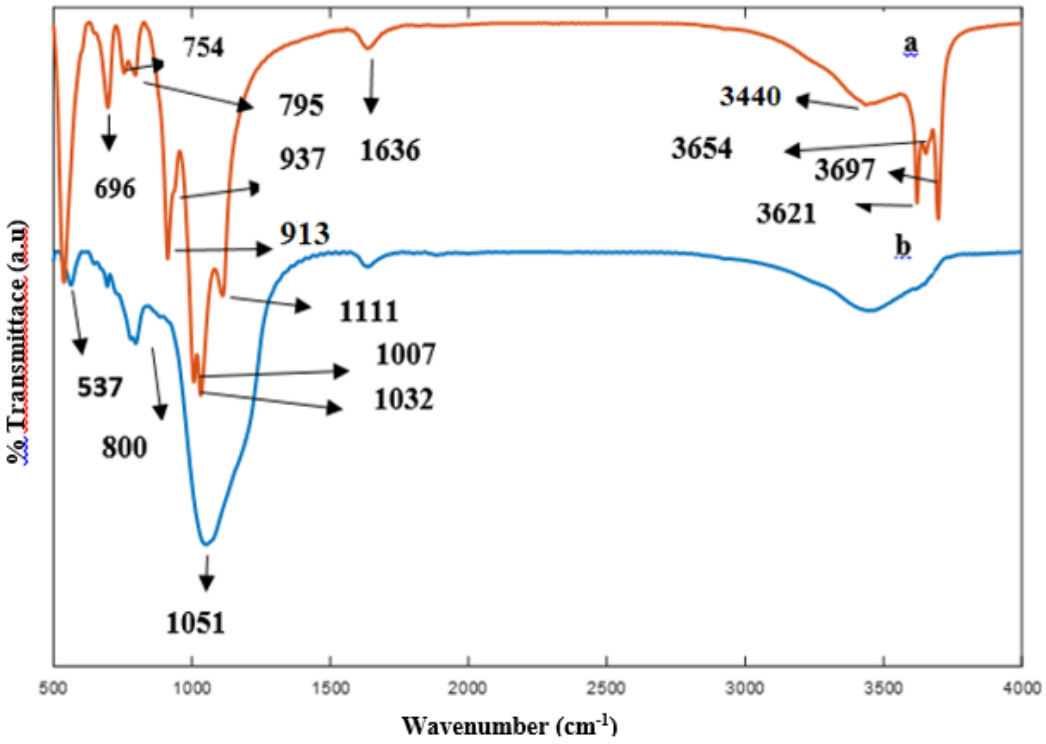

Figure 4.7: FTIR Spectra of (a) NK and and (b) N-MK

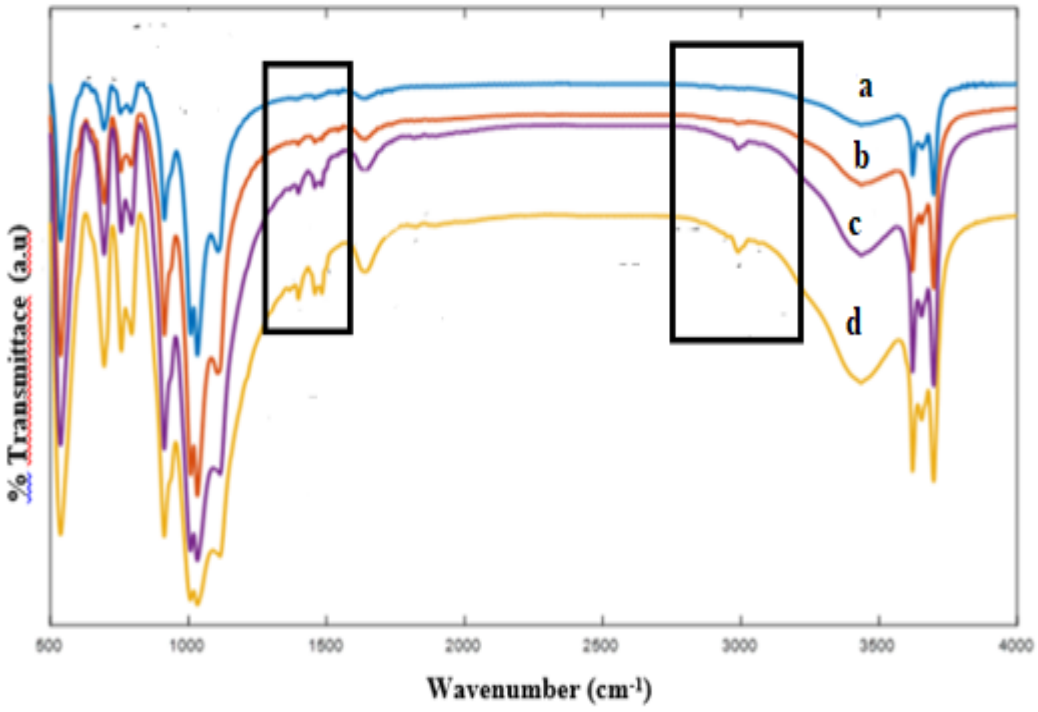

Figure 4.8: FTIR Spectra of (a) 0.5 NK, (b) 1.0 NK, (c) 1.5 NK and (d) 2.0 NK

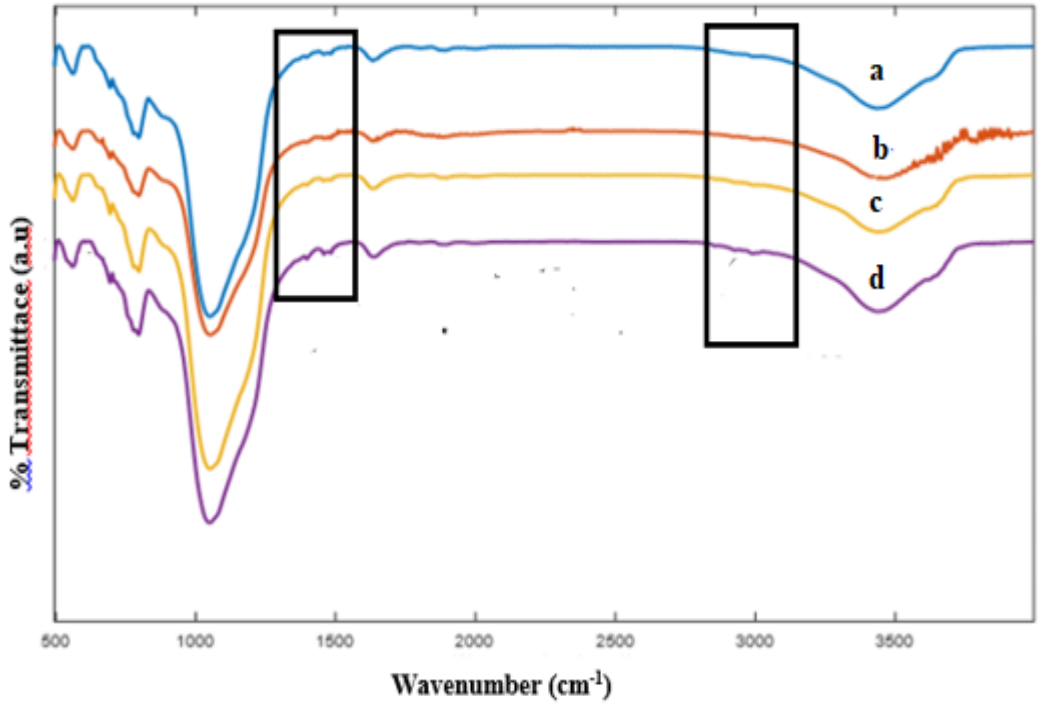

Figure 4.9: FTIR Spectra of (a) 0.5 MK, (b) 1.0 MK, (c) 1.5 MK and (d) 2.0 MK

Table 4.5: Vibrational Frequencies and Assignments for NK and Organo-Modified Kaolin

Wavenumbers (cm^{-1})					
2.0 NK	**1.5 NK**	**1.0 NK**	**0.5 NK**	**NK**	**Peak Assignment**
3699/3655	3697/3653	3697/3660	3699/3658	3697/3654	Al-O-H stretching
3621	3609	3601	3621	3626	OH stretching, crystalline hydroxyl (internal-OH group)
3439	3439	3439	3438	3440	H-O-H stretching of absorbed water
1644	1649	1641	1640	1636	H-O-H bending of water
538	538	538	536	537	Si-O-Al stretching
914	897	897	914	913	OH deformation, linked to $2Al_3$-
1034	1034	1034	1033	1032	Si-O stretching of clay minerals
1116	1140	1125	1113	1111	Si-O stretching
1008	1006	1006	1006	1007	Si-O stretching
695	695	695	695	696	Si-O quartz
795	796	795	797	795	Si-O quartz
2989	2989	2993	2991	-	$-CH_2-$ groups
1457	1457	1457	1458	-	CH_3 asymmetric bending
1474/1398	1474/1397	1475/1399	1471/1396	-	CH_2 symmetric bending

Table 4.6: Vibrational Frequencies and Assignments for N-MK and Organo-Modified Metakaolin

Wavenumbers (cm^{-1})					
2.0 MK	**1.5 MK**	**1.0 MK**	**0.5 MK**	**N-MK**	**Peak Assignment**
3451	3451	3451	3451	3450	H-O-H stretching of absorbed water
1648	1639	1642	1636	1634	H-O-H bending of water
566	565	576	564	563	Si-O-Al stretching
1059	1059	1056	1056	1051	Si-O stretching
731	727	723	668	695	Si-O quartz
801	830	801	802	800	Si-O quartz
608	-	-	600	-	C-H out of plane ring bending
2996	2996	2996	2987	-	$-CH_2-$ groups
1459	1459	1463	1463	-	CH_3 asymmetric bending
1485/1395	1487/1397	1487/1397	1486/1399	-	CH_2 symmetric bending

4.5 Analysis Using Scanning Electron Microscope (SEM)

SEM images of kaolin and metakaolin samples before and after organo-modification are shown in Figure 4.10 and Figure 4.11.

Referring to the SEM images, the micrograph of NK is characterized by distorted platelets, and its shape can be described as flaky and platy formation consisted of laminar particle aggregates of different sizes forming books of variable thickness. This indicates that the particles are not fully dispersed into individual layers. The platy structures are closely packed together and reducing voids between the particles. Such association development is likely because the domination of hydrogen bonds (Muhammad et al., 2014). The morphology of the NK changed when it was modified with $BTEA^+$. The organo-modification kaolin consisted of flaky type of particle aggregates, being considerably larger than NK and more voids are seen. The partial disintegration of small and glossy particles in kaolin treated with 2.0 CEC resulted in the production of a spongier texture, indicating that the $BTEA^+$ was evenly distributed over the kaolin surface.

Kaolin surface morphologies changed after thermal treatment, N-MK was also characterized using SEM to observe its particle morphology as presented in Figure 4.10(a). The laminate-layered plate used in the main structure is still present in the particles with indefinite in shape, more disordered morphology and more individualized platelets as a result of heating the kaolin at 650 °C for 5 hrs. Dehydroxylation process led to high distortion in the SiO_4 tetrahedral layers (Tanaskovic et al., 2017; Boukhemkhem & Rida, 2017) and disorganization of the crystalline structure of the material without a significant change on the morphology of the kaolin platelets. As a result, the thermal treatment has little effect on the morphology (Konan et al., 2009).

The calcination led to increase the friability of the kaolin layered structure, and alumina can be seen by whitish layer outside the metakaolin flakes was obviously seen compared to kaolin. Compared to the morphology of the metakaolin, the organo-modified metakaolin clays have many small and aggregated particles and the plates become relatively flat layers. The appearance of these plates increased with the increase in concentration of $BTEA^+$ leads to agglomeration of the metakaolin particles. The modified samples showed a rough surface than the unmodified clays, and this was probably due to the distribution of $BTEA^+$ cations on the surface of clay samples.

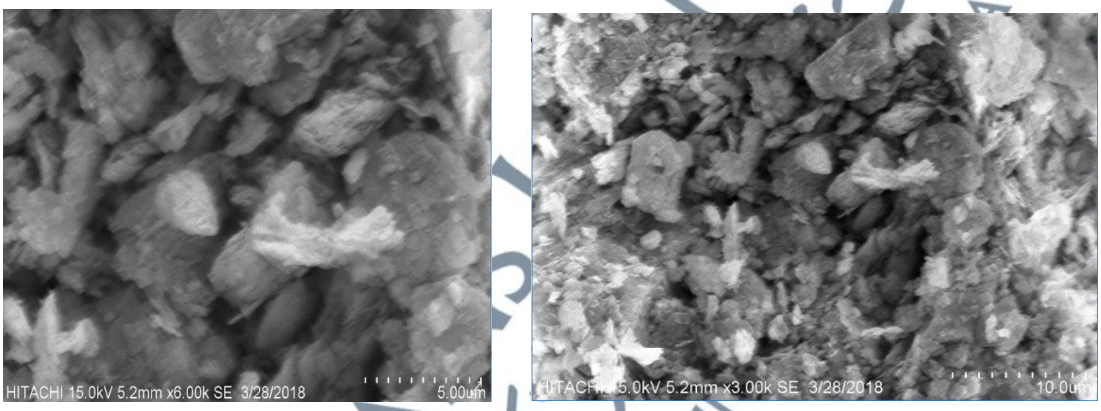

(a) NK

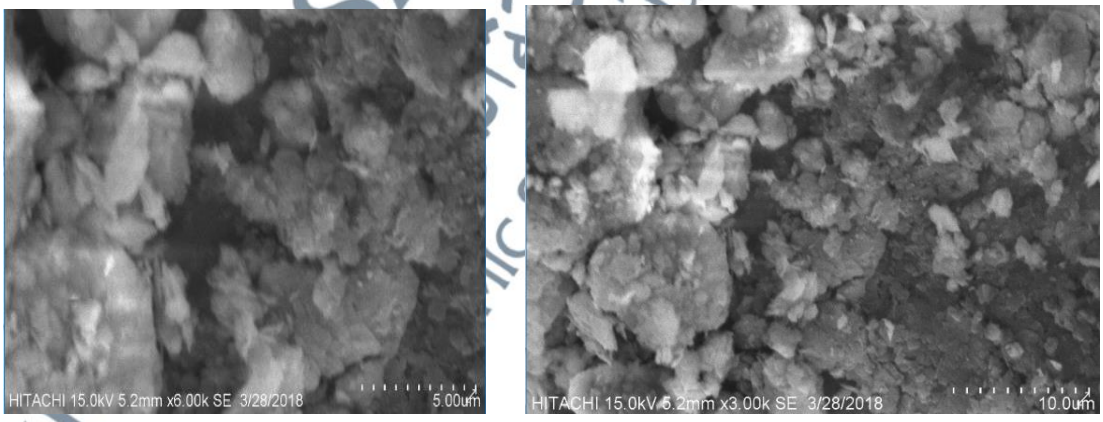

(b) 0.5 NK

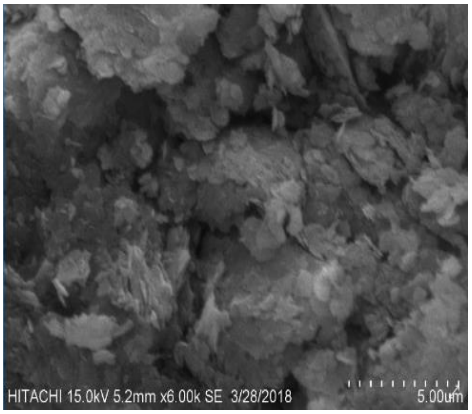

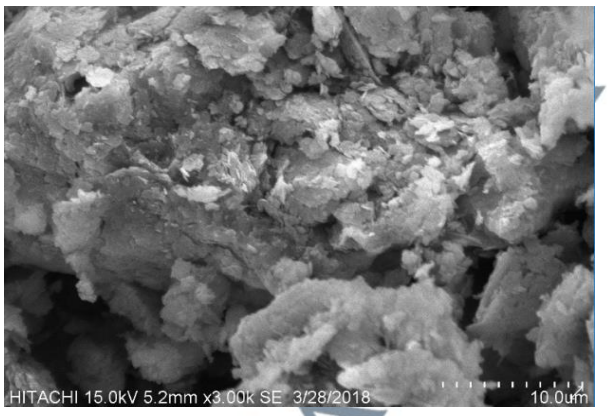

(c) 1.0 NK

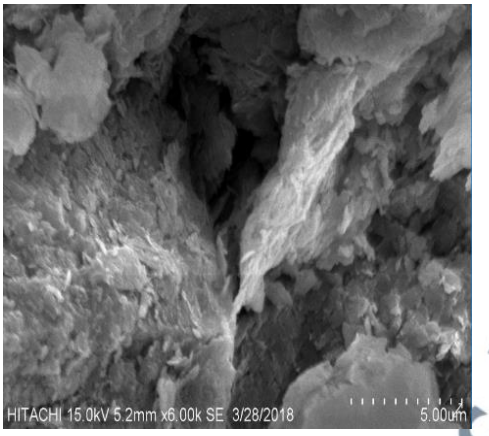

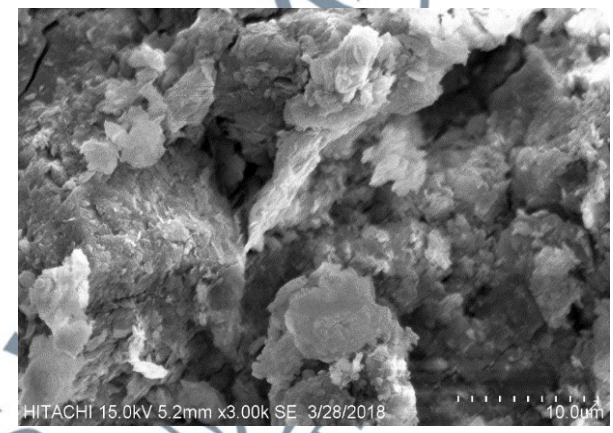

(d) 1.5 NK

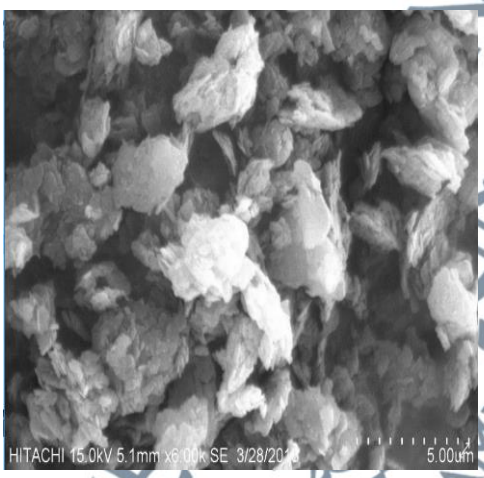

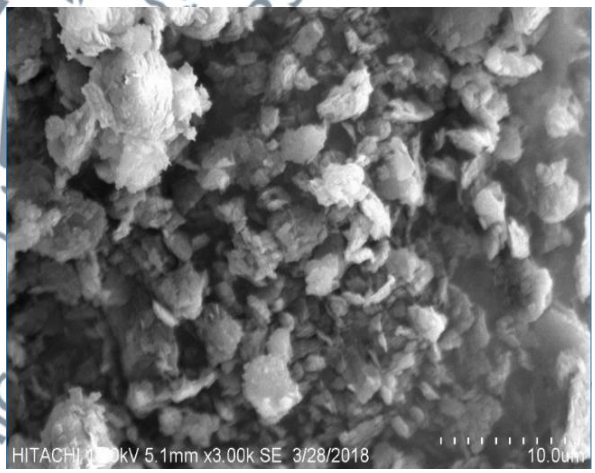

(e) 2.0 NK

Figure 4.10: SEM Images of (a) NK and Organo-Modified NK, (b) 0.5 NK, (c) 1.0 NK, (d) 1.5 NK and (e) 2.0 NK at 3,000x and 6,000x Magnifications

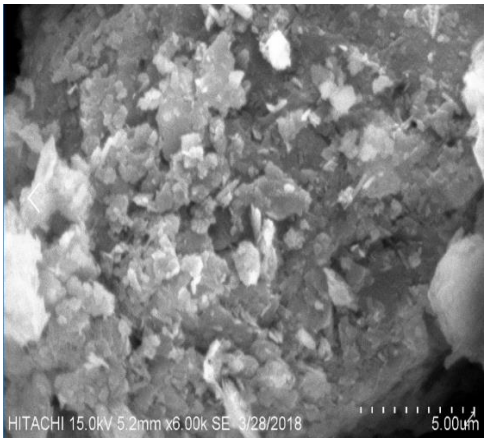

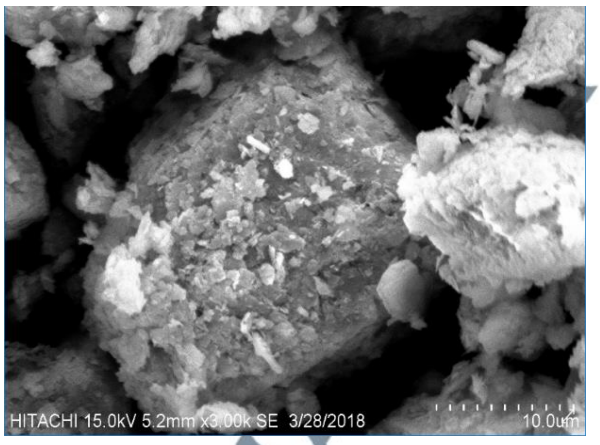

(a) N-MK

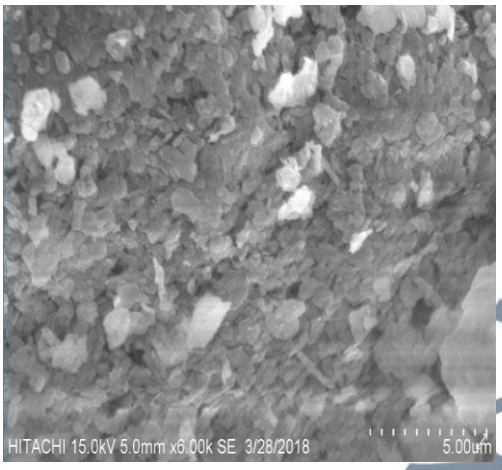

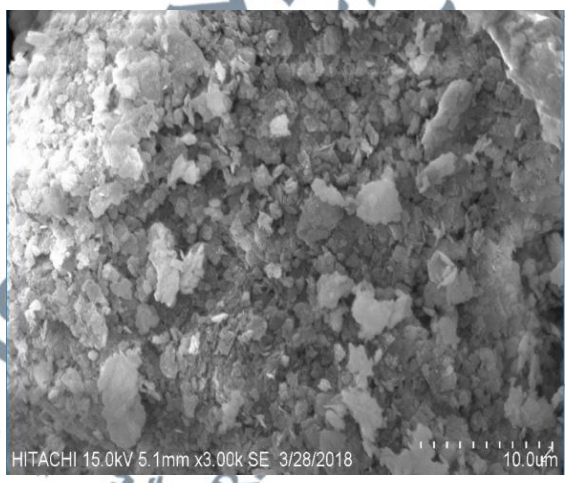

(b) 0.5 MK

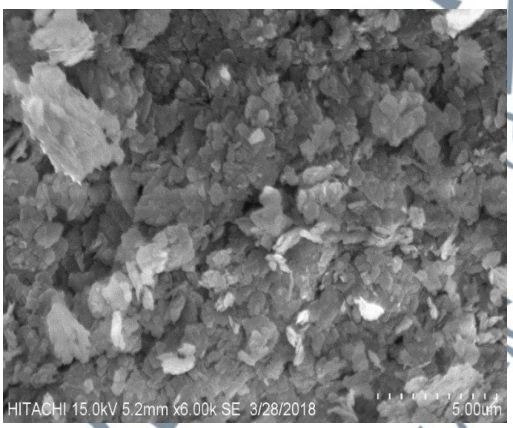

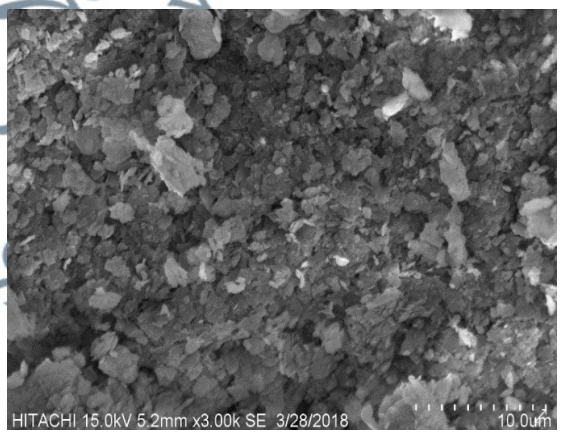

(c) 1.0 MK

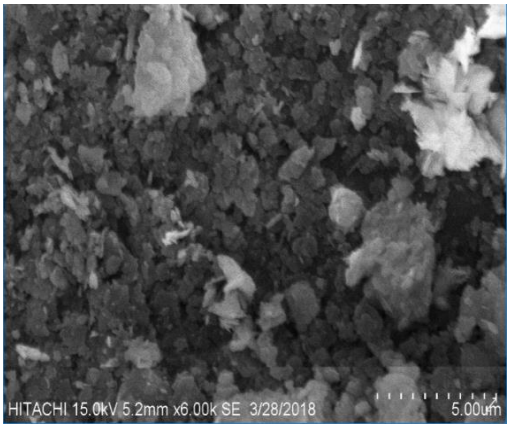

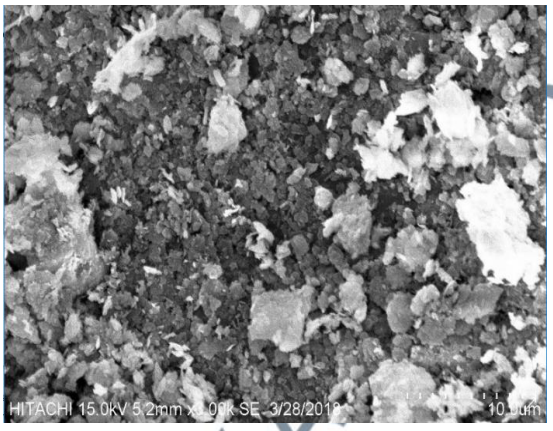

(d) 1.5 MK

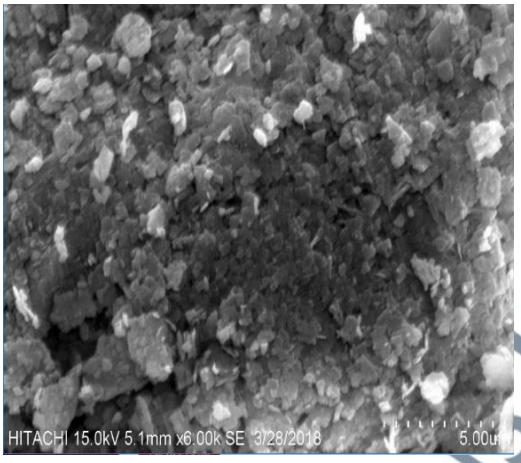

(e) 2.0 MK

Figure 4.11: SEM Images of (a) N-MK and Organo-Modified N-MK, (b) 0.5 NK, (c) 1.0 NK, (d) 1.5 NK and (d) 2.0 NK at 3,000x and 6,000x Magnifications

4.6 Analysis of Surface Area and Porosity Using Nitrogen Adsorption-Desorption Method

Table 4.7 illustrates the data of textural analysis; including the Brunauer, Emmett and Teller (BET) method to determine the surface area, pore volume and pore size obtained from the conventional analysis of nitrogen isotherms. From Table 4.6, it can be seen that NK sample had the highest BET surface area (25.34 m^2/g) which almost agreed with result obtained by Nascimento and co-authors (2011), where the value of BET surface area was 24 m^2/g for their kaolin sample. As reported by Yanguatin et al.

(2017) and Rashad (2013) the specific surface area of kaolin in the range between 5.8 m^2/g and 42 m^2/g, with the specific area of 10,000 - 29,000 m^2/kg.

According to Al-Asheh et al. (2003) the calcination of clays at high temperatures can change the surface properties of clays. In this study, the calcination of kaolin at 650 ^oC lead to decrease in BET surface area to19 m^2/g and this is in agreement with the result obtained by Timofeeva and co-authors (2016). They reported that after thermal treatment of kaolin at 650 ^oC for 4h, the BET surface area of kaolin decreased to 17 m^2/g. Gamelas et al. (2014) in their study mentioned that BET surface area of calcined kaolin decreased to 16.3 m^2/g.

Consider is of what happens during the heat treatment to explain the changes in specific surface area for both kaolin and metakaolin. The dehydroxylation tends to collapse the kaolin layers that brings particles closer to one another which leads to the agglomeration phenomenon among particles, as the aggregated particles sinter, the surface area of the aggregated particles decreases (Fabbri et al., 2013).

In comparison with the result obtained by Tanaskovic and co-authors (2016), they found that the surface area did not change after calcination of the kaolin. It demonstrates that the structural changes caused by the thermal treatment have no impact on the particular surface area. This may be due to the difference in temperature used during the calcination, which was 550 ^oC. According to Gamelas et al. (2014); the increasing in the calcination temperature lead to more decrease in BET surface area.

The pore volume of kaolin increased slightly after thermal modification from 0.113 cm^3/g to 0.121 cm^3/g. It can be a result of water loss and cavity expansions after water withdrawal, in other words the increase in pore volume due to the formation of wide interparticle voids, which contribute to more volume than to the surface (Díaz et al., 2017; Rostami et al., 2018). Moreover, large pore volumes imply that porosity is

caused by inter-particle spacing rather than pores within the structure (Duarte-Silva et al., 2014). Furthermore, the large pore size could indicate that pores grow only at the material's surface. The porosity of the support improved significantly after thermal treatment, indicating that the number of available attachment sites for the CRL molecule increased.

The organo-modification however led to decrease in surface area and pore volume of the modified samples. This is due to the modifier being incorporated into the clay's interlayer region (Ramos et al., 2014, Paroloa et al., 2014). The decrease of surface area for organo-modified kaolin was larger than organo-modified metakaolin; it may because kaolin has the largest CEC, thus the surfactant amount which modified the kaolin was more. The decrease in the value of BET surface area was also corresponded to the concentration of $BTEA^+$ where the higher concentration showed a smaller BET surface area. The SEM image of 2.0 NK also proved that the cations were largely distributed on the kaolin surface. This had caused decrease of the surface area and the pore volume of kaolin after the modification process.

Organoclays with a surfactant loading greater than 1.0 CEC, according to Park et al. (2011), have molecules intercalated in the clay mineral as well as the interparticle pores, resulting in a decrease in surface area and pore volume. The decrease in surface area can also be due to the $BTEA^+$ occupying exchanging sites that are covalently attached to the edge of -OH groups of individual clay platelets, which therefore obscure sections of the kaolin surface, preventing nitrogen gas from reaching the interior surface. Another reason for the decrease in BET surface area could be the pore blocking effect, in which the bigger exchanged cation clogs some of the smaller exchanged cations.

Table 4.7: Textural Properties of Unmodified and Modified Clay Samples

Sample	[a]Surface Area (m^2/g)	[b]Pore Volume (cm^3/g)	[b]Pore Size (Å)
NK	25.34	0.113	179
N-MK	19.91	0.121	225
0.5 NK	13.11	0.090	244
1.0 NK	9.59	0.075	286
1.5 NK	7.30	0.055	316
2.0 NK	5.90	0.054	385
0.5 MK	18.14	0.104	229
1.0 MK	12.79	0.103	302
1.5 MK	12.06	0.098	286
2.0 MK	9.04	0.092	413

[a]Surface area was determined using the BET method

[b] Pore volume and pore size were determined using the BJH t-plot method

Several studies had documented that the BET surface area of clay could be decreased after modification using cation exchange method (Romas et al., 2014; Paroloa et al., 2014; Díaz et al., 2017; Rostami et al., 2018).

Pore size, on the other hand, is critical for adsorbate entry into sorbents. It can be seen that after the organo-modification the pore size increased, Ramos et al. (2014), reported the same finding after modifying bentonite with quaternary ammonium cations. The huge pore sizes and low surface area of these samples indicated the creation of extensive inter particle cavities (Duarte-Silva et al., 2014).

All tested supports are characterized as mesoporous according to IUPAC and become a promising candidate for enzyme and protein adsorption, since the size of the most enzymes is about ~7.0 nm (Vulfson, 1994). Babaki et al. (2008) mention that the adsorption properties of a solid depend largely on the micropores (pores with diameter below 2 nm) and mesopores (pore diameter in the range of 2 nm to 50 nm), whereas macropores (pores with a diameter over 50 nm) have fiddling influence on the adsorption characteristics.

Figures 4.12 and Figure 4.13 show the nitrogen adsorption-desorption isotherms for all support samples. The profile of the isotherms is typical of type IV isotherm with narrow hysteresis loop of H3 type, which is typical of porous solids consisting particle aggregates. The lack of microporosity in the kaolin clay was shown by the low amount of N_2 adsorbed at relative pressures of $P/P_o < 0.2$. Beginning at $P/P_o \sim 0.8$, the volume of N_2 adsorbed increased rapidly due to the filling of the mesopores of the largest particle in the clay as well as those particles near the surface (Diaz et al., 2017).

The sharpness towards $P/P_o = 1.0$ indicated the uniformity of the mesopore size distribution, a typical phenomenon shown by mesoporous materials (Salis et al., 2003; Gregg et al., 1967). Duarte-Silva et al. (2014), reported a similar behaviour for their

kaolin sample and Babaei et al. (2014) revealed in their study to the same behaviour for mesoporous MnO_2 support.

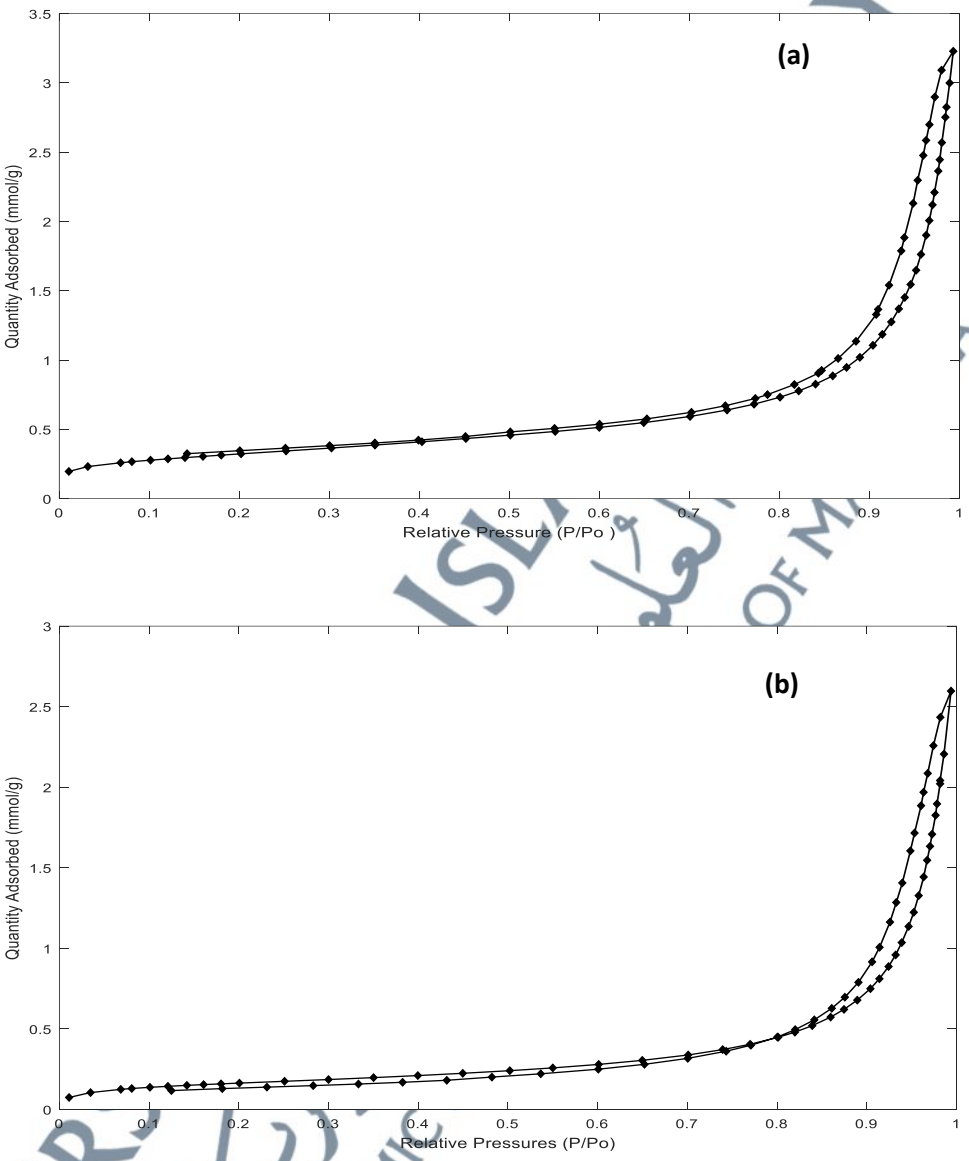

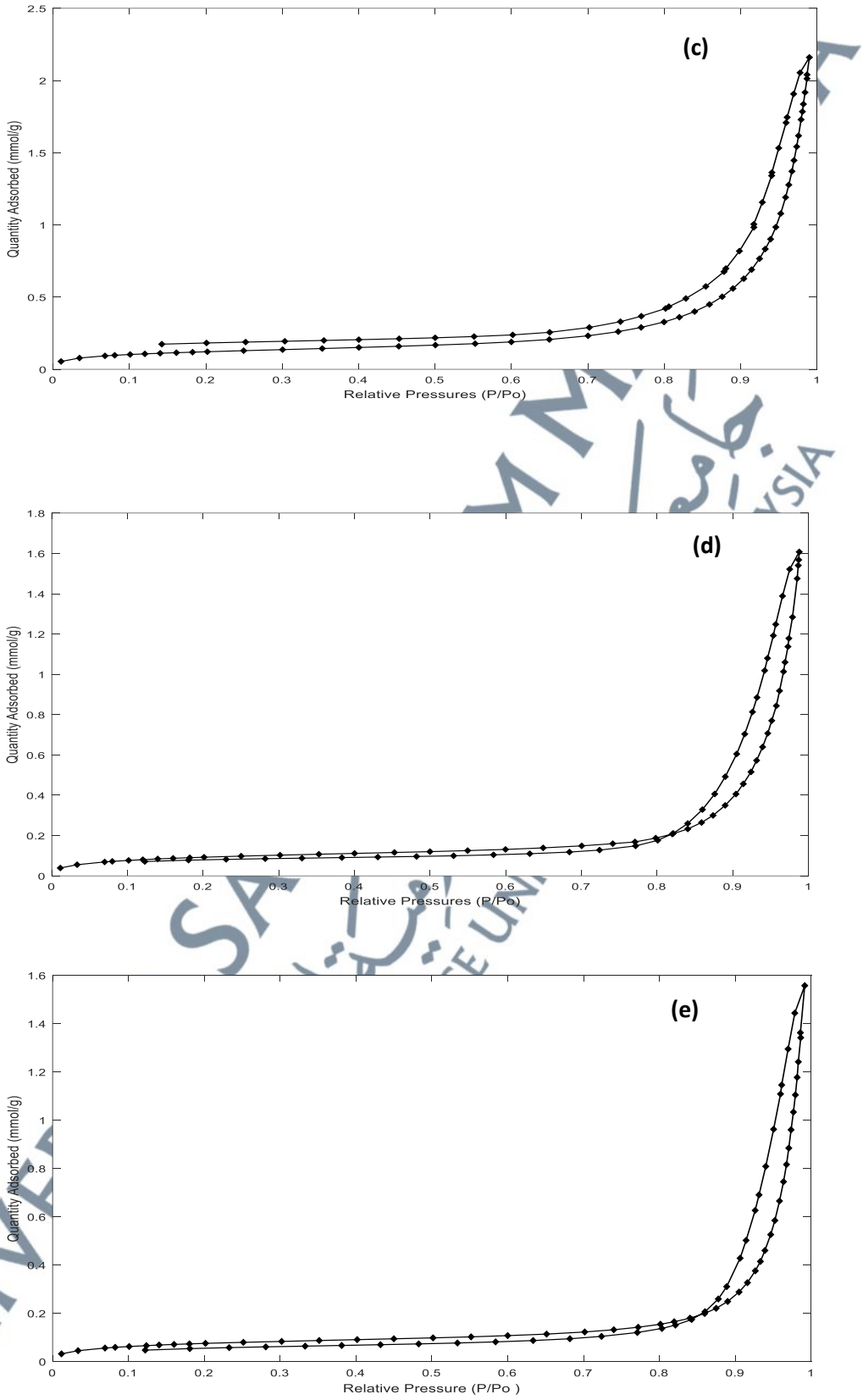

Figure 4.12: Nitrogen Adsorption-Desorption Isotherms for (a) NK, (b) 0.5 NK, (c) 1.0 NK, (d) 1.5 NK and (e) 2.0 NK

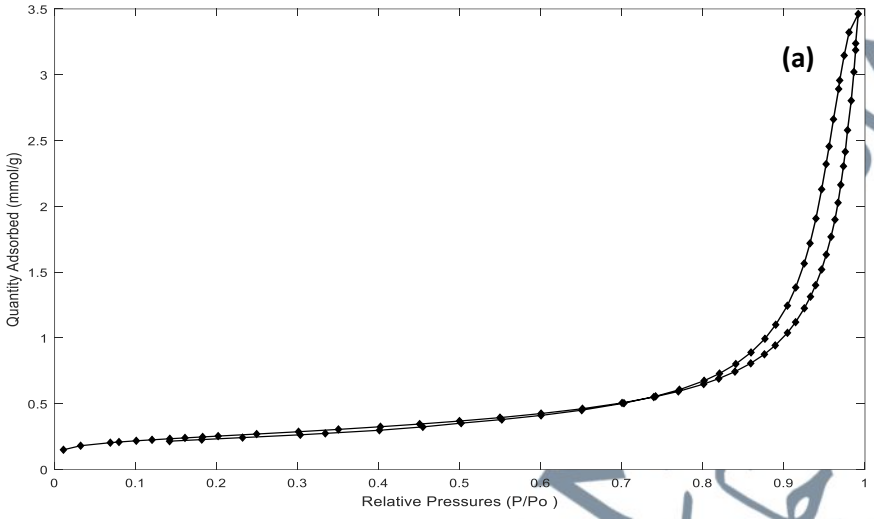
(a)
Quantity Adsorbed (mmol/g)
Relative Pressures (P/Po)

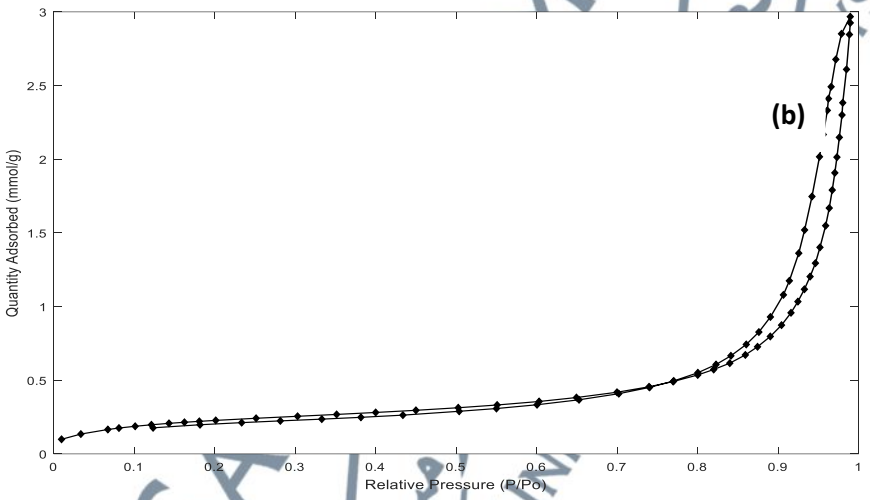
(b)
Quantity Adsorbed (mmol/g)
Relative Pressure (P/Po)

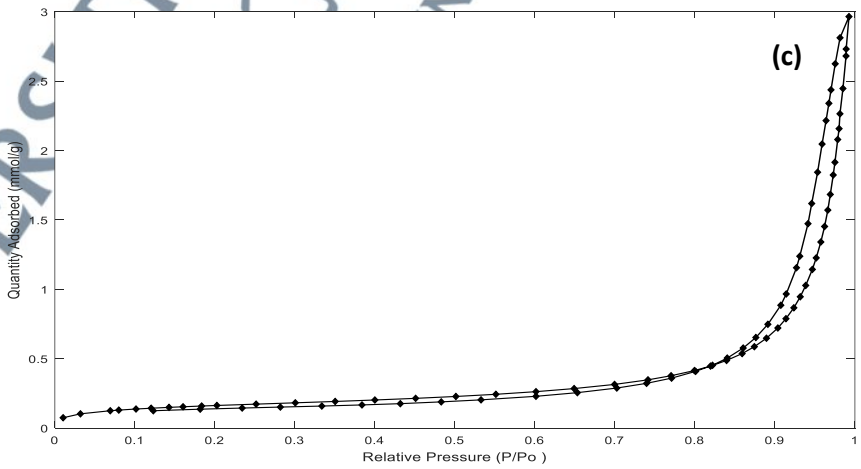
(c)
Quantity Adsorbed (mmol/g)
Relative Pressure (P/Po)

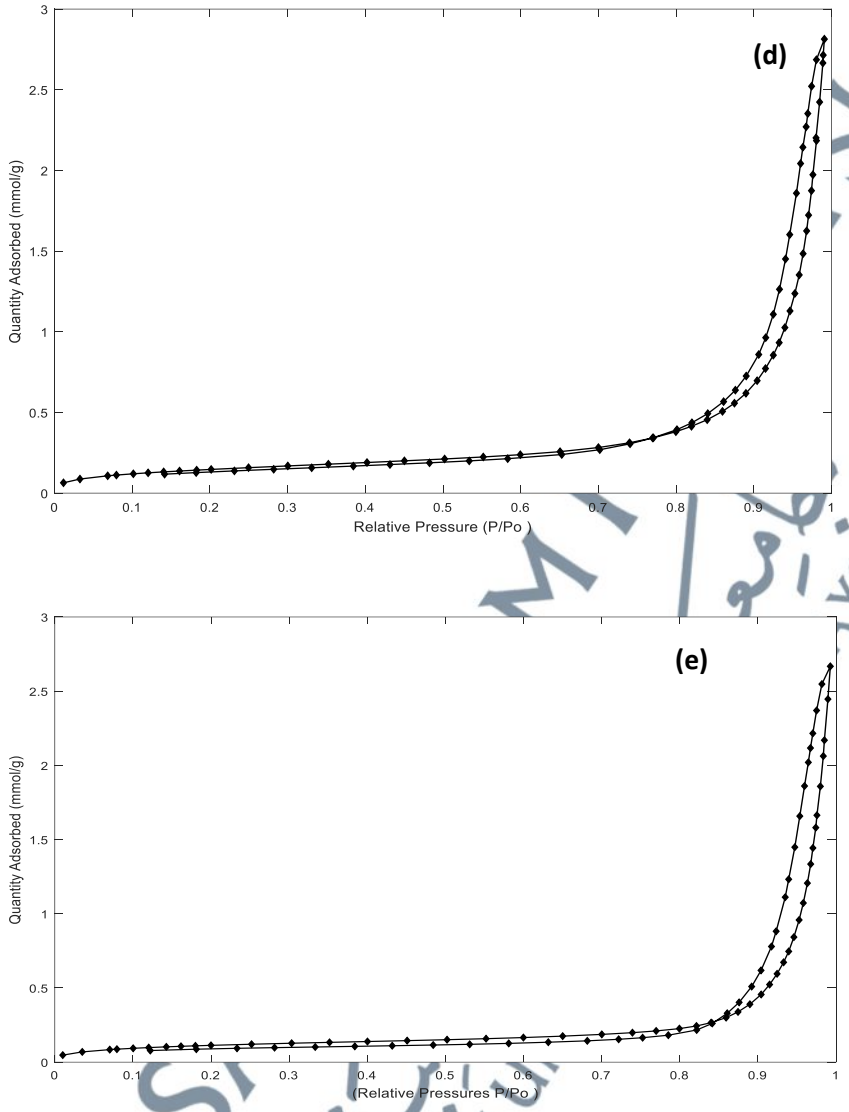

Figure 4.13: Nitrogen Adsorption-Desorption Isotherms for (a) N-MK, (b) 0.5 MK, (c) 1.0 MK, (d) 1.5 MK and (e) 2.0 MK

4.7 Effect of Support Modification on Lipase Immobilization

The immobilization of *Candida rugosa* lipase (CRL) following the physical adsorption method was performed on the natural kaolin, metakaolin and their organo-modified derivatives. The amount of protein in native and immobilized CRL were then determined according to Bradford (1976) method, and the results obtained are presented in Table 4.8.

Table 4.8: Percent of Immobilization and Protein Loading of CRL Immobilized onto NK, N-MK and Their Derivatives

Lipase Derivatives	Immobilization (%)	Protein Loading (mg/g support)
CRL-NK	52.99 ± 1.17	7.51 ± 0.38
CRL-N-MK	55.50 ± 0.54	7.85 ± 0.44
CRL-0.5 NK	49.72 ± 2.95	6.90 ± 0.50
CRL-1.0 NK	49.59 ± 0.49	6.52 ± 0.24
CRL-1.5 NK	48.34 ± 0.52	6.33 ± 1.08
CRL-2.0 NK	47.83 ± 1.52	5.85 ± 0.12
CRL-0.5 MK	42.14 ± 1.77	5.30 ± 0.52
CRL-1.0 MK	61.21 ± 2.96	10.81 ± 1.74
CRL-1.5 MK	59.33 ± 1.24	8.02 ± 1.01
CRL-2.0 MK	70.14 ± 2.41	14.83 ± 1.37

The amount of protein in the lipase immobilized support materials reflects the level of immobilization achieved in this investigation. CRL-2.0 MK displayed higher protein loading and consequently higher immobilization yield compared to other support samples as shown in Table 4.19. The CRL-2.0 MK achieved up to 70.14% ± 2.41 immobilization efficiency followed by CRL-1.0 MK and CRL-1.5 MK with 61.21% ± 2.96 and 59.33% ± 1.24, respectively. These values were lower than the value obtained by Rahman et al. (2019), who immobilized CRL onto diethylaminoethyl-cellulose (DEAE) through physical adsorption method, which was 84%. This could be because kaolin and metakaolin do not expand when wet, preventing the internal surface from being exposed, limiting the adsorption of big molecules like protein to the external surfaces and edges of the support (Duarte-Silva et al., 2014).

The great value of immobilization onto CRL-2.0 MK support is due to its characteristics such as has high pore size as shown in Table 4.7. This pore size value is suitable for biomolecules such as enzymes. Pore size contributes to the suitability of the support to immobilize the enzyme that leads to the increasing in enzyme activity. The porous structure enables a large quantity of the enzyme to be immobilized. According to a previous study, supports with smaller hole diameters (< 7.0 nm) can limit mass

transfer and enzyme molecule penetration, limiting protein interaction with the total surface area of the support particles. As a result, the substrates' interparticle diffusion impact was minimised (Musa et al., 2018).

The immobilization yield and amount of CRL-N-MK were slightly higher than those on CRL-NK, suggesting that the adsorption ability of metakaolin is better than that of kaolin. The maximum immobilization yield of kaolin and metakaolin reached 52.99% ± 1.17, 55.50% ± 0.54, respectively; while the maximum immobilization amount was 7.51 mg/g and 7.85 mg/g, respectively. Ajayi et al. (2012) stated that the thermal treatment carried out on the clay makes its pore relatively more available for occupation by the enzyme and create conducive environment for enzyme activities with less acidic and more reactive.

According to BET results in Table 4.7, the pore volume of metakaolin are higher than those of kaolin due to thermal treatment that caused loose of the structure and allowed more CRL immobilized on metakaolin and entrapment in the pores may also protect the enzymes from the surrounding media (Wang et al., 2011; Golbaha et al., 2016). Moreover; water molecules that filled the interstice were destroyed when the raw materials were heated, creating a structure with wide basal spacing between the brucite sheets. As a result, substantially more enzymes can be adsorbed.

Musa et al. (2018) immobilized Antarctic *Pseudomonas* AMS8 Lipase by adsorption method using different supports. Chitosan has the highest percentage of lipase immobilisation (76.2%) among the matrices or supports used, whereas kaolin has the lowest percentage of lipase immobilization (31.2%). The high value of immobilisation onto chitosan could be attributable to its particle size and diameter, and the difference in percentage values of immobilization and protein loadings were in accordance with the physicochemical parameters, according to their research.

Because of the wide surface area (25.34 m2/g) of NK, it adsorbed a higher percentage of protein than organo-kaolin. In addition, the steric restriction of surfactant in the modified kaolin interlayer reduced the quantity of lipase loaded on modified kaolin. Furthermore, the negative trend could be due to CRL aggregation produced by increased lipase interaction with organo-kaolin, preventing protein adsorption (Zhang et al., 2018). This result seems similar to those obtained by Ramos et al. (2014), who used organo-bentonite as support for the immobilization of CRL. It was found that the immobilization yield of organo-bentonite was approximately 48% in comparison with unmodified bentonite that achieved a protein immobilization yield of 81%. The differences in surface area and the interlayer space of these organo-clays resulted in differences in the adsorption efficiency (Puranik et al., 2010).

The low percentage of immobilization was achieved using CRL-0.5 MK and that was due to low pore size of the support (Table 4.6). This characteristic limits the process of migration of the enzyme into the support, and thus reduces the total efficiency of immobilization process. Handayan et al. (2011) stated that poor loading of enzyme can be caused by two reasons: (i) only the inner surface of mesopores is used for attachment of enzyme, (ii) received enzyme molecules can exert a steric hindrance against the other enzyme molecule penetrations into deeper mesoporous.

Golbaha et al. (2016) reported that the hydrophobic interactions of lipase-support molecules can contribute to the adsorption process. At this point, it should be noted that hydrophobicity of the support would have an effect on the extent of enzyme binding. Lipases have a unique property known as 'interfacial activation,' in which they can be hyperactivated at hydrophobic matrix interfaces and induce conformational changes in the lipase (by removing the lid covering their active sites), which are required to allow substrates free access to their active centres (Gittlesen et al., 1997). This method is

intriguing not only because it allows lipase derivatives to have high activity, but it also shows that surfaces may be steering enzyme molecules towards a specific orientation that keeps them active (Blanco et al., 2004; Zaidan et al., 2010). From these results, it can be concluded that the pore size, and specific surface area had influence on the enzyme loading values.

4.8 Characterization of Immobilized Lipase

The characterization of biocatalysts is of great importance to explain and predict some of their main properties, such as activity, selectivity and stability. The resulting modified and unmodified clays-lipase conjugates were characterized by a combination of techniques such as powder X-ray diffraction (XRD), Fourier transform infrared spectroscopy (FTIR), Scanning electron microscopy (SEM), Branauer, Emmet and Teller (BET) method.

4.8.1 Characterization Using X-Ray Diffractometer (XRD)

XRD was used to determine the position of the adsorbed enzyme in the CRL immobilised clays. The effect of lipase immobilisation on the internal microenvironment of the clay was also evaluated between modified and unmodified clay minerals. Figures 4.14 and 4.15 depict X-ray diffraction patterns of immobilised lipase on various platforms.

The values in d-spacing after immobilization process are shown in Table 4.9. The d-spacing (d_{001}) for CRL-NK showed an increase slightly from 7.12 Å to 7.22 Å upon immobilization compared to the d-spacing of kaolin and that corresponds to an inter sheet separation. Enzymes are polymeric species of very high molecular size. CRL has a molecular size of 50 - 70 Å, globular protein with a molecular weight of 60 kDa, hence the possibility of attachment within the inter lamellar space could be ruled out. Thus,

the whole enzyme was not involved in the intercalation in the interlayer space of kaolin. Probably, the side chains of different amino acid residues take part in intercalation while the polypeptide backbone was immobilized at the external surface and the edges of the adsorbents which was in accordance to previous studies obtained by Sinegani et al. (2005) who stated that Immobilization of cellulase on K-montmorillonite resulted an increase of the d-spacing from 11.77 Å to 11.94 Å.

The value of d-spacing did not change considerably in basal spacing after the immobilisation of lipase on modified kaolin, indicating that the enzyme did not enter the interlayer space. This was most likely owing to the limitation of intercalated surfactants, with the most adsorbed CRL being immobilised at the organic clay derivatives' external surfaces and edges via hydrogen bonding, Van der Waals, and electrostatic interactions (Secundo et al., 2008).

Table 4.9: *d*-spacing Value of Unmodified and Modified Kaolin After Immobilization of Lipase

Sample	**2θ (º)**	**$d_{(001)}$ Å**	**Intensity**
CRL-NK	12.26	7.22	166.63
CRL-0.5 NK	12.33	7.17	198.45
CRL-1.0 NK	12.32	7.18	183.72
CRL-1.5 NK	12.41	7.12	207.21
CRL-2.0 NK	12.44	7.11	178.55

There was a slight shifting of the peak to a higher $2\theta^{o}$, suggesting that very few of the layers are intercalated by the enzymes. It could happen, only if the immobilization occurred inside the clay mesopores, as well as on the external surfaces. Filling of the pores of the support materials have already been confirmed by the decrease in surface areas in the following result. Similar results were obtained with lipase on hydrophobic clay support (Reshmi & Sugunan, 2013) and lipase adsorbed on montmorillonite K10

(Golbaha et al., 2016). The finding was also compatible with result obtained by Ghaici et al. (2009), who reported that the CRL did not intercalate into unmodified and modified bentonite. Other enzymes, such as amylase, glucoamylase, and invertase, when applied to synthetic montmorillonite, cause side chains to intercalate into the clay layers while the polypeptide backbone does not enter the interlayer gap (Gopinath and Sugunan, 2007; Tzialla et al., 2010).

The hydroxyl groups in the unmodified kaolin layers interacted with the functional groups of lipase amino acid chains, causing lipase amino acids to intercalate the interlayer and the hydrophobic parts of lipase to be selectively bound to the embedded hydrophobic surfactants via interfacial adsorption in the modified clay interlayer (Dong et al., 2013).

After CRL adsorption onto the support materials, a change in XRD peak intensity was observed (shown in Figures 4.4, 4.5, 4.14, and 4.15), which was responsible for the lower surface crystallinity caused by CRL loading and likely due to the loss of the small partial meso structure during the adsorption process (Yu et al., 2015). The peak shape, on the other hand, remained unchanged during the immobilisation procedure, indicating that the CRL can be immobilised without compromising the structural integrity of the support materials (Zhang et al., 2017). A new reflection for XRD patterns of CRL-1.0 MK and CRL-2.0 MK was observed with low intensity as illustrated in Figure 4.31, so it can be concluded that the XRD profile is not changed, suggesting that the structure of the support remained almost unchanged after enzyme attachment. This is to be expected, as kaolin contains strong hydrogen bond connections between platelets,

making organic molecules difficult to intercalate (de Souza Lima et al., 2019).

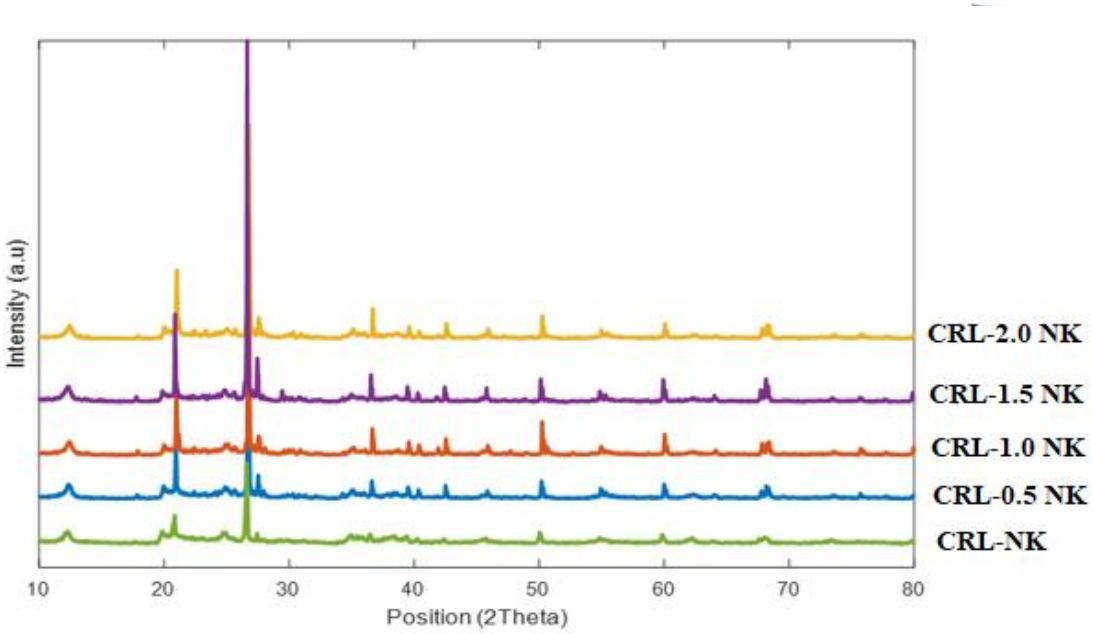

Figure 4.14: XRD Spectrum of Immobilized CRL on Unmodified and Modified Kaolin

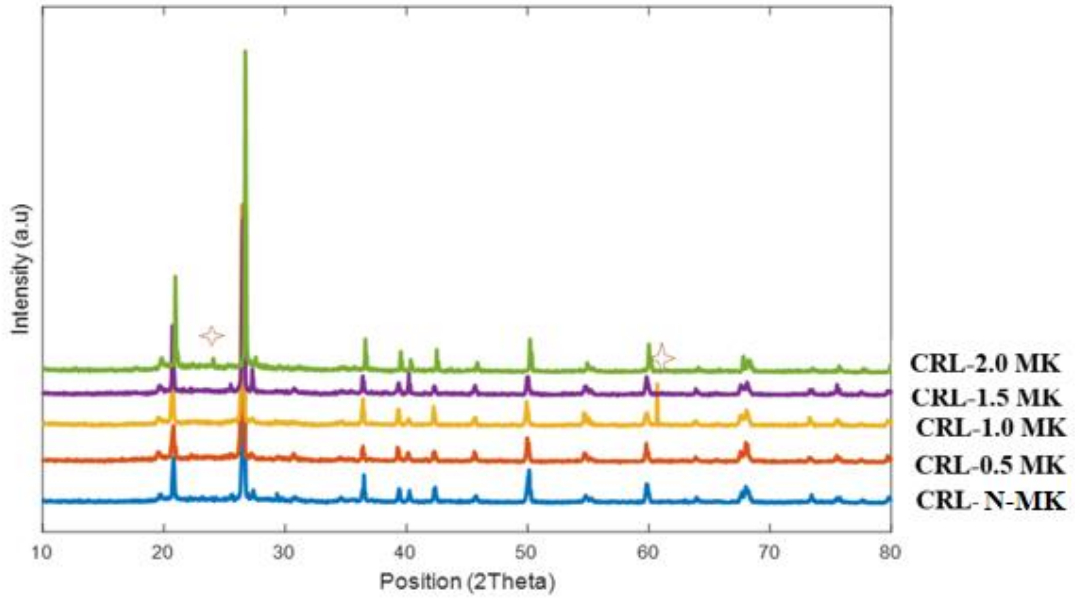

Figure 4.15: XRD Spectrum of Immobilized CRL on Unmodified and Modified Metakaolin

4.8.2 Characterization Using Fourier Transform Infrared (FTIR) Spectrometer

The vibrational frequency and assignments for free CRL is summarized in Table 4.10. The spectrum of free CRL is shown in Figure 4.16. It can be seen the presence

with maxima at the following wavenumbers: the amide I peak of the free lipase which originates mainly from the C=O stretching vibration was observed at 1656 cm^{-1}. This band consists of a group of overlapped signals, which is also responsible of enzyme secondary protein structure of the enzyme and the backbone shape and hydrogen bonding arrangement within the protein molecule defined the exact band position. The discrepancy in presence could be attributable to the Amide I band's conformational sensitivity (Sarno et al., 2017).

Amide II of free lipase was shown at 1541 cm^{-1} indicative of the existence of amino groups. This band is connected with side chain vibrations and hydrogen bond modifications in the protein, and it is mostly due to N-H in-plane bending with a contribution from the C-N stretching vibration. Peak found around 3400 cm^{-1} for -OH and -NH groups (stretching vibrations), and the band at 2934 cm^{-} for -C-H bonds (stretching vibrations). While the bands at 1125 cm^{-1} and 1095 cm^{-1} corresponded to the characteristic peaks of lipase and were attributed for stretching vibrations of C-O bonds. At 1416 cm^{-1}, a weak peak can be observed, which is due to -OH groups (bending vibration) (Yu et al., 2015; Zdarta et al., 2017).

Table 4.10: Vibrational Frequencies and Assignments for Free CRL

Wavenumber (cm^{-1})	Peak assignment
1656	C=O stretching vibration (amide I)
1541	N-H in-plane bending with a contribution of the C-N stretching vibration (amide II)
3368	-OH and -NH groups (stretching vibrations)
2934	C–H bonds (stretching vibrations)
1125 and 1095	stretching vibrations of C–O bonds
1416	-OH groups (bending vibration)
1456	C-H deformation vibrations
657	N-H vibration

The FTIR spectra of support samples after immobilization of CRL are shown in Figure 4.17, Figure 4.18 and Figure 4.19. The absorption bands associated with their characteristic amide I group that was ascribed the peak of the bending vibrations of the hydroxyl group of clay samples at 1634 cm^{-1} - 1649 cm^{-1} (seen in Figures 4.24, 4.25, and 4.26) likely disrupted the -C=O stretching, resulting in an increased intensity of the immobilized lipases' amide I peak. The side chains of lipase were properly fixed on the supports by hydrogen bonds and van der Waals forces at the hydrophobic interface between lipase and the supports, as evidenced by a sharp reduction in the intensity of amide II in all samples when compared to the free CRL, implying that some changes in the conformation of the enzyme occurred after adsorption to the support. The loss of -helix structure and the likely rise of -sheet and/or self-aggregates could be to blame for these conformational alterations (Babaei et al., 2014). However, appearance of these two bands in spectrum were used as markers for the presence of the enzyme on the support surface by physical adsorption because these bands are the most prominent bands of the protein (Golbaha et al., 2016).

It was observed that after immobilization the bands at 2851 cm^{-1} and around 2920 cm^{-1} - 2940 cm^{-1} appeared confirming the presence of -C-H group. These bands indicated the existence of asymmetric stretching vibration of aliphatic -C-H group with contributions from the organo surfactant, and the enzyme (Monteiro & Airoldi 1999; Airoldi & Monteiro 2000). At about 656 cm^{-1}, a weak peak was observed, which was due to the bending of N-H vibration (George, 2013) which then causes decrease in the amount of amino on immobilized CRL (Yu et al., 2015). However, because the bands were overlapped with the Si-O-Si band at 1054 cm^{-1} and 1149 cm^{-1}, the presence of a C-O bond at 1125 cm^{-1} and 1095 cm^{-1} was barely discernible in the spectra. (Zaidan et al., 2010).

In addition, it can be seen after enzyme immobilization that the band which originated from stretching vibrations of free water molecules located in the range between 3100 cm^{-1} - 3550 cm^{-1} had increased intensity and width. These results suggest that the overlapping of -NH stretching vibration of the inserted lipase protein interacts with the -OH bond of the supporting material via hydrogen bonding and confirmed the presence of the enzyme (Monier et al., 2010).

The band at around 1448 cm^{-1} - 1456 cm^{-1} was attributed to -C-H deformation vibrations of alkyl groups and originated from the adsorbed lipase molecules (Tanasković et al., 2017). It should be noted that small changes in the intensity of peaks in the spectra corresponded to certain particular functional groups existing on the clay materials upon immobilization, was due to the existence of hydrogen interactions between the matrix and the enzyme particles. The presence of major bands originating from the support materials and from the enzyme confirmed that effective immobilization had taken place. The vibrational frequency and assignments for CRL immobilized on different supports are summarized in Table 4.11.

Table 4.11: The Vibrational Frequencies and Assignments for CRL Immobilized onto NK, N-MK and Their Derivatives

Wavenumbers (cm^{-1})										
CRL-2.0 MK	**CRL-1.5 MK**	**CRL-1.0 MK**	**CRL-0.5 MK**	**CRL-2.0 NK**	**CRL-1.5 NK**	**CRL-1.0 NK**	**CRL-0.5 NK**	**CRL-N-MK**	**CRL-NK**	**Peak Assignment**
1659	1659	1658	1658	1655	1658	1659	1658	1647	1647	–C=O stretching (amide I)
1545	1545	1549	1541	1541	1545	1541	1540	1538	1533	N-H in-plane bending with a contribution of the -CN stretching vibration (amide II)
2855, 2938	2938	2851, 2938	2932	2851, 2926	2859, 2924	2855, 2928	2851, 2924	2854, 2923	2854, 2924	asymmetric stretching vibration of aliphatic -CH group with contributions from the organo surfactant, and the enzyme
1460	1460	1456	1456	1456	1456	1456	1456	1449	1451	-CH deformation vibrations of alkyl groups and originated from the adsorbed lipase molecules
660	660	660	660	657	656	656	656	656	656	-NH vibration

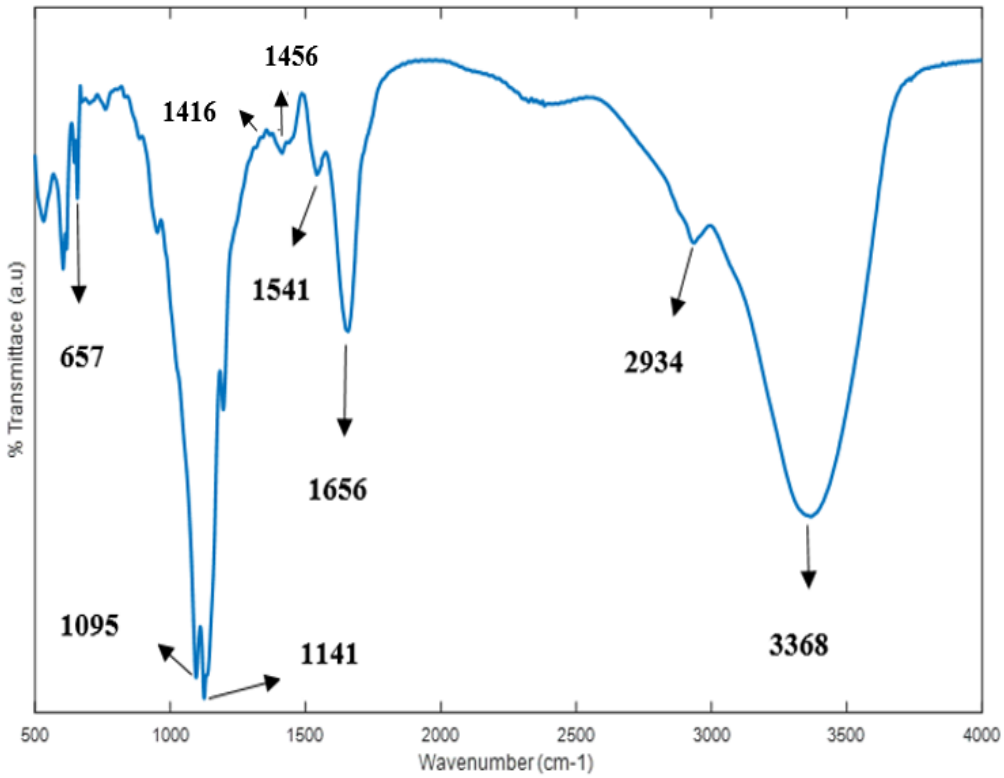

Figure 4.16: FTIR Spectrum of Free CRL

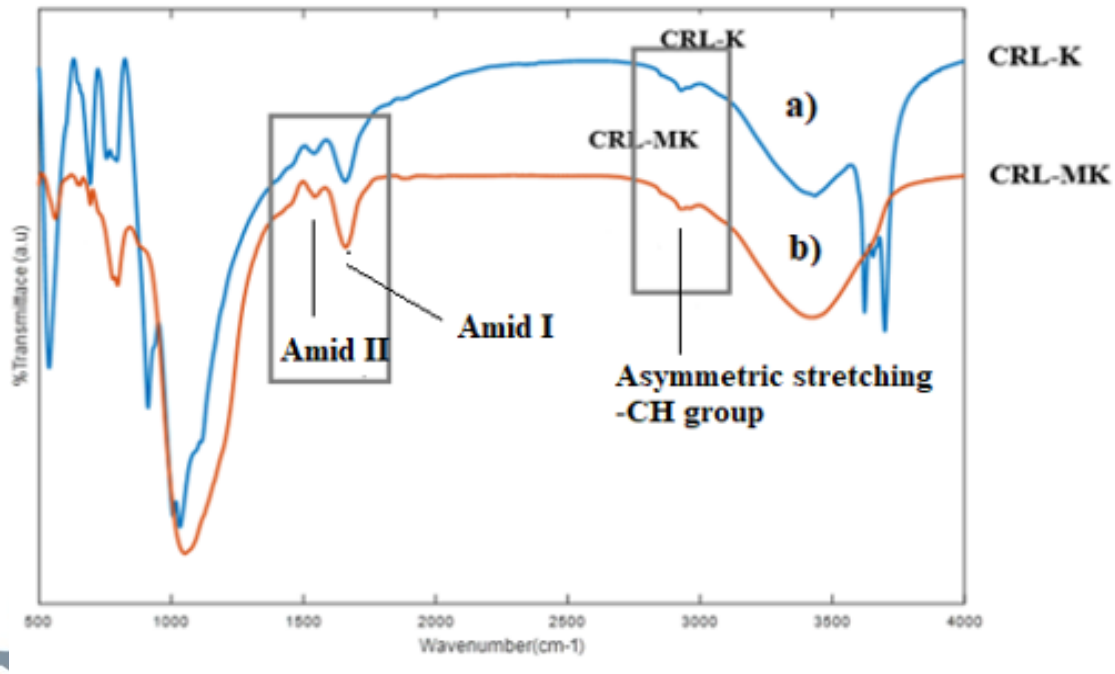

Figure 4.17: FTIR Spectrum of CRL Immobilized onto (a) Natural NK (CRL-NK and (b) Metakaolin (CRL-N-MK)

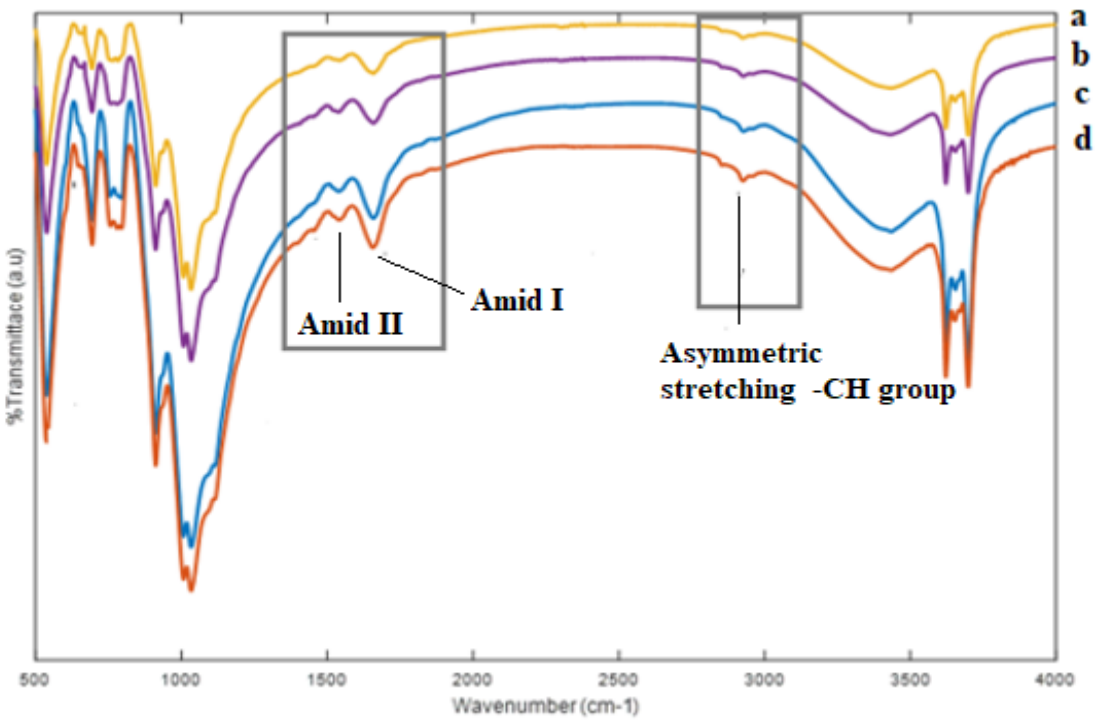

Figure 4.18: FTIR Spectrum of CRL Immobilized onto Organo Modified Kaolin (a) CRL-0.5 NK, (b) CRL-1.0 NK, (c) CRL-1.5 NK and (d) CRL2.0 NK

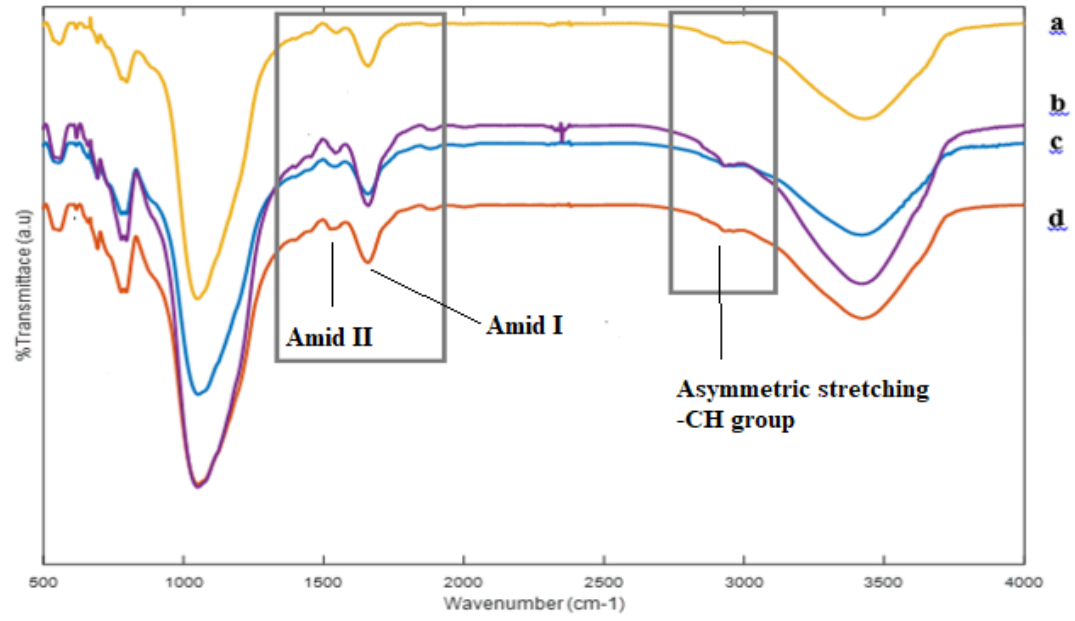

Figure 4.19: FTIR Spectrum of CRL Immobilized onto Organo Modified Metakaolin (a) CRL-0.5 MK, (b) CRL-1.0 MK, (c) CRL-1.5 MK and (d) CRL-2.0 MK

4.8.3 Analysis Using Scanning Electron Microscopy

The morphology of the supports as affected by enzyme adsorption was studied using SEM. SEM of free CRL and immobilized lipase on different support samples are shown in Figure 4.20, Figure 4.21 and Figure 4.22. In general, the CRL can be observed as oval and elongated particulate as shown in Figure 4.20. It can also be seen that the CRL are spherical in shape but shrinked when present in a colony. This is in agreement with reports which claimed that CRL is a spherically shaped unicellular micro fungus. CRL can also be found as single, paired or in a colony (Cygler & Schrag, 1999; Amin, 2013).

Through the images of the morphological structures and dimensions of immobilized lipases, similar features and surface patterns can be observed. Lipase immobilization should be considered at much finer, on the other hand, Lipase had a significant impact on particle structure, resulting in the formation of ball-like structures on the surface (small beads) with higher concentration versus with before immobilization very likely formed by protein aggregates and there was increase in particle size after immobilization.

The external surface of the supports used became substantially thick, rough surface and irregular domains upon immobilization because of lipase molecule aggregation on the support surface. Also, the filling of the pores between layers of the support which have already been confirmed by the decrease in surface areas (Table 4.11). Thus, the SEM images confirmed that the lipase seemed to change the porosity of the aggregate's particles, which will be discussed in detail in Section 4.8.4. SEM images also showed more compact agglomerations of particles due to the existence of enzyme molecules on the surface of the support materials.

These results suggest that the enzyme has been immobilized within the pores and on the surface of the support which led to a change in the morphology of the supports which is in accordance to that observed after lipase immobilization on organo modified smectite nanoclay and on activated chitosan (Tzialla et al., 2009; Santos et al., 2017).

.

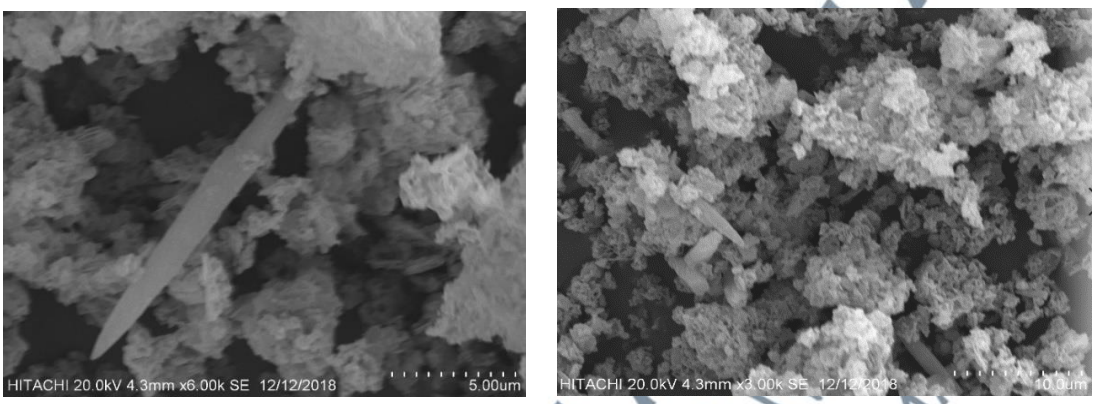

Figure 4.20: SEM Images of Free CRL at 3,000x and 6,000x Magnifications

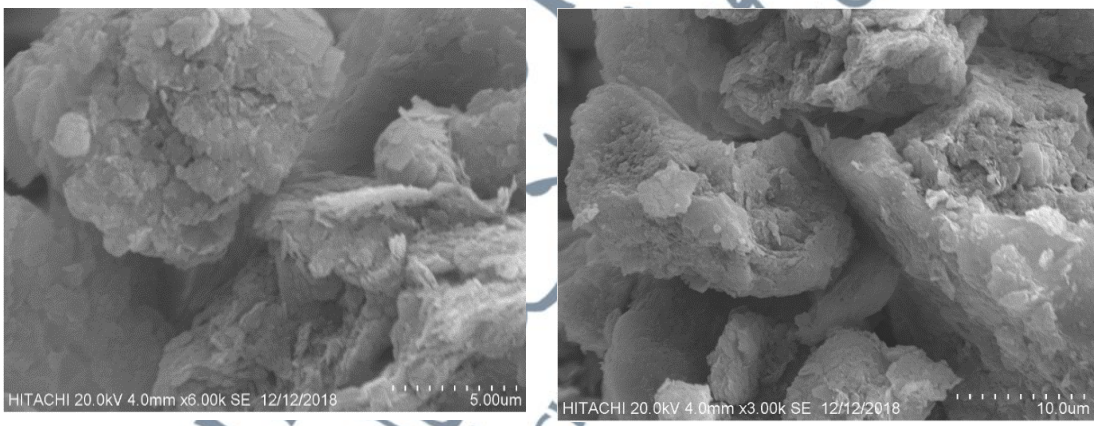

(a) CRL-NK

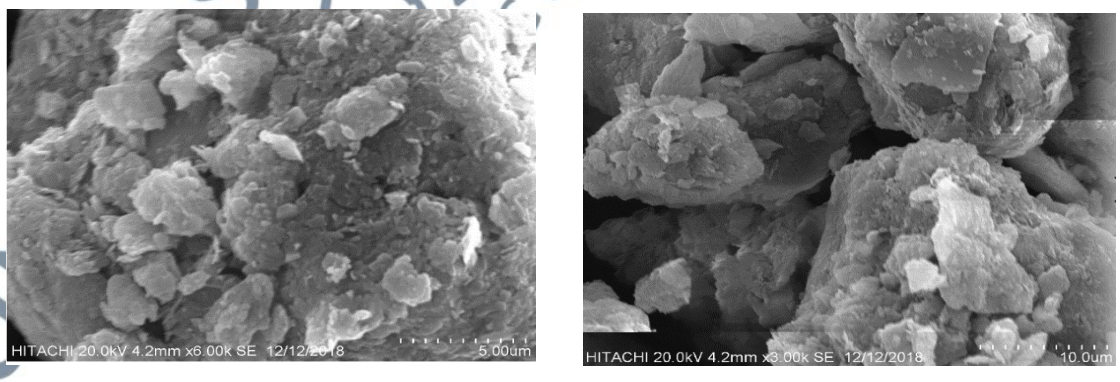

(b) CRL-0.5 NK

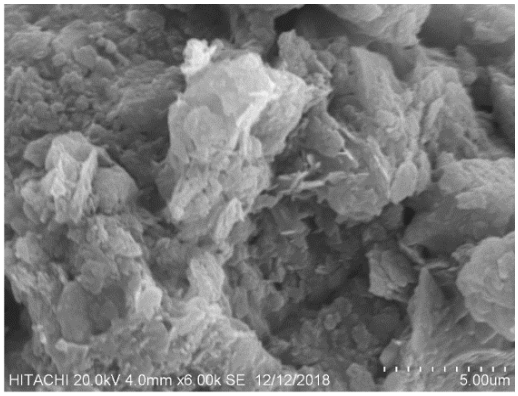

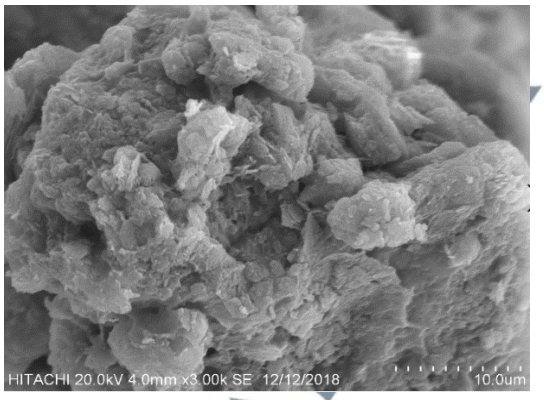

(c) CRL-1.0 NK

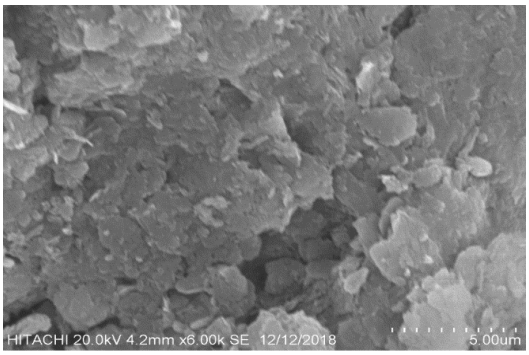

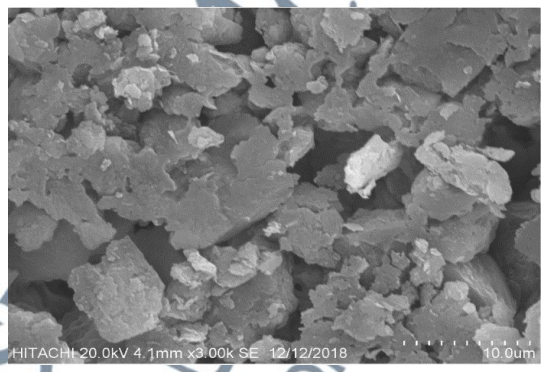

(d) CRL-1.5 NK

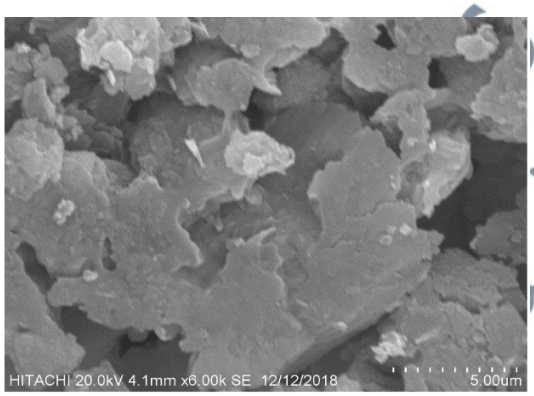

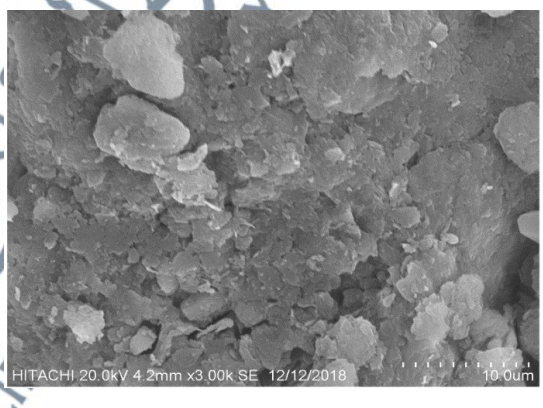

(e) CRL-2.0 NK

Figure 4.21: SEM Images of CRL Immobilized onto Natural Kaolin (a) CRL-NK and Organo Modified Kaolin (b) CRL-0.5 NK, (c) CRL-1.0 NK, (d) CRL-1.5 NK and (e) CRL-2.0 NK at 3,000x and 6,000x Magnifications

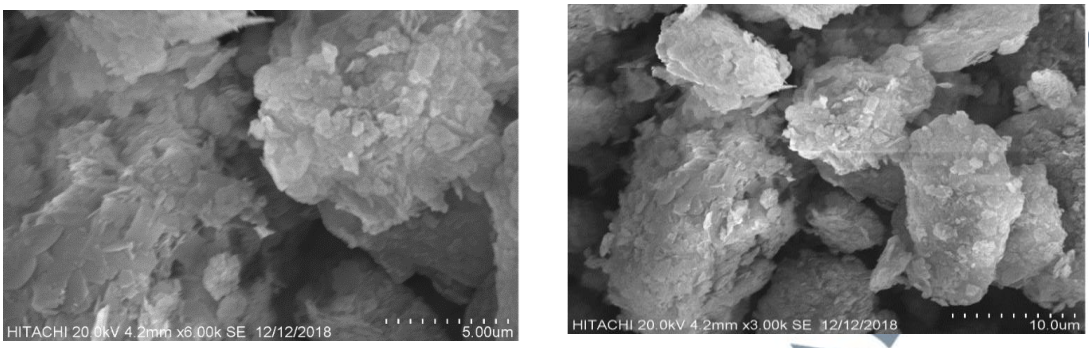

(a) CRL-N-MK

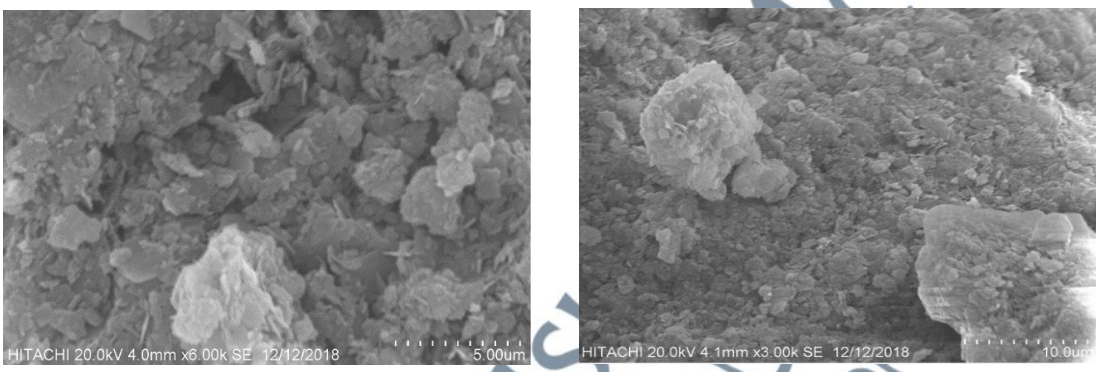

(b) CRL-0.5 MK

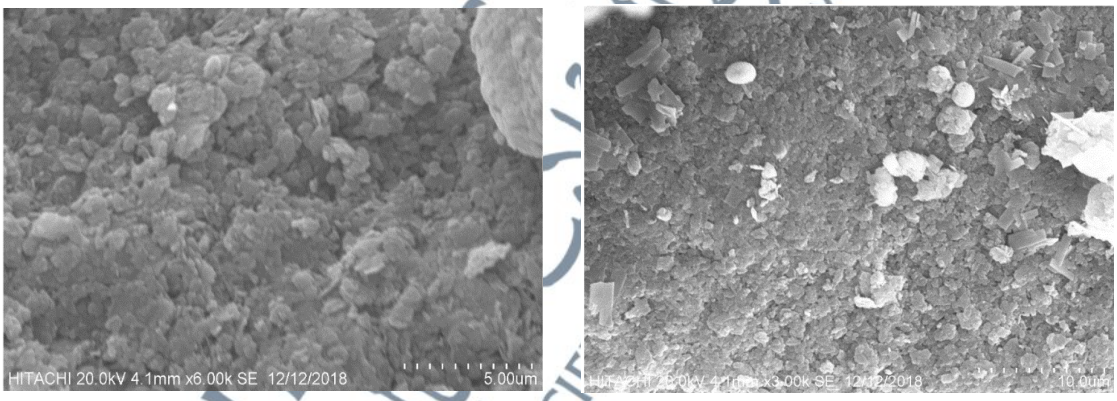

(c) CRL-1.0 MK

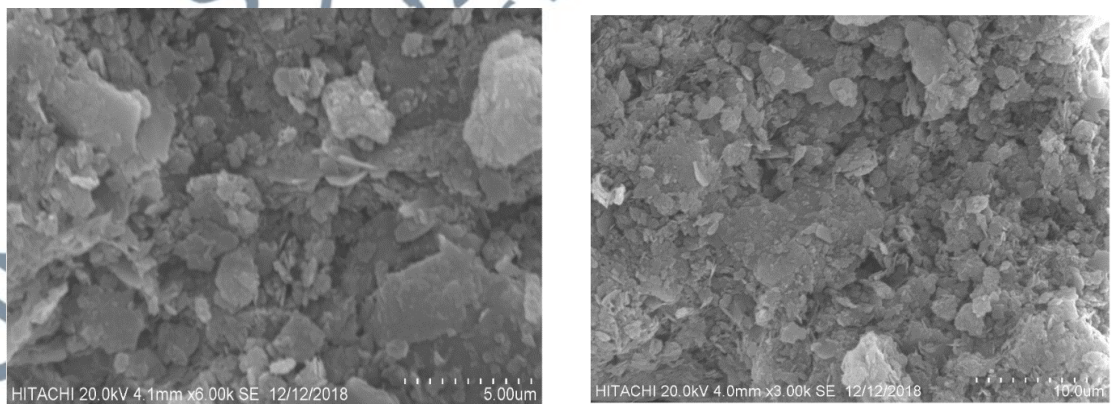

(d) CRL-1.5 MK

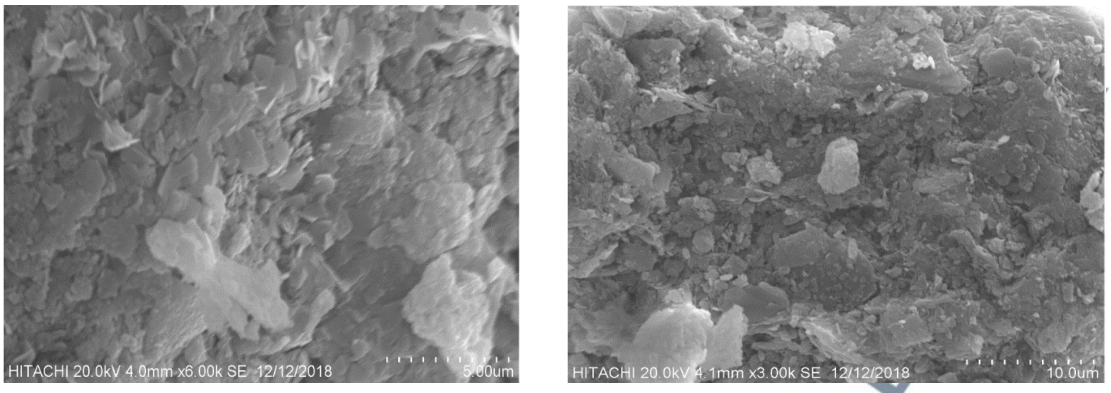

(e) CRL-2.0MK

Figure 4.22: SEM Images of CRL Immobilized onto Metakaolin (a) CRL-N-MK and Organo Modified Metakaolin (b) CRL-0.5 MK, (c) CRL-1.0 MK, (d) CRL-1.5 MK and (e) CRL-2.0 MK, at 3,000x and 6,000x Magnifications

4.8.4 Characterization Using Physisorption of Nitrogen Technique

Morphological changes of support materials as affected by immobilized lipase were determined by measuring porosity characteristics such as total surface area, pore diameter and pore volume using nitrogen adsorption/desorption technique and BET equation. Table 4.12 exhibits the porosity characteristics of immobilized enzymes. The amount of N_2 adsorbed decreased after lipase adsorption, however the P/P_o value did not change substantially (Figure 4.23 and Figure 4.24), which confirmed that the adsorption occurred mostly on the surface of the clay and with almost no sign of intercalation based on the N_2 physisorption isotherms and XRD images.

The hysteresis loops of the N_2 adsorption-desorption isotherms of lipase immobilized clay supports are of type IV, with H_3-hysteresis loops according to the Brunauer et al. (1940). These were similar to the properties of mesoporous materials. At low relative pressures, there is no steep uptake of nitrogen, indicating limited micro porosity. At relative pressures near to one, the adsorption limit is not well defined, indicating the presence of macroporosity in the materials. The slope can be attributed to the exterior area of the particles at relative pressures P/P_o between 0.1 and 0.9, and

the large volume uptake at $P/P_o > 0.9$ to the meso- and macropores formed by the inter particular space.

Adsorption of CRL resulted in the modification of the support microstructure, which led to substantial decline in the specific surface area and pore volume of the resultant catalysts as compared to the values before immobilization (Table 4.6) was done, indicating the adherence of the enzyme on the cavities of the supports. Large areas of the surface, as shown by N_2 molecule adsorption, are located in cavities into which the protein cannot enter, reducing the binding area accessible to CRL. CRL molecules occupied pore channels, blocked pore openings, or were eclipsed by the inserted enzyme, resulting in a decrease in surface area. As a result of the enzyme connections, pores became severely clogged, and the surface area shrank dramatically. This finding could be also due to the layered structure of clay samples which has been collapsed during the immobilization process (Rodrigues et al., 2008; Golbaha et al., 2016). The decrease in the pore volume was attributed to the occupation of the enzyme in the pore channel, which indicated that CRL had been immobilized on support samples. Pang et al. (2016) obtained the similar result when immobilized CRL on wrinkled silica nanoparticles.

All support samples had a wide range of pore diameters, demonstrating bimodal porosity in the mesoporous and macroporous. This type of porosity would allow for efficient transport of reactants into the interior of clay samples, which is advantageous for catalytic capabilities (Zhao et al., 2011). After immobilisation, all samples showed an increase in pore size, which was most likely owing to the enzyme's entry into the clay structure. Coghetto et al. (2012) employed natural montmorillonite as a support for the immobilisation of inulinase from Kluyveromyces marxianus NRRL Y-7571 and obtained similar findings. Reshmi and Sugunan (2013) also reported similar findings as

this phenomenon is a conformation that lipases were adsorbed onto the surfaces of the supports. The enzyme's entry into the pores of the supports gives it a more stable habitat and protects it from external shear stresses (Forde et al., 2010).

It is a known fact that the amount lipase immobilized by adsorption often depends on the porosity of the support materials. In the immobilization procedure, the support pore size is fundamental parameter which should be sufficiently large to allow the enzyme accommodation. Therefore, the globular enzymes like lipases are macromolecules of protein with molecular weight about 40,000 - 60,000 mDa and they possess a typical diameter of ~4.0 - 7.0 nm, whereby most supports in this study have pores large enough to accommodate the molecules of lipases. As stated in most literatures, CRL could be found attached to the surface of clays through the interactions between its amino groups with the carboxyl groups of the clays.

The support with small pore diameter such as unmodified kaolin and metakaolin, however, will not allow CRL to enter their mesopores. Even if there are CRL molecules in the mesopores of NK and N-MK, the enzymes would probably face difficulties to interact with the substrate due to its confinement in the limited space of the mesopores.

The internal diffusion of the substrate to the active site of the encapsulated enzyme and of the product back into the reaction media is the principal consequence of the porous structure. In general, increasing pore diameter leads to more substrate diffusion toward the immobilised lipase active site. Furthermore, large pore surfaces can accommodate protein molecules, whereas small pores may obstruct or even prevent enzyme access to the internal structure of the support, making diffusion difficult, thus limiting mass transfer, and possibly causing conformational and flexibility restrictions, which could result in further denaturation of the enzymes (Anastasescu et al., 2018; Cea et al., 2019). It may be concluded that the variations in surface area, pore volume, and

pore size seen in N_2 adsorption-desorption isotherms show that lipase was adsorbed or dispersed, validating lipase immobilization on clay supports.

Table 4.12: Surface Area, Pore Volume and Pore Size of CRL Immobilized onto NK, N-MK and Their Derivatives

Immobilized Lipases	[a]Surface Area (m^2/g)	[b]Pore Volume (cm^3/g)	[b]Pore Size (Å)
CRL-NK	8.16	0.087	315
CRL-N-MK	6.77	0.093	402
CRL-0.5 NK	3.67	0.064	518
CRL-1.0 NK	4.75	0.071	531
CRL-1.5 NK	3.13	0.049	593
CRL-2.0 NK	2.22	0.031	673
CRL-0.5 MK	8.15	0.102	486
CRL-1.0 MK	6.16	0.049	557
CRL-1.5 MK	6.52	0.105	551
CRL-2.0 MK	3.69	0.048	710

[a]Surface area was determined based on the Brunauer, Emmett and Teller (BET) method
[b]Pore volume and pore size were determined based on the Barret, Joyner and Halenda (BJH) t-plot method

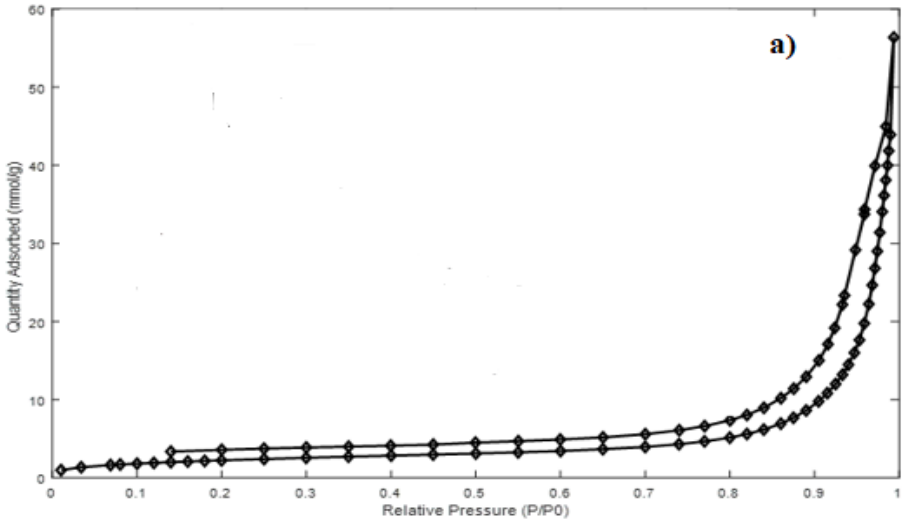
a)
Quantity Adsorbed (mmol/g)
Relative Pressure (P/P0)

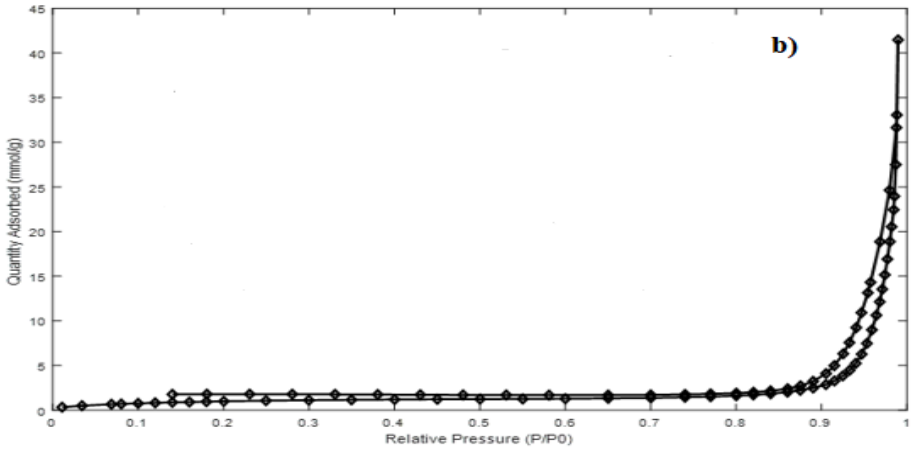
b)
Quantity Adsorbed (mmol/g)
Relative Pressure (P/P0)

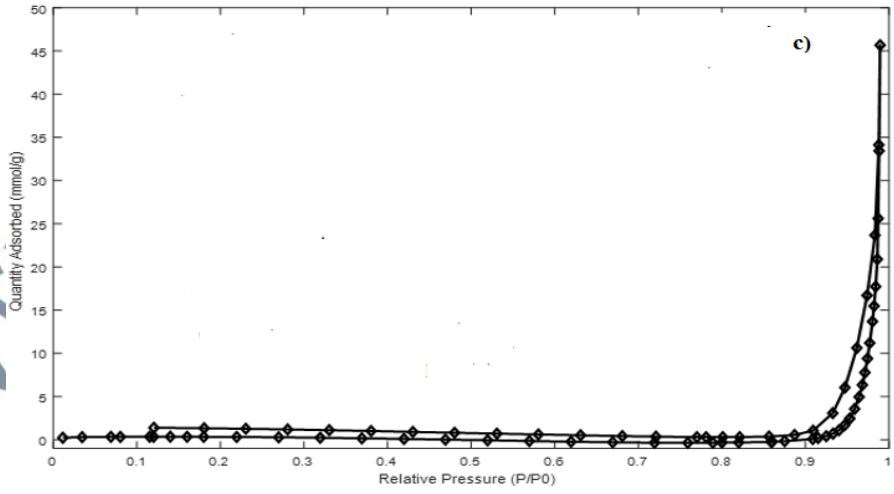
c)
Quantity Adsorbed (mmol/g)
Relative Pressure (P/P0)

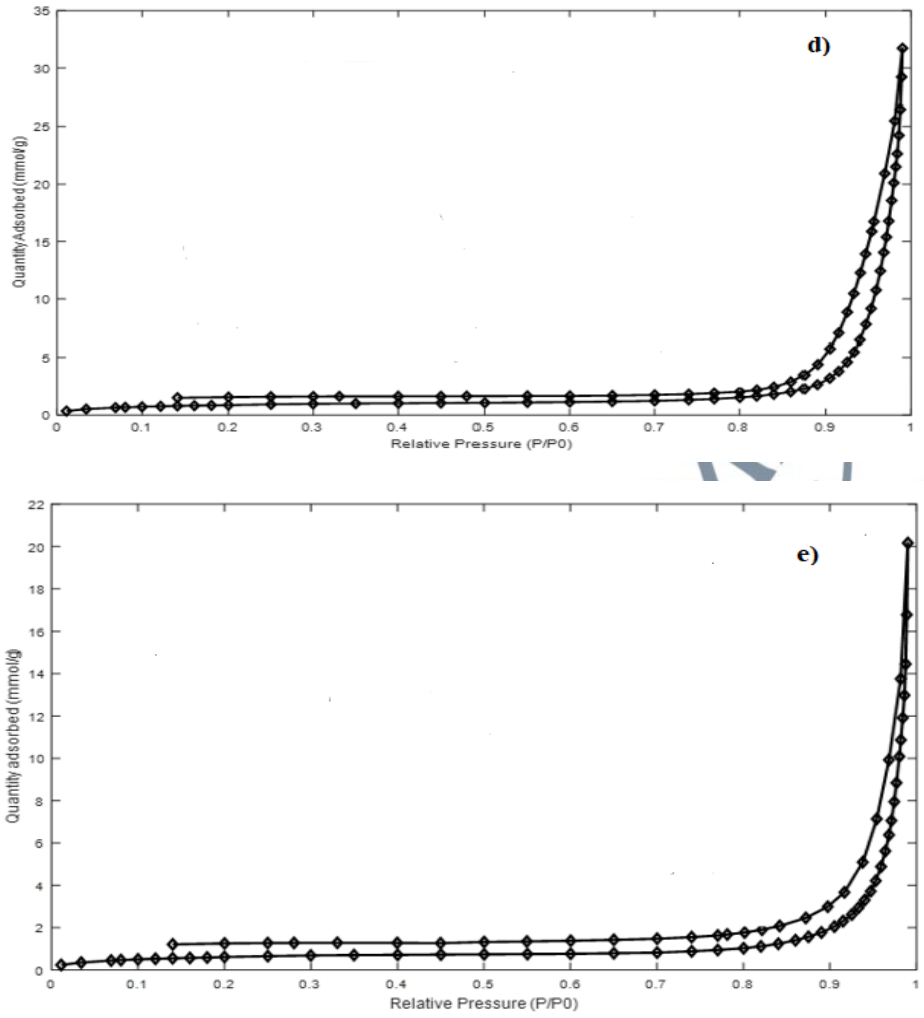

Figure 4.23: Nitrogen Adsorption-Desorption Isotherms for CRL Immobilized onto Natural Kaolin and Its Derivatives (a) CRL-NK, (b) CRL-0.5 NK, (c) CRL-1.0 NK, (d) CRL-1.5 NK and (e) CRL-2.0 NK

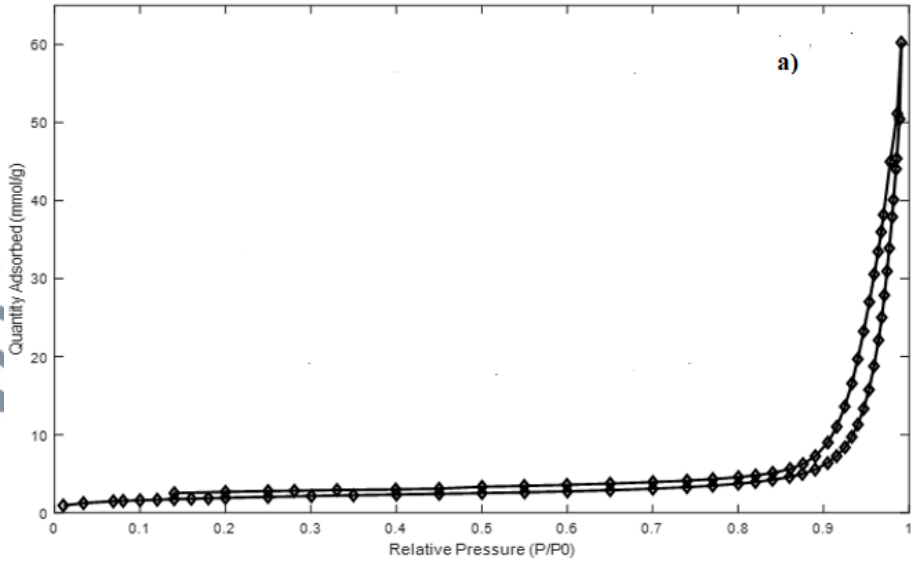

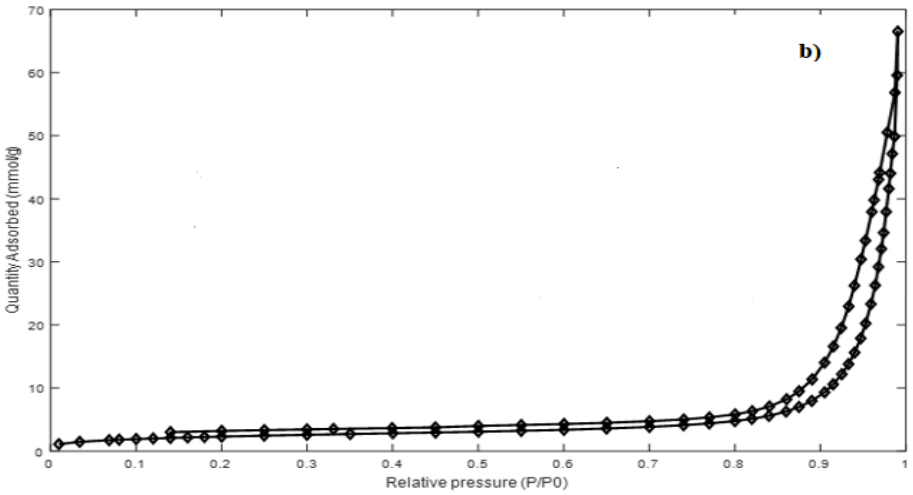
b)
Quantity Adsorbed (mmol/g)
Relative pressure (P/P0)

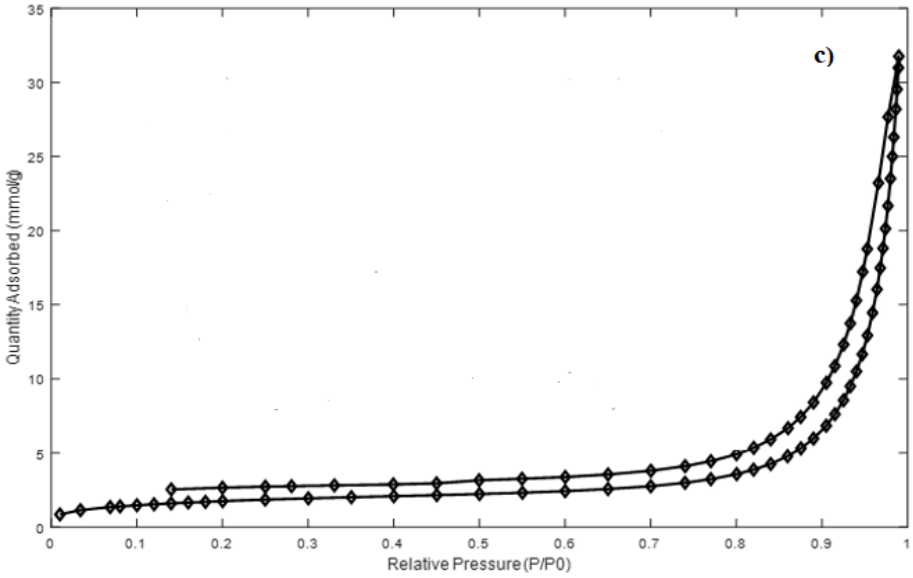
c)
Quantity Adsorbed (mmol/g)
Relative Pressure (P/P0)

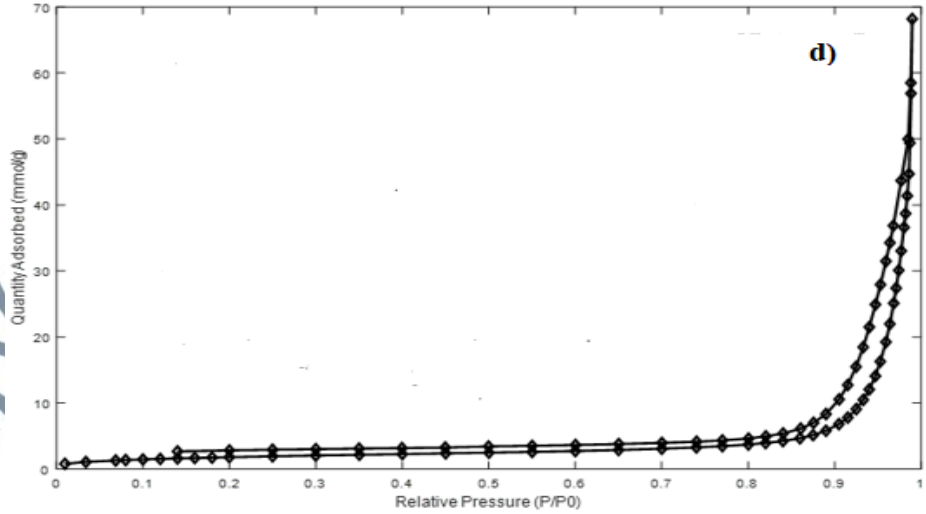
d)
Quantity Adsorbed (mmol/g)
Relative Pressure (P/P0)

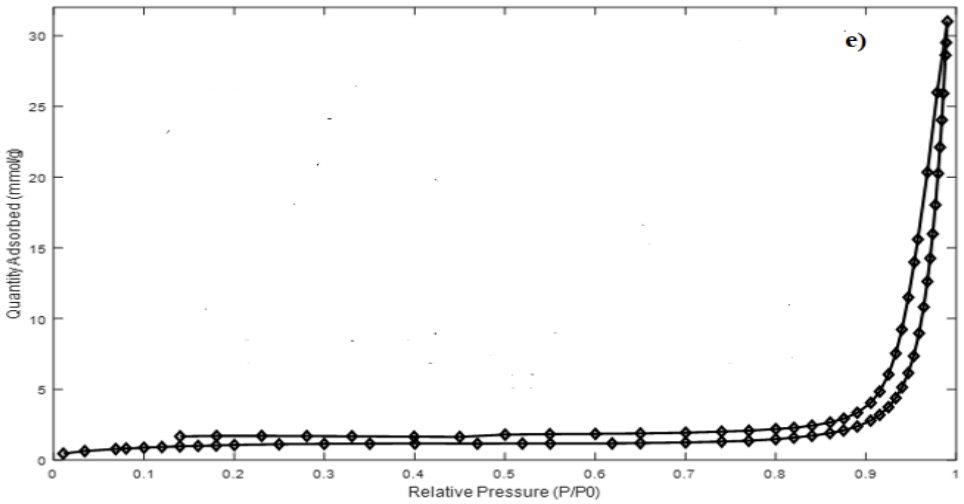

Figure 4.24: Nitrogen Adsorption-Desorption Isotherms for CRL Immobilized onto Metakaolin and Its Derivatives (a) CRL-MK, (b) CRL-0.5 MK, (c) CRL-1.0 MK, (d) CRL-1.5 MK and (e) CRL-2.0 MK

4.9 Enzymatic Synthesis of Nonyl Hexanoate

The esterification reaction was used to successfully complete the enzymatic production of nonyl hexanoate between nonyl alcohol and hexanoic acid. Lipase from *Candida rugosa* was employed in this reaction since it had previously been used in various stereo selective esterification reactions under mild reaction conditions in organic medium (Rahman et al., 2019). In addition, because of its high activity in synthesis and hydrolysis reactions, CRL is used in a number of activities. To dissolve the reaction components and move the equilibrium to the synthetic process, the reaction was carried out in the presence of hexane as a medium.

4.9.1 Screening of Immobilized Lipase

In this study, the immobilized lipases were tested for suitability as biocatalyst in the esterification of nonyl hexanoate. A screening step was achieved to select the support that had a high affinity for lipases and facilitate effective contact with the substrate at the enzyme-support interface. The conversion of ester of free and lipase immobilized on support derivatives is displayed in Figure 4.25. A percentages

conversion of ester ranging from 50.71% to 68.03% and esterification were achieved during 5 hours of experiment. Muhamad et al. (2010) obtained 82% for nonyl caprylate as flavour ester. The fact that enzymes from different sources have varied properties makes comparing with previous study results difficult.

All immobilized lipase performed higher specific activity compared to the free lipase which achieved 3.27 $\times 10^{-3}$ µmol/min/mg as shown in Figure 4.26. This is owing to the increased in surface area supplied by these supports, as well as the distribution of lipase on the support surface, resulting in better active-site exposure, while free lipase aggregated because it was insoluble in the organic medium, this aids lipase dispersion in the reaction media (Rahman et al., 2005; Garcia-Galan et al., 2011; Reshmi & Sugunan, 2013; Romero et al., 2018). Similarly, with the previous study was done by Rahman et al. (2004) who reported that the activity and stability of the lipase after immobilization on both layered double hydroxides (LDHs) were found to be increased compared to in native lipase. In contrast; Aghababaie et al. (2018) found the specific activity of CRL reduced after immobilization on membrane. When an enzyme is immobilised on a membrane, mass transfer restrictions diminish the amount of substrate available to the enzyme, lowering its activity in contrast to a free enzyme (Ye et al., 2006; Chen et al., 2012).

The activity followed the order: CRL-2.0 MK> CRL-2.0 NK> CRL-1.5NK> CRL-1.0 MK>CRL-1.5 MK> CRL-1.0 NK> CRL-0.5 NK> CRL-0.5MK> CRL-N-MK>CRL-NK> Free-CRL. It can be seen that all prepared lipases clearly improved the esterification after modifying the surface of support with $BTEA^{+}$. The presence of silanol groups, which act as sites of linkage for bioactive species after being activated by the modifier (Scherer et al., 2011). Due to proportionality with the 'open lid' of the lipase, making it better accessible to any substrate, these qualities may favour high

binding capacity and boost the catalytic of the conjugated enzyme. (Zaidan et al., 2010; Romero et al., 2018).

This research demonstrated that when utilising organo-modified clays, the lipase molecules preferentially associated with the organo-modifier (ammonium salt), resulting in superior structural placement and accessibility to the active centre of the enzyme, as described by Oztürk et al (2016). NK support showed the lowest enzymatic activity (3.63×10^{-3} µmol/min/mg) with yield of synthesized nonyl hexanoate ester (52.53% ± 1.56) compared with other supports. The decrease of ester conversion might be due to its negatively charged surface, which may be not fully appropriate for catalytic activity and may also the formation of enzyme aggregates on these supports (Golbaha et al., 2016; Ramos et al., 2014). This result in agreement with result obtained by Musa and co-authors (2018) where the kaolin support showed the decrement of synthesize ethyl hexanoate ester compared with other supports. Other enzymes such as porcine pancreatic lipase and acid phosphatase (Scherer et al., 2011; Huang et al., 2005) also have reported the unsuitability of this support.

Abolhasani et al. (2017) and Tzialla et al. (2010) stated that the enzymes that form complex and become immobilized in organic compounds are resistant against protein-decomposing enzymes. That is due to the hydrophobic microenvironment created by organic modification could influence the diffusion and distribution of substrates and products in the microenvironment of the immobilized enzyme increasing the accessibility to hydrophobic substrate and enhancing the activity of enzyme.

The discrepancy in ester conversion between organoclay samples could be related to differences in physical structures and surface hydrophilic/hydrophobic qualities generated by varying surfactant ratios utilised in the manufacture of organoclay (Yu et al., 2015).

However, the lipase immobilized on modified metakaolin with 2.0x CEC showed higher enzymatic activity (5.24×10^{-3} µmol/min/mg) with ester conversion (68.03% ± 0.61) as compared with control. The internal diffusion of the substrate to the active site of the encapsulated enzyme and of the product back into the reaction media appears to be the main consequence of the porous structure, and tiny pores can cause mass transfer restrictions in both directions (Paul et al., 2016). With thinner layers of immobilised enzymes, 2.0 MK may have a better adsorption capacity, resulting in more active sites accessible for catalysis and less space available for the lipase to distribute itself as the amount of lipase adsorbed increased. As a result, more of its active conformation is preserved, and the activity loss is decreased (Golbaha et al., 2016).

It should also be noted that at low immobilization yield which was achieved by CRL-0.5MK (Table 4.8), this support also showed less activity (3.73×10^{-3} µmol/min/mg) and the lowest ester conversion (57.79 ± 0.91) compared to the other organoclay samples. This could be because the lipase has some surface area to occupy and is attempting to optimise its contact with the surface, resulting in a loss of conformation and hence a decrease in activity (Golbaha et al., 2016). Blanco et al. (2004) found that in low loaded derivatives, enzyme-support interactions are particularly strong, resulting in activity reduction.

Although, immobilization yield for both supports CRL-1.0 NK and CRL-1.5 NK were almost similar (Table 4.7), they showed differences in the specific activity. The specific activity for both supports were 4.43×10^{-3} and 4.88×10^{-3} µmol/min/mg, respectively, while the ester conversion obtained by both supports were 61.91 ± 0.96 % and 64.33 ± 0.63%, respectively. The variation in these values for both supports is presumably due to the dispersion of the pore size that is larger for CRL-1.5 NK, and this makes it easier for the enzyme to connect with the substrate (Ramos et al., 2014).

The specific activity for CRL-1.0 MK and CRL-1.5 MK were 4.81×10^{-3} and 4.59×10^{-3} µmol/min/mg, respectively. Thus, it can be noticed that the increase in the amounts of bound proteins does not necessarily mean the activity increase (Golbaha et al., 2016). That was observed for CRL-1.0 MK and CRL-1.5 MK with the activity is lower than that of the enzyme it contains. In order to find the causes of the drop in final activity, several hypotheses were investigated, (Öztürk et al., 2016): which are

(a) production of enzyme aggregates on the support's surface;

(b) tertiary structural deformation due to intense interaction with the support;;

(c) structural damage of the protein caused by the protein–protein interactions which are the consequence of deficiently space between adsorbed proteins which leads to structural rearrangements and activity decrease;

(d) due to increase in the mass of loaded protein enzyme molecules and because some enzymes get "buried" and hence less accessible to the substrate, thicker layers of adsorbed lipases typically result in a loss of specific activity.

Overall, the efficiency of immobilised lipase catalysts is greatly improved by organo-modification of the clay surface, and due to its superior immobilization performance by CRL-1.0 MK, CRL-2.0 MK, CRL-1.5 NK, CRL-2.0 NK were used for lipase immobilization in the rest of the study.

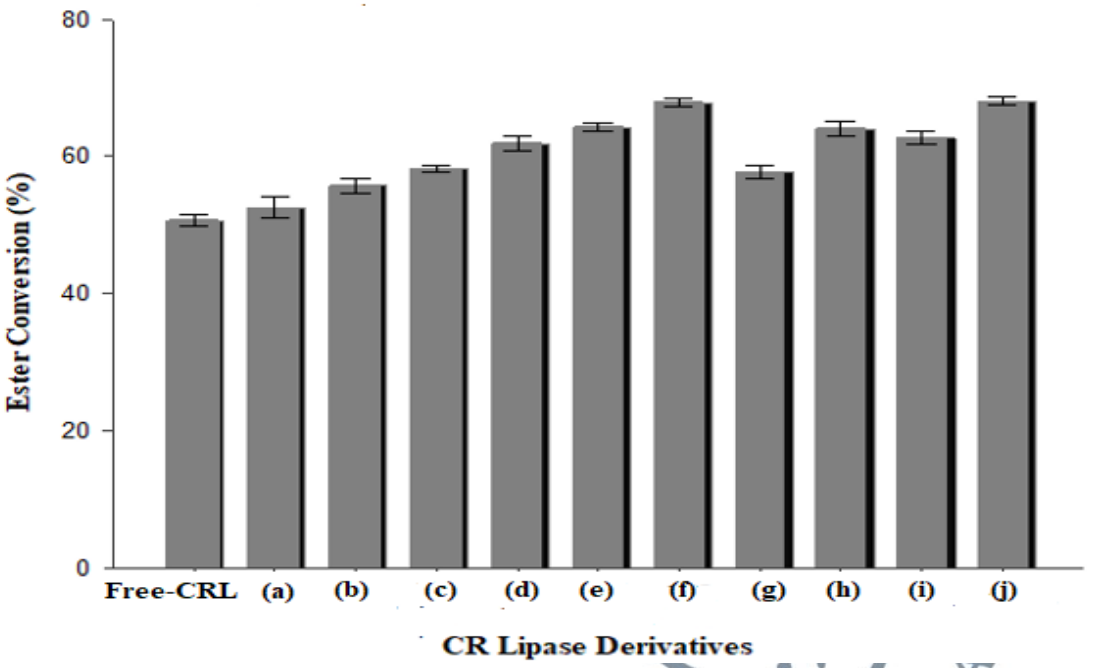

Figure 4.25: Percent of Nonyl Hexanoate Conversion in the Synthesis Using Free and Immobilized CRL [(a) CRL-NK-(b) CRL-N-MK-(c) CRL-0.5NK-(d) CRL-1.0NK-(e) CRL-1.5NK-(f) CRL-2.0NK-(g) CRL-0.5MK-(h) CRL-1.0MK-(i) CRL-1.5 MK-(j) CRL-2.0MK]. Reactions were Performed at 30 ^{o}C for 5 Hours with 1:1 Molar Ratio of Nonanol and Hexanoic Acid in Hexane. Bars Represents Standard Deviations

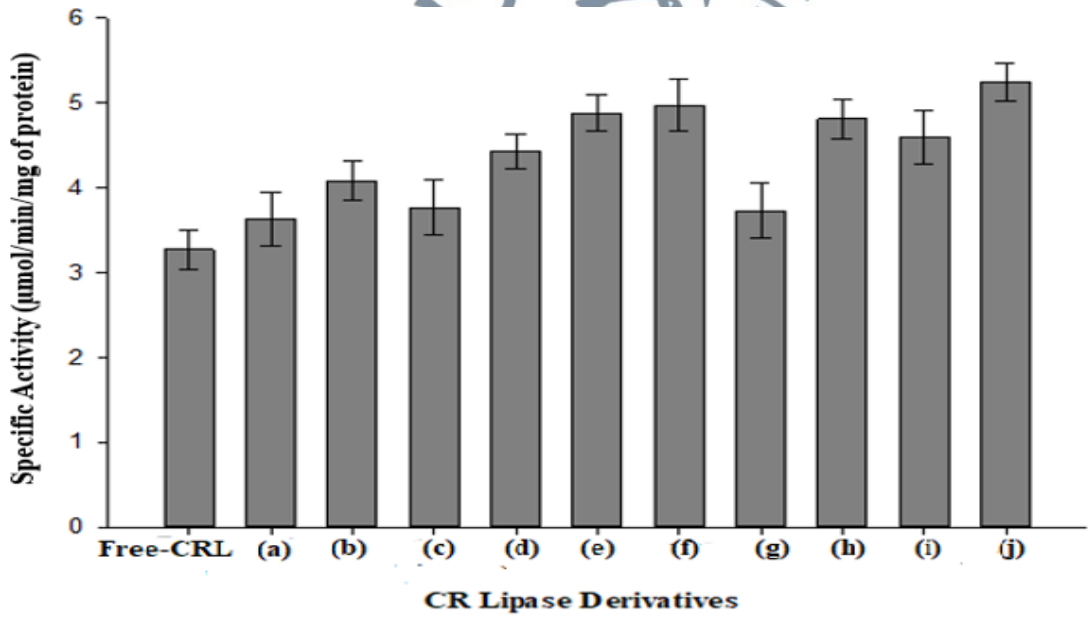

Figure 4.26: Specific Activity of Free and Immobilized CRL [(a) CRL-NK-(b) CRL-N-MK-(c) CRL-0.5NK-(d) CRL-1.0NK-(e) CRL-1.5NK-(f) CRL-2.0NK-(g) CRL-0.5MK-(h) CRL-1.0MK-(i) CRL-1.5 MK-(j) CRL-2.0MK] in the Synthesis of Nonyl Hexanoate. Reactions were Performed at 30 ^{o}C for 5 Hours with 1:1 Molar Ratio of Nonanol and Hexanoic Acid in Hexane. Bars Represents Standard Deviations

4.9.2 Effect of Time Course

A good measure of enzyme performance and reaction progress is a time course study. When an enzyme produces good product yields in a shorter amount of time, it is said to have good performance (Rahman et al., 2008). The progress curves can be used to calculate the lowest time required to achieve a good conversion yield while minimising energy consumption and, as a result, lowering process costs. Figure 4.27 depicts the reaction time curve of hexanoic acid esterification with nonanol catalysed by free CRL and the both immobilized lipase on organo-modified kaolin and metakaolin, which gave high conversion of ester. Generally, the conversion of nonyl hexanoate increased with increasing reaction time.

In this study, the percentage conversion shows a different profile where the reaction took about 5 hours to achieve equilibrium with percentage conversion (~70%) for immobilized lipases. Whereas it was only 51.39% for the free CRL. Hence, this was taken as the basis and subsequent experiments, where the reactions were conducted over the course of 5 hours. The percentage conversion shows high increment at 8 hours for CRL-2.0 NK and CRL-2.0 MK (75.97% - 80.11%, respectively). Incubation beyond 8 hours led to decrease the conversion of ester. In contrast, reactions with free-CRL only achieved about 61.52% of nonyl hexanoate within 12 hours and subsequently the conversion has decreased back. The enhanced efficiency of immobilized lipase over native CRL in producing higher nonyl hexanoate conversion degrees can be due to CRL being more stable on both supports. Because of the additional stiffness conferred by multipoint interactions (e.g. hydrophobic interaction, hydrogen bond, electrostatic, and van der Waals forces) and greater dispersion of the enzyme molecule over the support surface, immobilized CRL can better preserve their activity than free CRL. As a result,

immobilised lipase is less susceptible to denaturation in the reaction vessel due to solvents, temperature, or substrates (Mohamad et al., 2015; Elias et al., 2019).

The declined percentage of synthesis the nonyl hexanoate may be explained by increasing production of water molecules during catalysis. Large amounts of water in excess of what is required for a complete hydration layer may give some protection from organic solvent denaturation, but this may pose mass transfer issues for the substrate. Increased water is more likely to cause hydrolysis of the ester generated. In addition, as indicated in another similar study, water adsorption on the supports could be one of the key factors contributing to biocatalyst inactivation (Onojaa et al., 2018).

The increased amount of water produced by the reaction results in water-organic solvent immiscibility, lowering the substrate's solubility in organic solvent (Rahman et al., 2001). The evaporation of hexane from reaction medium would decrease the volume of organic solvent, hence the substrate solubility would decrease and the accessibility of substrate and lipase would decrease (Radzi et al., 2010). In addition, the ionisation of water molecule produced ion H^+ and OH^-, which may alter the salt bridge and charges on the surface of lipase molecule. The concentration of substrates reduced as the reaction progressed, resulting in a decrease in the degree of saturation of the enzyme with substrate (Radzi et al., 2005; Ozyilmaz & Yağız, 2012; Mohamad et al., 2015).

Because just a little amount of water was made during the initial stage, the initial reaction rate was rather insensitive to the amount of water produced. After the specified time intervals (12 hours for nonyl hexanoate synthesised by immobilized synthesis) the conversion of ester was relatively constant, which may be due to the attainment of reactions at the equilibrium (Garlapati & Banerjee, 2013) and the rate of forward reaction was expected to be equal to the rate of backward reaction.

In the literature, reaction times for enzymatic synthesis of flavour esters varied within 2 - 5 hours (Martins et al., 2014), 6 hours (Manan et al., 2016), 8 hours (Eliasa et al., 2019), 12 hours (Muhamad et al., 2010), 24 hours (Raghavendra et al., 2010), 48 hours (Ozyilmaz et al., 2010), 96 hours (Annapurna Devi et al., 2018). This is due to variety of enzyme, support system, and variety of carbohydrate types and fatty acids used. The reduction in reaction time in this study could be due to accumulation of reaction by product to clay support, thus limiting the contact surface area between substrates and lipase. Its decreased hydrophilicity can also be attributed to lower and non-inhibitory concentrations of both substrates (hexanoic acid and nonanol) in the enzyme's microenvironment.

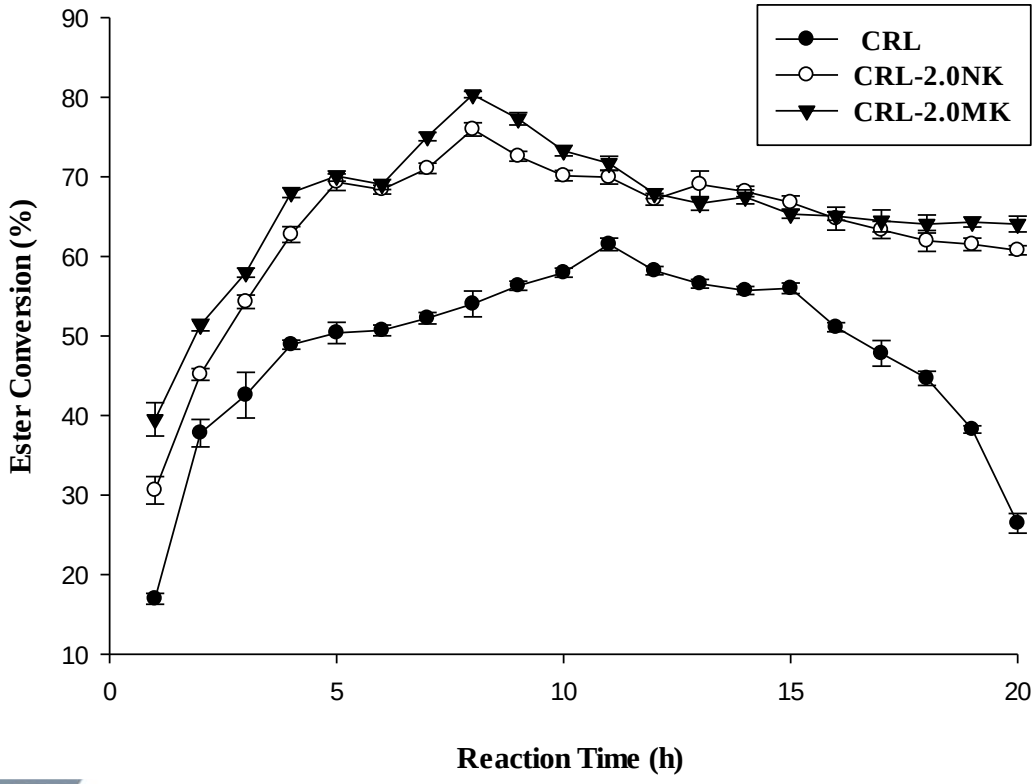

Figure 4.27: Percent of Nonyl Hexanoate Conversion in the Synthesis Using Free CRL, CRL-2.0 NK and CRL-2.0 MK, as Affected by Incubation Time. Reactions were Performed at 30 ^{o}C with 1:1 Molar Ratio of Nonanol and Hexanoic Acid in Hexane, at Different Time Intervals. Bars Represents Standard Deviations

4.10 Verification of Nonyl Hexanoate

Product of the reaction was ascertained using FTIR and GC-MS. The aim of these analyses is to verify major product of the reaction based on the existence of the functional groups it possesses.

4.10.1 Verification of Nonyl Hexanoate Using Fourier Transform Infrared (FTIR) Spectrometer

The use of FTIR on determination of ester product has been reported in many papers (Salmahaminati & Jumina, 2017; Musa et al., 2018). In this study, FTIR is used to identify the product obtain which is nonyl hexanoate. Figure 4.28 shows the FTIR spectra of hexanoic acid, nonanol, and nonyl hexanoate, respectively. Infrared spectrum for hexanoic acid showed a strong broad peak in the region above 2520 cm^{-1} indicative the -OH stretch. There are also strong peak in the spectrum at 1706 cm^{-1} indicates the carboxylic group. The C-O stretching also detected at 1106 cm^{-1} and 1380 cm^{-1}. Finally, the CH_2 bend was observed at 1413 cm^{-1} and 1459 cm^{-1}.

The second spectrum which is nonanol also showed the broad peak at 3322 cm^{-1} which indicates the -OH stretch with the medium intensity. The C-O stretching also detected at 1055 cm^{-1}. The -CH_2 bend was observed at 1465 cm^{-1}. The third spectrum for the product which is nonyl hexanoate, have three major absorption bands that observed for ester product (Table 4.13). The aliphatic -C-H stretching vibration occurred in the range of 2800-3000 cm^{-1} was confirmed by the sharp peak at 2931 cm^{-1}. The two or more stretching bands are shown by some peaks in the range of 1000-1300 cm^{-1} which revealed the presence of C-O bond. The existence of carbonyl group conjugated to a double bond (C=O) was represented by the strongest peak at 1713 cm^{-1} which strongly suggested the existence of the corresponding ester due to (COOR)

formed by esterification process. This shifted in the carbonyl peak of C=O from 1706 cm^{-1} to 1713 cm^{-1} which confirms the change from acid to ester. In addition, the uptake area in 1466 $cm^{-1}$and 1357 cm^{-1} indicate the presence of -C-H vibration bends of methylene group ($-CH_2-$) and vibration of -C-H bend of a methyl group ($-CH_3$).

The other functional group detected in the compound was -OH, due to the existence of a weak band in the region above 3016 cm^{-1}. This was assumed to originate from the traces of substrates left in the product of the reaction.

Table 4.13: Fourier Transform Infrared Spectrum of Nonyl Hexanoate

Wave number (cm^{-1})	Peak Assignment
1714	v(C=O)
2931	v(C-H) stretch
1250	v(C-O)
1466	($-CH_2-$)
1357	($-CH_3$)

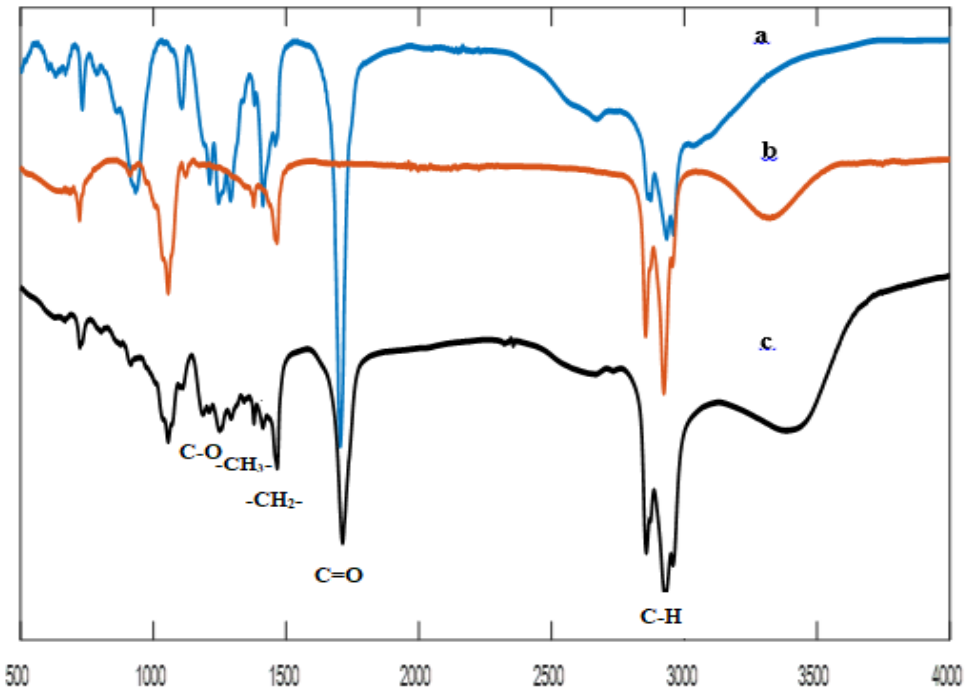

Figure 4.28: FTIR Spectra of Substrates, (a) Hexanoic Acid, (b) Nonanol and Product of the Reaction, (c) Nonyl Hexanoate

4.10.2 Verification Using Gas Chromatography-Mass Spectrometer (GC-MS)

In Figure 4.29, the gas chromatogram shows 5 major peaks corresponding to the existence of different compounds as listed in Table 4.14. The peak corresponding to nonyl hexanoate was detected at retention time of 34.492 minutes. The ester showed highest retention time compared to the substrates. This is due to the low polarity of nonyl hexanoate as compared to the substrates used in its synthesis. The results which showed the presence of other interfering compounds was not surprising and could be due to the partial purification and isolation which have taken place prior to the analysis.

After the analysis using gas chromatography, the sample was further analysed using mass spectrometer where fragmentation into single ions was done and depicted in the spectrum. Figure 4.30 showed the molecular ion fragmentation at m/z 242 (M^{-1}) which corresponded to the existence of nonyl hexanoate. The corresponding ester compound of nonyl hexanoate ($C_{15}H_{30}O_2$) can be recognized by mass spectra. Fragmentation begins with a loss of pently ion, with of m/z 171 (M^{-1}), which is the base peak ion. Further fragmentation of the ester resulted in loss of a compound at m/z 126 (M^{-1}). The positive charge commonly resides on the smaller fragments, so a homologous series of pentyl (m/z = 71), propyl (m/z = 43) and ethyl (m/z = 29) can be seen. Furthermore, the peaks at m/z 61 and m/z 99 corresponded to $[C_2H_5O_2]^+$ and $[C_6H_{11}O]^+$ ions, respectively, detected in the spectra. Other bonds cleavage occurred through some pathways and gave further fragmentation ions as shown in Scheme 4.1.

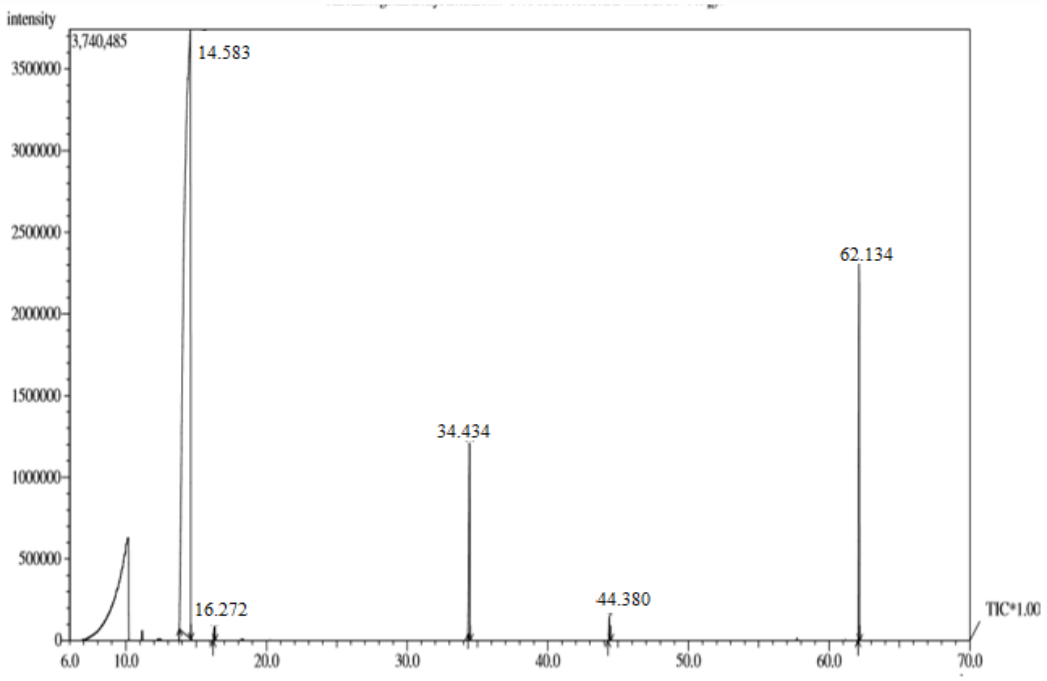

Figure 4.29: GC-MS Chromatogram in the Verification of Nonyl Hexanoate

Table 4.14: Molecular Ion Fragments of Nonyl Hexanoate

m/z	Fragmentation of Molecular Ion
29	$CH_3CH_2^+$
43	$CH_3CH_2CH_2^+$
56	$CH_3CH_2\ CH_2CH_2^+$
61	$CH_3\overset{\overset{+OH}{\|}}{C}OH$
71	$CH_3CH_2\ CH_2CH_2CH_2^+$
84	$CH_3CH_2CH_2CH_2CO^+$
99	$CH_3CH_2CH_2CH_2CH_2CO^+$
117	$CH_3CH_2CH_2CH_2CH_2\overset{\overset{+OH}{\|}}{C}OH$
126	$CH_3CH_2CH_2CH_2CH_2CH_2CH_2CH_2CH_2^+$
143	$CH_3CH_2CH_2CH_2CH_2CH_2CH_2CH_2CO^+$
171	$CH_3CH_2CH_2CH_2CH_2CH_2CH_2CH_2COO^+$
175	$CH_3CH_2CH_2CH_2CH_2CH_2CH_2CH_2CH_2COO^+$
242	$CH_3CH_2CH_2CH_2COOCH_2CH_2CH_2CH_2CH_2CH_2CH_2CH_2CH_3$

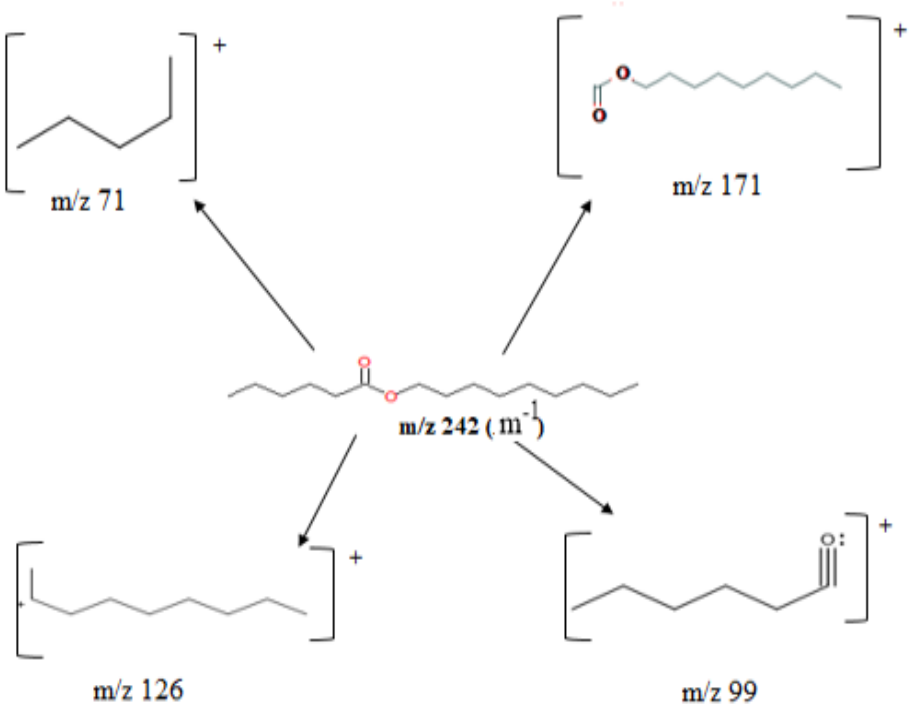

Scheme 4.1: Ion Fragmentation of Nonyl Hexanoate

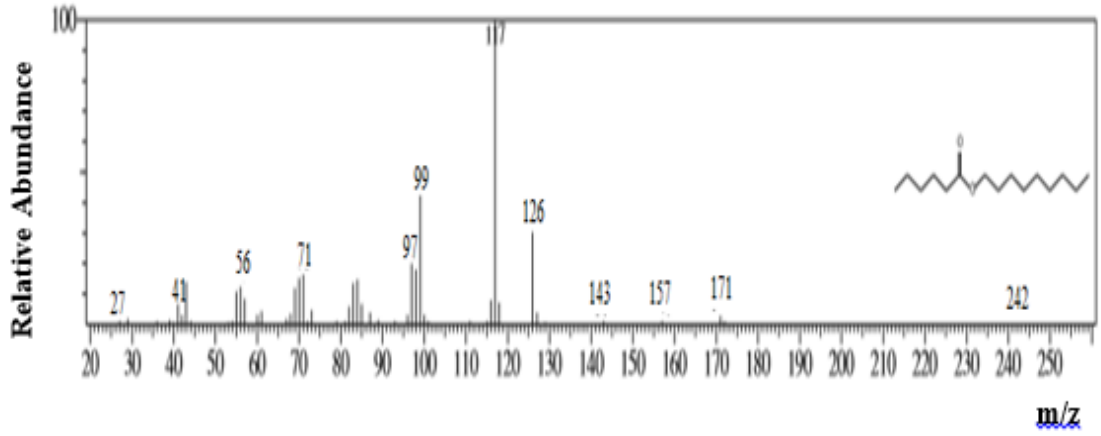

Figure 4.30: Mass Spectrum of Nonyl Hexanoate

4.11 Free and Immobilized Lipases Stability Assay

4.11.1 Thermal Stability

Figure 4.31 shows the influence of temperature on the activities of free and immobilised CRL after 1 hour of incubation. The relative activities were calculated by comparing the percentage yield of activities at various temperatures to the activity of the reaction at 40 °C. Lipase's thermal stability has been demonstrated to correlate with its structure, according to Zhu et al. (2001), and decreased with an increase in temperature and exposure time.

At 50, 60 and 70 °C, the residual activity free CRL was approximately 47.58%, 32.82% and 28.24%, respectively. Whereas, the immobilized lipases retained residual activity 90.04% to 56.97% at the same temperature conditions (50 - 70 °C). The high affinity between the CRL and modified clay supports may explain this improvement in thermostability. This stability was most likely owing to the microcrystalline lipase structure's enhanced stability as compared to free CRL (Scherer et al. 2011; Benamia et al., 2017; Huang et al., 2015).

Figures 4.32 and 4.33 show the percent conversion of nonyl hexanoate and specific activity of free and immobilized lipases as affected by temperature. As an observation, the optimum temperature of free and immobilized lipases was at 40 °C. At the optimum temperature, the ester conversion and specific activity for free CRL were 58.52 % and 3.86×10^{-3} µmol/min/mg, respectively. Whereas, the ester conversion for immobilized lipases 65.53% to 69.31%, while their specific activity 4.9×10^{-3} to 5.43×10^{-3} µmol/min/mg at the optimum temperature. It can be noticeable rapidly loss in activity of free lipase occurred with further increase in temperature, while the immobilized lipase seemed to be more stable to heat. However, after that point, the thermal stability decreased because of the disturbance of globular structure of the

protein by high temperature, which lead to unfolding and loss of enzymatic activity (Rahman et al., 2005).

Similar results were reported by Zhang et al. (2017) and Zhang et al. (2018), who noticed that the optimum temperature for the CRL immobilized onto graphene oxide decorated with ZnO nanoparticles and onto polyvinylpyrrolidone, respectively did not change. After immobilization on chitin and chitosan by adsorption method and cross-linking with glutaraldehyde, Kilinc et al. (2006) reported a change in the optimum temperature of lipase activity from 30 to 45 °C, which is highly desirable because the higher optimum temperature leads to lower risk of microbial contamination. The rise in optimal temperature can be explained by the enzyme's covalent link, which restricts conformational flexibility and so takes more activation energy for the molecule to reorganise itself into the appropriate shape for substrate binding, stabilising the enzyme (Reshmi & Sugunan, 2013; Babaei et al., 2014; de Souza Lima et al., 2019). While the optimal temperature for both free and immobilised lipases was similar, physical adsorption had no effect on the physical or chemical properties of lipase (Dong et al., 2012).

At 70 °C, CRL-2.0 NK shows the highest ester conversion (57.67%) and the highest specific activity (4.12 10^{-3} µmol/min/mg), followed by CRL-2.0 MK, which shows about 51.39 % of ester conversion and about 3.84 × 10^{-3} µmol/min/mg. While the ester conversion for CRL-1.5 NK and CRL-1.0 MK 46.67 % and 43.72 %, respectively, and their specific activity 3.01 × 10^{-3} µmol/min/mg and 2.9 × 10^{-3} µmol/min/mg, respectively. It is possible that the best stability might be attributed to the appropriate balance of hydrophobicity/hydrophilicity on the surface of organo-modified clay (Dong et al., 2013). Small differences in activity can be attributed to differences in enzyme distribution in support samples (Paul et al., 2016), as well as the

increased stiffness with which the enzyme is adsorbed to the organoclay; consequently, the enzyme did not lose its structure over high temperatures (Ramos et al., 2014).

Karagulyan et al. (2007) were found that the thermostability of enzyme slightly decreased after immobilization on kaolin, it. The thermal stability of the CRL enzyme was significantly increased after immobilization on functionalized clay samples, according to our findings. It's probable that the support samples' improved hydrophobic contacts will improve the thermal stability of immobilized CRL (Cabrera-Padilla et al., 2012). Because the protein has buried hydrophobic amino acid residues on the surface, the contact area between the proteins and the support's hydrophobic groups should grow, resulting in an increase in the adsorbent's hydrophobic interaction at higher temperatures (Reshmi and Sugunan, 2013).

Similar result was obtained by de Oliveira et al. (2000), they showed that the C. *rugosa lipase* immobilized on styrenedivinylbenzene have lost 50% of its activity after only 1 h of heat treatment at 60 °C. Under the same conditions, the free enzyme lost 94% of its activity. A study by Tajudin et al. (2018) show the relative activity of the free CRL about 32% of the initial activity at 65 °C. In contrast, immobilised lipase retained up to 50% of activity at the same temperature. Tu and co-authors (2017) found that immobilising lipase on clay/chitosan composite beads significantly improved its thermal stability, with the improving range equal to the amount of clay in the composite beads. Similar observation reported with other enzymes like glucoamylase where the adsorbed it retains all activity even at 80 °C (Gopinath & Sugunan, 2007). This can be explained due to *Aspergillus niger* is a good source of thermostable enzymes, and their enzymes are less mobile and so resist denaturation of protein.

In general, higher temperatures destabilise the bonds in the lipase molecule, disrupting the long-range interactions that are necessary for the three-dimensional

posture of the stabilised lipase molecule. Eventually the breaking of the helical structure occurs, with loss of lipase activity (Ali et al., 2017). However, the activity of immobilized enzyme is known to minimize the effect of external factors like temperature. Thus, to be more resistant against heat than native state due to preserve structure of the enzyme from thermal degradation (Tutar et al., 2009; Miranda et al., 2011) which attributed to its multiple attachment point of functional group of lipase molecule (-COOH) of enzyme on the support (protein-surface interaction) and protect it from unfolding. The location of lipase inside the pores of support could protect it against alterations (Kharrat et al., 2011).

In addition, physical adsorption between enzyme and support was proportional increasing the stability of enzyme, which locks the enzyme into the active conformation. This prevents irreversible unfolding of the protein by limiting movements caused by electrostatic contact and hydrogen bonds between the support and enzyme, or by a low limitation in the diffusion of the substrate at high temperatures (Lenders et al., 1985; Kharrat et al., 2011; Samui et al., 2016).

As previously stated, immobilized lipase's temperature endurance is a significant benefit for practical applications. Inorganic supports, on the whole, provide higher thermal stability, therefore there is a lot of room for research in this field (Gopinath & Sugunan, 2007). As a result, immobilized lipase samples have a higher potential for biotechnological applications than free lipase.

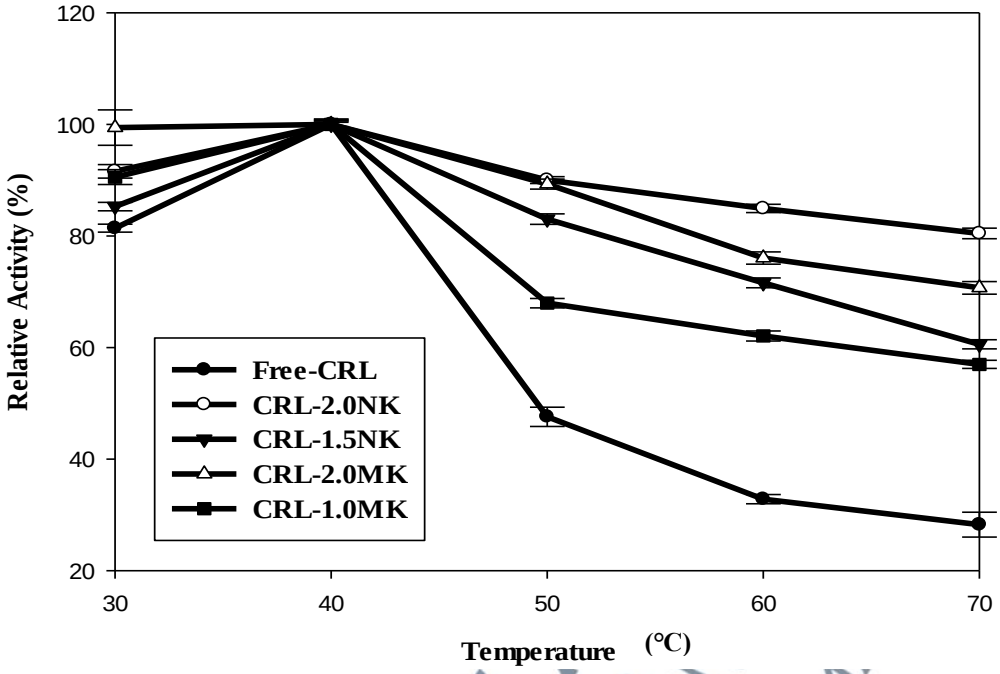

Figure 4.31: Relative Activity of Free (Free-CRL) and Selected Immobilized Lipases (CRL-1.5 NK, CRL-2.0 NK, CRL-1.0 MK, CRL-2.0 MK) as Affected by Temperature in the Synthesis of Nonyl Hexanoate. Reactions were Performed in Hexan at 30 °C for 5 Hours with 1:1 Molar Ratio of Nonanol and Hexanoic Acid in Hexane. Bars Represents Standard Deviations

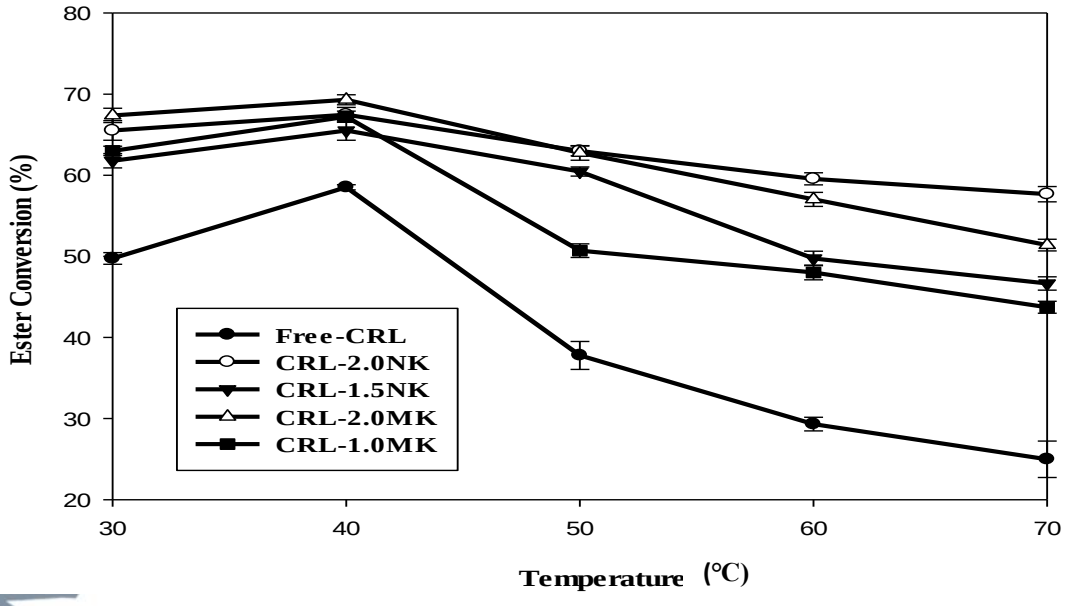

Figure 4.32: Percent Conversion of Nonyl Hexanoate by Free (Free-CRL) and Selected Immobilized Lipases (CRL-1.5 NK, CRL-2.0 NK, CRL-1.0 MK, CRL-2.0 MK) as Affected by Temperature. Reactions were Performed in Hexan at 30 °C for 5 Hours with 1:1 Molar Ratio of Nonanol and Hexanoic Acid in Hexane. Bars Represents Standard Deviations

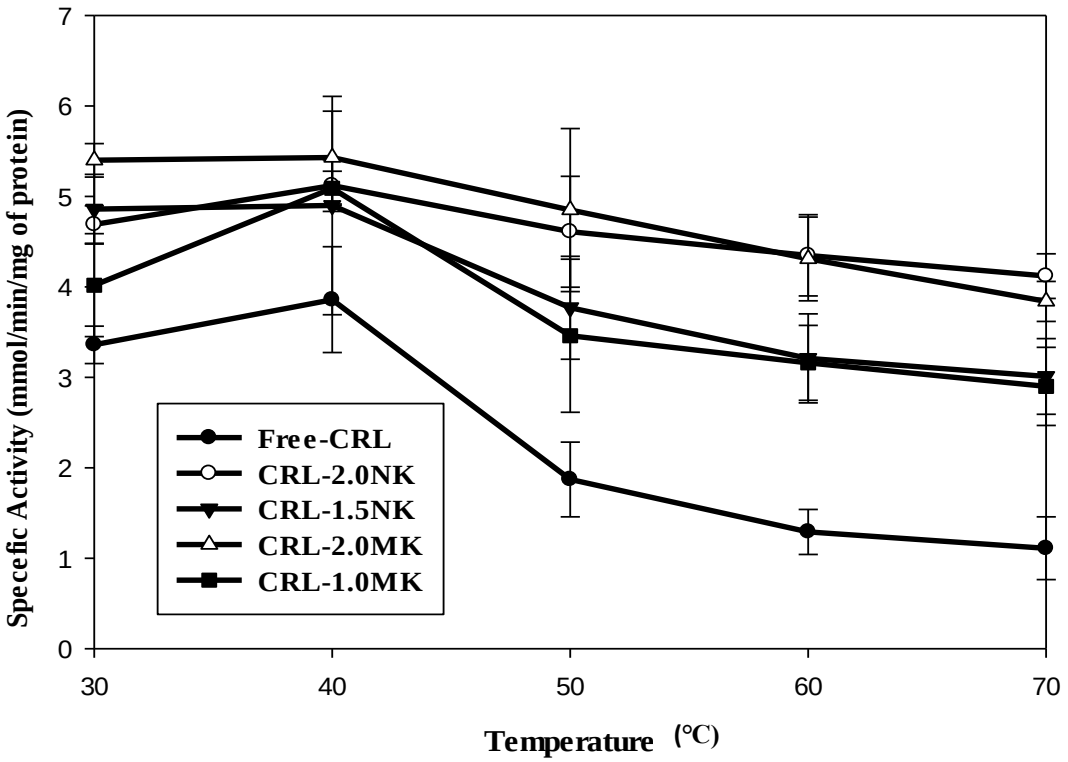

Figure 4.33: Specific Activity of Free (Free-CRL) and Selected Immobilized Lipases (CRL-1.5 NK, CRL-2.0 NK, CRL-1.0 MK, CRL-2.0 MK) as Affected by Temperature in the Synthesis of Nonyl Hexanoate. Reactions were Performed in Hexan at 30 °C for 5 Hours with 1:1 Molar Ratio of Nonanol and Hexanoic Acid in Hexane. Bars Represents Standard Deviations

4.11.2 Operational Stability

Operational stability or reusability of the selected immobilized lipases were used in ten subsequent cycles in the esterification reaction of hexanoic acid and nonanol and the results of relative activity are shown in Figure 4.34. The capacity to use the same enzyme repeatedly in the desired reaction significantly increases operational stability, which is a key aspect in determining the economic feasibility of using enzymes on an industrial scale. Because it's difficult to extract free lipase from the reaction media for reuse, thus it was excluded from this study. In contrast, attachment of the protein to the solid matrix preserve the enzyme from changes in its structure, making the whole particles more stable (Zdarta et al., 2017; Zhang et al., 2018).

The biocatalyst particles were separated by filtering after each cycle, and the flask content was determined by titrating. The immobilized lipase particles were isolated and utilised in a new chemical cycle. For each reaction, the final conversions and relative activities were measured, with relative activities defined as the percentage of ester converted by each successive cycle compared to the ester converted by fresh enzymes in the first cycle. When an immobilized enzyme is utilised repeatedly, the reaction behaviour visibly changes.

Particularly, Immobilized CRL demonstrated good capacity in the first treatment cycle. Due to the growing number of uses, the percentage of relative yield of the immobilised lipase samples rapidly reduced. The lipase immobilized on support samples was clearly preserved its high activity after five cycles (83.15% - 71.91%). This result of reusability represented better results when compared to previous work obtained by Jafarian et al. (2018) who achieved 58.03% as the highest residual activity of CRL immobilized on graphene oxide nanosheet after 5th. Huang et al. (2011) also reported that after the 8th cycle, the remaining activity of *Candida rugosa* lipase immobilized on a cellulose nanofiber membrane being about 30%.

After 10 times of reusing, reduction of activity was between 36.11%- 65.15%. The result of this study was also better than the result obtained by Edama et al. (2014) who obtained 32% of remaining activity of immobilized enzyme on clay. The organoclay was more efficient in this aspect because the hydrophobically interfacial activation and stabilisation, as well as hydrogen bond interactions, caused the immobilized lipases on organo-modified kaolin to be more reusable. The hydrophobic surface of modified clay samples prevented lipase protein leakage in an aqueous solution, resulting in better reusability (Dong et al., 2013). Reusing the immobilized

enzyme necessitates a tight bond between the lipase and the matrix in order to ensure that activity is retained after numerous processes (Babaei et al., 2014).

Figures 4.35 and 4.36 show the percent conversion of nonyl hexanoate and specific activity of free and immobilized lipases as affected by operational stability. As an observation, The CRL-2.0 MK maintained the highest specific activity (1.96×10^{-3}µmol/min/mg of protein) and the highest ester conversion (44.32 %) after 10 repeated use, followed by CRL-1.0 MK, which shows about 33.74 % of ester conversion and about 1.56×10^{-3} µmol/min/mg. While the ester conversion for CRL-2.0 NK and CRL-1.5 NK 26.44 % and 23.23 %, respectively, and their specific activity 1.12×10^{-3} µmol/min/mg and 1.03×10^{-3} µmol/min/mg, respectively

The excellent reuse stability of CRL-2.0 MK can be explained by the following aspects: (i) the agglomeration of CRL was greatly suppressed; (ii) the reusability could be related to the loading capacity, so that a suitable amount of protein can be spread on the surface area, avoiding conformational changes, (ii) Because this support has the highest pore size, it was able to withstand the filter layer better than the support with the smallest pore size. That is why the carrier with the biggest pore size had the maximum reusability (Handayani et al., 2011; Zhang et al., 2017; Jafarian et al., 2018).

The loss of the activity was probably attributed to leakage part of immobilized CRL upon filtration and washing for the instability of physical adsorption. Reuse can cause the binding strength between the support and the immobilised enzyme to diminish, resulting in the enzyme being physically removed from the support. However, bonding forces in physical adsorption are weak and do not protect the enzyme from conformational changes (unfolding), that may be caused by the interaction with the solvent during the esterification reaction (Rodrigues et al., 2008),

Furthermore, the loss of activity can be caused by the active site being distorted as a result of repeated contact with the substrate, resulting in a partial or complete loss of catalytic efficiency and it is possible that the confirmation of lipase was affected by organic solvent (Guldhe et al., 2015). Reactants and products appear to bind to the solid enzyme phase in organic media, resulting in significant alterations in the enzyme esterification activity for the next cycle. Hexane was employed as a solvent in this study since previous investigations had shown that it could be used to dehydrate immobilized lipase preparations for many batch runs (Pereira et al., 2003), Furthermore, formation of the reaction products layer across the enzyme active site, which thus became inaccessible for the substrate (Šekuljica et al., 2016), (iv) the natural inactivation of an enzyme as a result of the enzyme protein's denaturation over time (Gopinath & Sugunan, 2007).

The idea of reusing the enzyme, on the other hand, necessitates a high level of stability in the final enzyme preparation. Based on these findings, physical adsorption of CRL onto organo-modified supports has been shown to be a useful approach for increasing enzyme activity through direct contact with the lipase and protecting it from solvent inactivation.

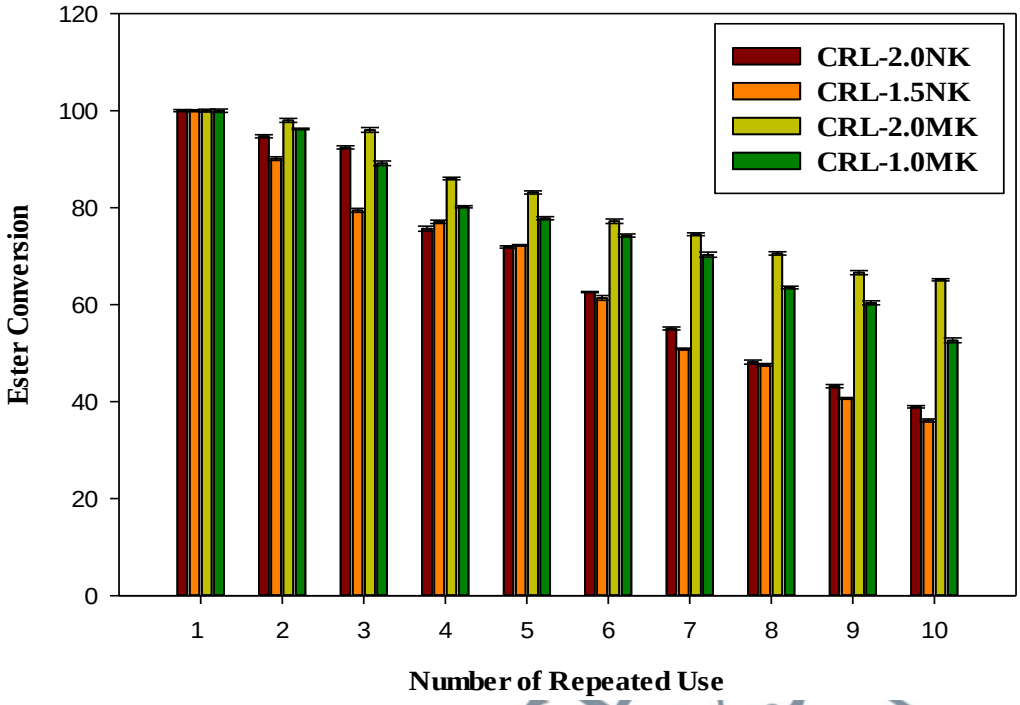

Figure 4.34: Percent of Relative Activity as Affected by Operational Stability of Selected Immobilized Lipase (CRL-1.5 NK, CRL-2.0 NK, CRL-1.0 MK, CRL-2.0MK) in the Synthesis of Nonyl Hexanoate

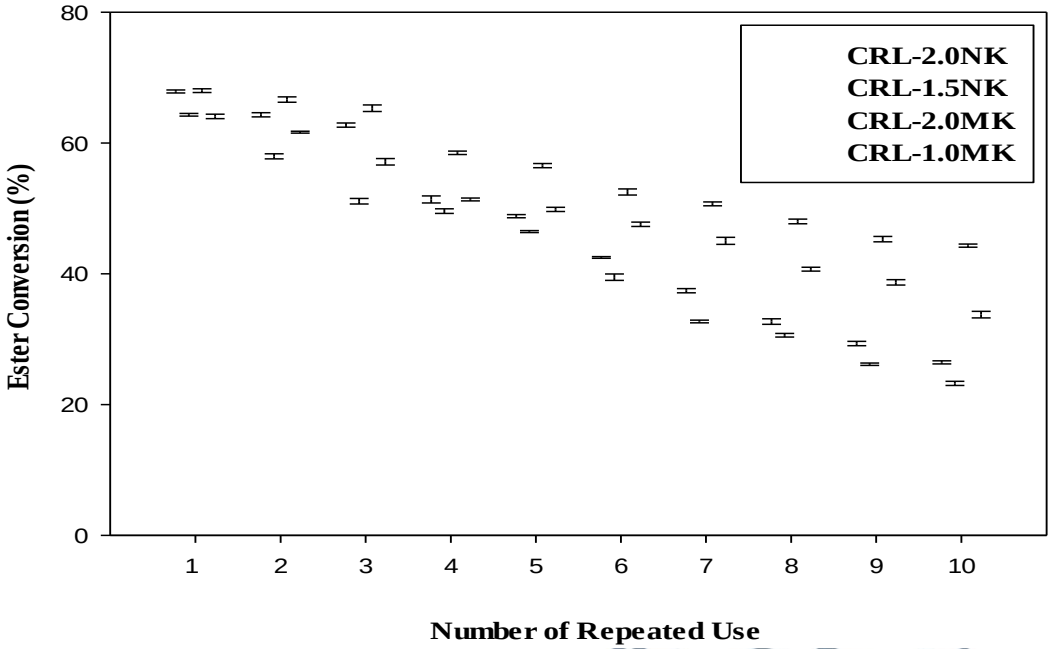

Figure 4.35: Percent Conversion of Nonyl Hexanoate as Affected by Operational Stability of Selected Immobilized Lipase (CRL-1.5 NK, CRL-2.0 NK, CRL-1.0 MK, CRL-2.0MK) in the Synthesis of Nonyl Hexanoate

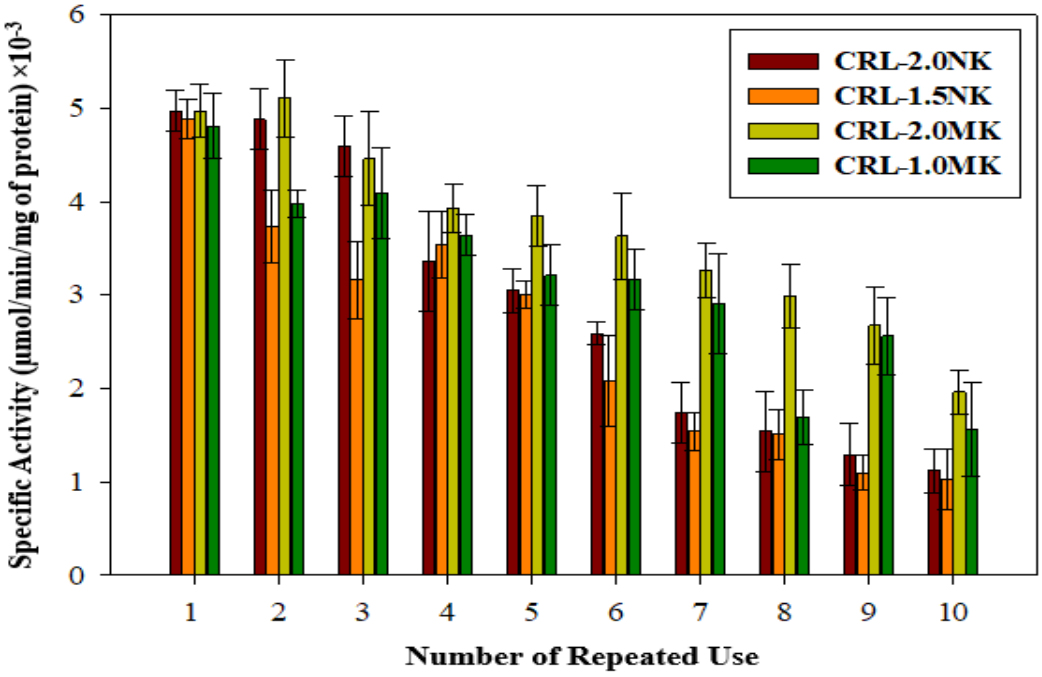

Figure 4.36: Specific Activity of Selected Immobilized Lipase (CRL-1.5 NK, CRL-2.0 NK, CRL-1.0 MK, CRL-2.0MK) as Affected by Operational Stability in the Synthesis of Nonyl Hexanoate

4.12 Kinetic Study in the Synthesis of Nonyl Hexanoate Using Selected Immobilized *Candida rugosa* Lipase

The study of kinetics is essential for enzyme catalysed reactions in order to determine the factors that affecting the reaction rate, and to check if, the Michaelis constant or maximal activity was affected through immobilization process. The substrate concentration was found to have a significant influence on the esterification rates. Hence, kinetic models of free *Candida rugosa* lipase and selected immobilized lipases (CRL-2.0 NK and CRL-2.0 MK) were constructed on the basis of the initial rate determination by maintaining one substrate (hexanoic acid) at constant concentration while varying the concentration of the other reactant (nonanol), or vice versa.

4.12.1 Kinetic Modelling of Michaelis-Menten Plots

As shown in Figures 4.37 and 4.38, the effects of substrate concentrations on initial rate were depicted by representative curves at different concentrations of each substrate. When fixed the nonanol concentration, the initial reaction rates increase rapidly with increasing acid concentration and there was no evidence of inhibition by the hexanoic acid in the range of values studied (Figure 4.37). This type of behaviour can be seen for CRL-2.0 NK and CRL-2.0 MK. In contrast of Free-CRL, at high hexanoic acid concentrations (> 2000mmol/L), an inhibitory effect was noticed for Free-CRL.

It can be explained that for the acid inhibition at higher concentrations, the lower reported conversions could be a consequence of an accumulation of water in the catalytic triad pocket of the lipase as the reaction progresses, causing ester hydrolysis.

On the other hand, the excess of acid may cause acidification of the micro-aqueous layer interface Fermentation leading to enzyme inactivation and/or high local concentration of OA near the active site with further hindrance for the diffusion of the alcohol to the acyl enzyme (Krishna et al., 2001, Cavallaro et al., 2019). By other words, hexanoic acid, being a medain-chain polar acid, concentrates in the microaqueous layer and causes a pH drop in the enzyme microenvironment leading to enzyme inactivation. In the case of immobilization, the immobilized enzyme was not in direct contact with the acid as well as the microenvironment associated to the location of the hydrophobic support at the aqueous-organic interface, thus, it has the ability to retain activity in such high hexanoic acid concentration (Oliveira et al., 2001, Amin, 2013). In addition, broad range pH is the one of benefits the enzyme immobilization, thus it may overcome the negative pH effect (Fopase et al., 2020).

The acid inhibition behavior observed in our studies is different from several studies on enzymatic kinetics which indicate inhibition by alcohol but not acid (Raita et al., 2015, Abd Manan et al., 2018). Bezbradica et al., (2013) were reported that inhibition with an excess of ascorbic acid occurs, while inhibition with oleic acid does not. Furthermore, Devi et al., 2017 reported competitive enzyme inhibition by butyric acid during CR lipase catalyzed transesterification reaction, indicating some effect of the length structure of the acid molecule.

On the other hand, when the concentration of hexanoic acid is fixed, the initial reaction rates for immobilized lipases increase rapidly with increasing substrate concentrations until it reached a maximum level at a 3:1 (for CRL-2.0 MK) and 2:1 (for CRL-2.0 NK) molar ratio of nonanol to hexanoic acid. A further increase in the concentration of nonanol led to decrease the rate of enzymatic reaction (Figure 4.38).

For free-CRL, increasing concentrations of nonanol led to decrease of initial rates from 2000 to 5000 mmol/L nonyl hexanoate esterification. Du et al., (2004) stated that the high concentration of an alcoholic compound is a substrate inhibitor for lipase-catalyzed esterification. The higher tolerance of immobilized CRL can be ascribed to the multipoint attachment of CRL onto the organo support that increased robustness and reduced inhibition by substrates (Elisa et al., 2019).

Similar observation was made by Raghavendra et al., (2014) during the kinetic study of synthesis of Pentyl Valerate by CRL immobilized in microemulsion based organogels (MBGs), wherein higher concentrations of alcohol resulted in inhibition while higher concentrations of the acid did not. However, there are other studies have proved that inhibition can be due to both of the substrates (Cavallaro et al., 2019).

The result can be attributed to the inhibition effect of nonanol on the lipases, which lead to increase propensity of irreversible binding the nonanol molecules to form the inactive dead-end complex. In effect, the nonanol being a polar substrate may have been accumulated in the aqueous microenvironment around the enzyme, reaching the level of concentration sufficient to make a denaturation of the protein and/or to a modification of the protonation state by the acidic or basic species in the microenvironment (Pires-Cabral et al., 2009). Moreover, complex interaction between the hydrophobic pockets of the lipase and alcohol, which leads to larger conformational mobility and finally formation of dead-end inhibition complex. All of which obstruct the proper interactions at the active sites of the lipase and reduce reaction rates (Abd Manan et al., 2018).

From the results described above, it can be concluded that all the reaction followed a Michaellis-Menten kinetic with or without substrate inhibition. However, it

was further confirmed by the Lineweaver-Burk plots to prove the inhibitory effects of the substrates on the lipase, and for better comprehension of the reaction kinetics. Somashekar et al., (2007) reported the similar substrate inhibition profile.

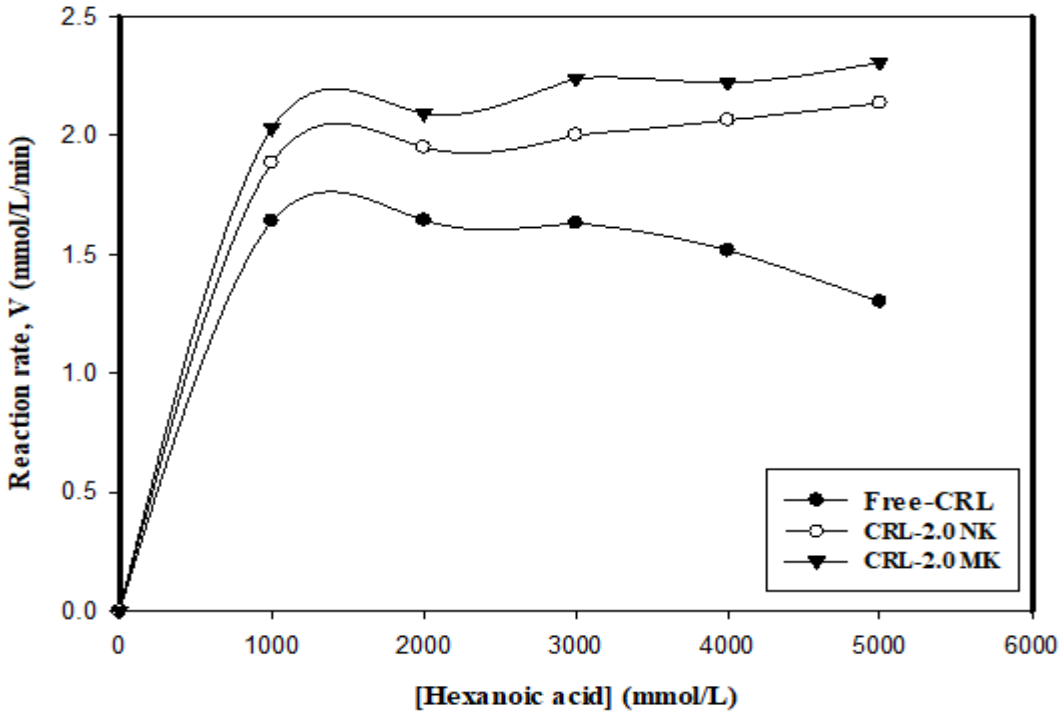

Figure 4.37: Michealis-Menten Plots on the Reaction Rates of Nonyl Hexanoate Synthesis at Various Hexanoic Acid Concentrations for Free-CRL, CRL-2.0 NK, and CRL-2.0 MK.

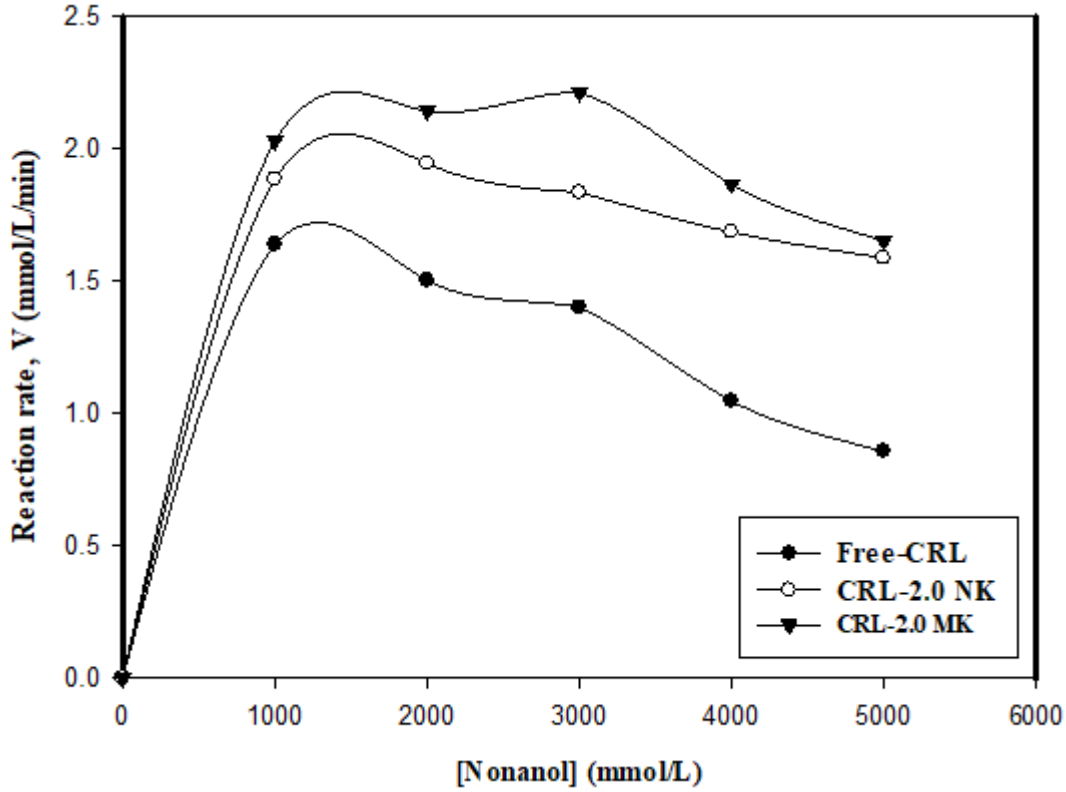

Figure 4.38: Michealis-Menten Plots on the Reaction Rates of Nonyl Hexanoate Synthesis at Various nonanol Concentrations for Free-CRL, CRL-2.0 NK, and CRL-2.0 MK.

4.12.2 Determination of Kinetic Constants

The experimental results show that the highest initial reaction rates are reached when using equimolar amounts (1:1 molar ratio) in the certain esterification condition. Furthermore, an excess of either substrate lead to loss of the lipase activity (except no inhibition of hexanoic acid for CRL-2.0 NK and CRL-2.0 MK). This mechanism is characterized by the parallel lines in the Lineweaver–Burk double reciprocal representation at concentrations in which there is no inhibition.

The kinetic constants of nonyl hexanoate esterification were determined for both free and immobilized lipases (Table 4. 15) to check if the maximal activity and Michaelis constant were affected by immobilization.

Table 4.15: Kinetic Constants Obtained for the Enzymatic Esterification of Nonyl Hexanoate

Kinetic Constants	Selected Lipases		
	Free-CRL	CRL-2.0 NK	CRL-2.0 MK
[a,b]V_{max}(mmol/L/min)	1.5810	2.1786	2.3504
[a] $K_{m\ (Hex)}$ (mmol/L)	100.0182	209.283	183.268
[b] $K_{m(Non)}$ (mmol/L)	3493.1	399.315	1349.554
[a] $K_{i(Hex)}$ (mmol/L)	5572.9	-	-
[b] $K_{i(Non)}$ (mmol/L)	495.7	6401.8	2505.1

[a] Condition where concentration of nonanol was kept constant, while concentration of hexanoic acid was varied

[b] Condition where concentration of hexanoic acid was kept constant, while concentration of nonanol was varied

It can be seen that the kinetic parameters for the immobilized enzyme may be different from those of the free enzyme because of diffusion restrictions and interactions active sites of enzymes with the support or deactivation due to immobilization (George & Sugunan, 2014). Hence, by creating a Lineweaver-Burk plots, the K_m and V_{max} were estimated from nonlinear regression method (Ek-Sigma Plot module) through the values for 1/intial rate versus 1/[substrate] (Figure 4.39 and Figure 4.40). V and V_{max} are the rate and maximum rate of the reaction, respectively, K_m is the Michaelis constant, K_i is the inhibition coefficient and S is the substrate concentration.

Using the immobilization technique, the kinetic constants are noted as 'apparent', since the interaction between the support and both substrates, which can result in different substrate concentrations near the enzyme, was not accounted (Oliveira et al., 2001). In this study, CRL-2.0 MK displayed the highest V_{max} value in varying substrate concentration reaction. Where, high value of Vmax indicates that there is greater tendency for enzyme substrate complex to split and form product. In general, both immobilized lipases displayed higher V_{max} value that the free enzyme indicating an improved activity upon immobilization. On the other hand, high values of K_m indicate that there is lesser affinity of enzyme towards substrate. Comparison of the K_m value

for a given free and immobilized enzyme could provide information about interaction between enzyme and its support (Quiroga et al., 2011).

In this study, the lower $K_{m(Hex)}$ values comparing with $K_{m(Non)}$ suggested that the free and immobilized lipases showed higher affinity towards hexanoic acid (Hex) than towards Nonanol (Non) with $K_{m(Hex)} < K_{m(Non)}$, whereby $K_{m(Hex)}$ and $K_{m(Non)}$ are the Michaelis constants for hexanoic acid and nonanol, respectively. As the apparent Michaelis-Menten constant normally falls between 10^{-1}–10^{-7} M (Kuperkar et al., 2014), hence the values seen in this study were well within the satisfactory range.Other kinetic studies regarding immobilized lipases have also shown a higher K_m for alcohols than towards acids. For example, in a study using CRL immobilized on nanoporous mica, the Km values for butyric acid and sulcatol were 14.5 mmol/L/mg and 9308 mmol/L/mg, respectively (Zaidan et al., 2011). However, the affinity for both substrates changed after immobilization as a result to conformational changes to the active site of the enzyme (Ghiaci et al., 2009). In addition, high value of K_i indicates that there is increased binding to non-catalytic sites leading to inhibition. From the relatively large value of $K_{i(Hex)}$ of free CRL, it is apparent that acid inhibition is much less significant than $K_{i(Non)}$. The inhibition constant is smaller than previously reported in similar kinetic models (Chen et al., 2017). Ki for octanoic acid in their result was 0.078 mol/L, indicating that hexanoic acid has stronger lipase inhibitor effect.

Furthermore, $K_{i(Non)}$ for immobilized lipases is much less significant comparing with free lipase. Where $K_{i(Non)}$ for CRL-2.0 NK and CRL-2.0 MK (6401.8 and 2505.1 mmol/L) are 12.9 and 5.1 fold higher than free CRL (495.7 mmol/L) implying that the inhibitory effect of the substrates was more severe on aggregated CRL. The data strongly indicated that immobilization of CRL on the organo-modified kaolin and

metakaolin imparted favorable changes on the lipase and became less susceptible to substrate-related inhibition during reaction.

The calculated efficiency factor (η), determined as the ratio of the maximum reaction rate of immobilized CRL ($V_{immobilized}$) over that of free-CRL (V_{free}) (Equation 4.1), which was 1.4 (for CRL-2.0 NK) and 1.5 (for CRL-2.0 MK). The value of efficiency factor in this study is smaller than obtained by Zaidan et al., (2011), which was 1.6.

$$\textbf{\textit{Efficiency factor}}\ (\eta) = \frac{\boldsymbol{V_{immobilized}}}{\boldsymbol{V_{free}}} \qquad (4.1)$$

The high value of Efficiency immobilized lipase (η) suggest that diffusional limitations are minimized and the native conformation of lipase is maintained after immobilization (George & Sugunan, 2014).

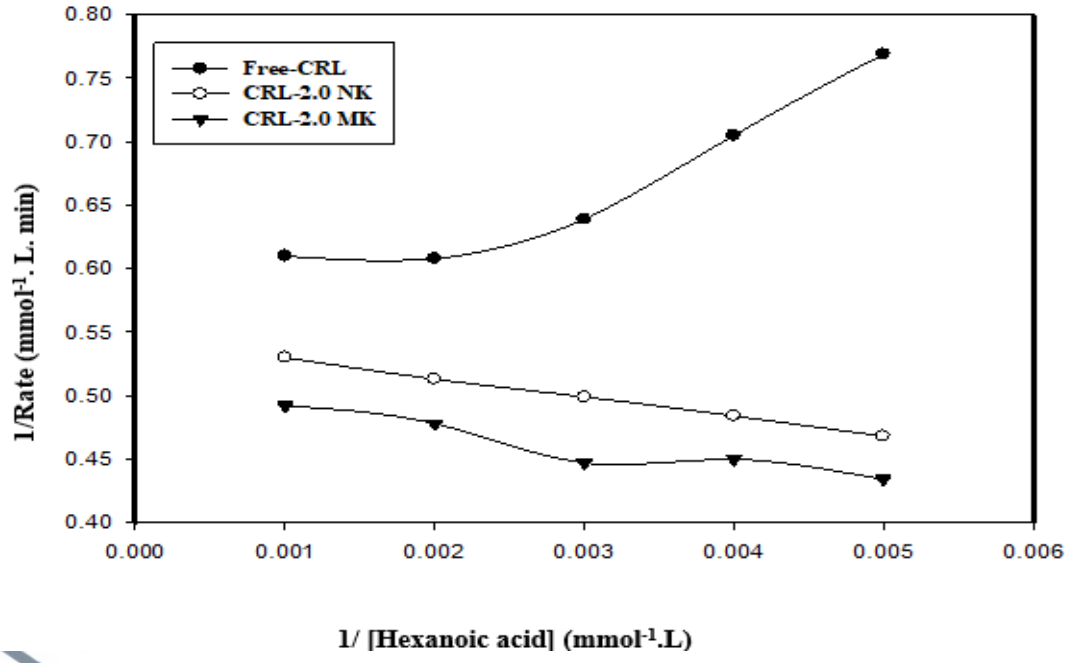

Figure 4.39: Double-Reciprocal Plots of Initial Rate of Nonyl Hexanoate Synthesis at Varied Hexanoic Acid Concentration and Fixed Nonanol Concentration For Free-CRL, CRL-2.0 NK and CRL-2.0 MK. Reactions were Performed at 30 °C with 1:1-1:5 Molar Ratios of Nonanol and Hexanoic acid in Hexane.

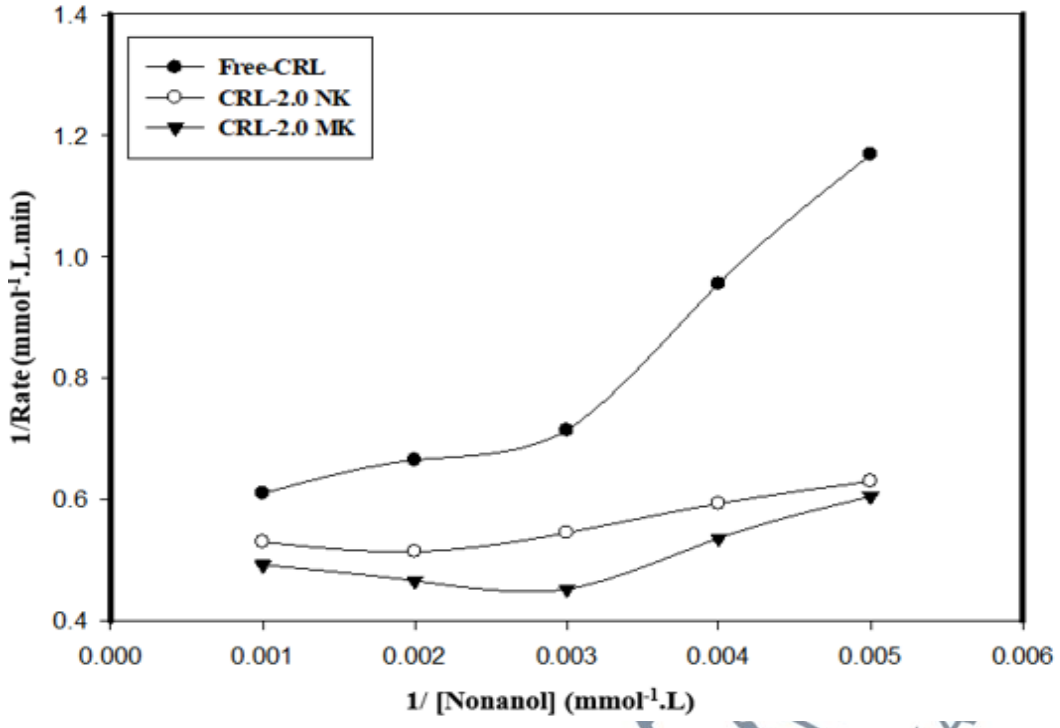

Figure 4.40: Double-Reciprocal Plots of Nonyl Hexanoate Synthesis at Varied Nonanol Concentration and Fixed Hexanoic Acid Concentration For Free-CRL, CRL-2.0 NK and CRL-2.0 MK. Reactions were Performed at 30 °C with 1:1-1:5 Molar Ratios of Hexanoic acid and Nonanol in Hexane.

As in this work, previous studies have shown that the lipase-catalyzed esterification and transesterification in organic media can be described by the Ping–Pong mechanism (Orrego et al., 2009, Razak & Annuar, 2015, Abd Manan et al., 2018, Elias et al., 2019). This mechanism is characterized by the parallel lines in the Lineweaver–Burk double reciprocal representation at concentrations in which there is no inhibition, as it happened in the present study. Further, the lines do not intersect at a common point (Yadav & Devi, 2004). In addition, the kinetic constants in Table 4. 15 show that K_i value is very smaller than $K_{m(Non)}$ ($K_{m(Non)} > K_i$) using Ping–Pong mechanism. According to Segal, this reaction follows the Ping–Pong mechanism (Segel,1975, Rahman et al., 2011).

The Ping-Pong Bi-Bi model with one substrate inhibition and Ping-Pong Bi-Bi mechanism with two substrates inhibition are illustrated by the Cleland conventional diagram as shown in Scheme 4.2 and Scheme 4.3. In this type of the reaction mechanism, the enzyme binds first with the hexanoic acid (Hex) forming lipase-acid complex, which then transformed to acyl-enzyme intermediate with the release of water. The second step, nonanol (Non) binds to acyl-enzyme and forms another complex, which is isomerized by a unimolecular reaction to lipase-ester complex, which finally yields nonyl hexanoate and the lipase. Both nonanol and hexanoic acid for free enzyme, and nonanol for CRL-2.0 NK and CRL-2.0 MK assumed to react with the lipase and acyl-enzyme complex, respectively, to form dead-end complexes with no formation of the product (Zaidan et al., 2011)

.

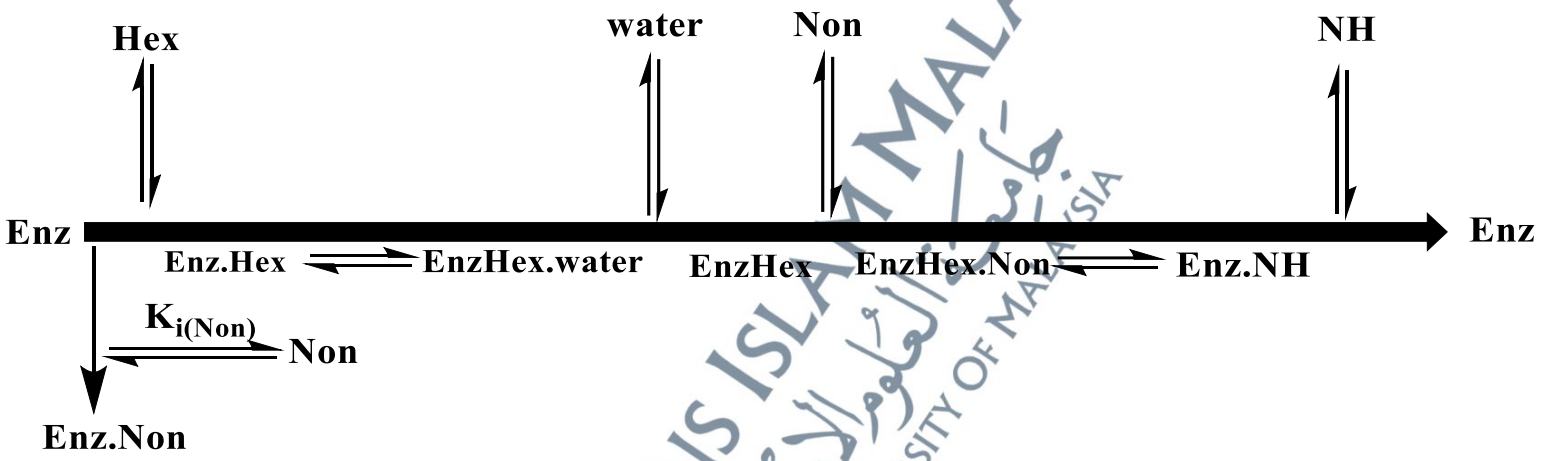

Scheme 4.2: Graphical Repreentation of the Ping-Pong Bi-Bi Model with One Substrate (Nonanol) Competitive Inhibition Catalyzed by CRL-2.0 MK and CRL-2.0 NK which Indicated High Affinity to Hexanoic Acid

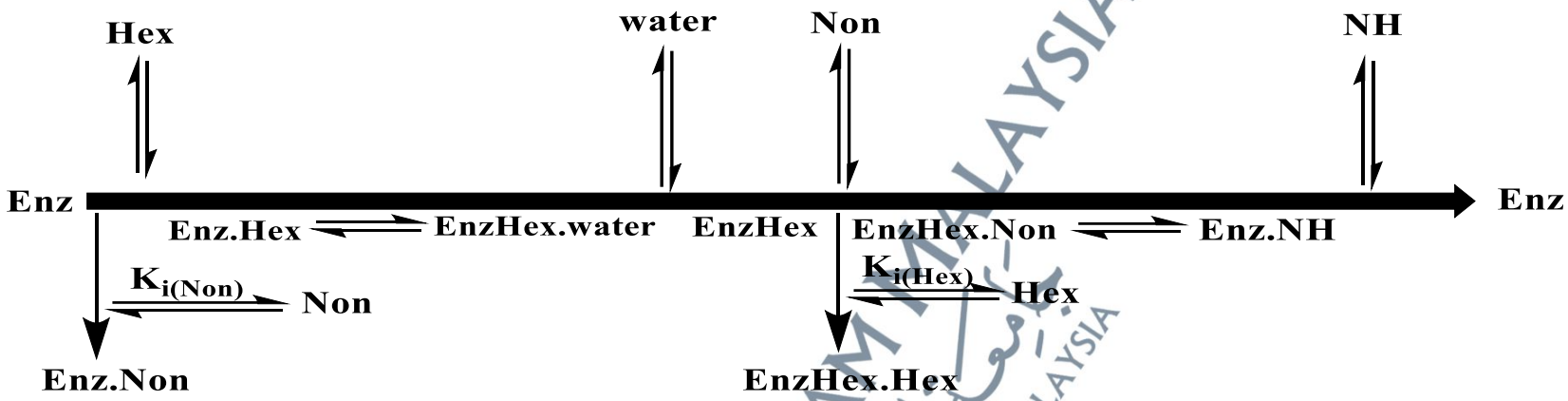

Scheme 4.3: Graphical Representation of the Ping-Pong Bi-Bi Model with Two Substrates (Hexanoic Acid and Nonanol) Competitive Inhibition Catalyzed by Free-CRL

Whereby, Enz = enzyme

NH = nonyl hexanoate

Non = nonanol

Hex = hexanoic acid

$K_{i(Non)}$, $K_{i(Hex)}$ = inhibition constant oftt nonanol, hexanoic acid

The correlation between substrate concentration and reaction rate can be determined by Michaelis-Menten equation. In this study, similar characteristics for the effect both substrates were observed for CRL-2.0 NK and CRL-2.0 MK, whereby nonanol acted as an inhibitory substrate, with hexanoic acid serving to advance the reaction and the reaction models can be simplified as in the Equation 4.2. Otherwise, the inhibition of both substrates (Free-CRL), the equation gets more complex (Equation 4.3). Thus, the rate equations that describe these models are schematically presented as below:

$$\boldsymbol{V = \frac{V_{max}[Non][Hex]}{K_{m(Hex)}[Non](1 + [Non]/K_{i(Non)}) + K_m[Hex] + [Non][Hex]}}$$

(4.2)

$$\boldsymbol{V = \frac{V_{max}[Non][Hex]}{K_{m(Non)}[Hex](1 + [Hex]/K_{i(Hex)}) + K_{m(Hex)}[Non](1 + [Non]/K_{i(Non)}) + [Non][Hex]}}$$

(4.3)

Whereby,

V = initial reaction rate

[Non] = concentration of nonanol

[Hex] = concentration of hexanoic acid

V_{max} = maximum velocity

$K_{m(Non)}$, $K_{m(Hex)}$ = Michaelis constant of nonanol, hexanoic acid

$K_{i(Non)}$, $K_{i(Hex)}$ = inhibition constant of nonanol, hexanoic acid

The validation of the Ping-Pong Bi-Bi model with inhibition by substrate for this reaction was also evaluated by constructing parity plot for the theoretical versus the experimental esterification rate Figures 4.41 (a), (b), and (c). R_2 values between simulated and experimental rates were 0.9935, 0.8517 and 0.8416 for Free-CRL, CRL-2.0 NK and CRL-2.0 MK, respectively. Thus, it indicates that the model developed was in agreement with the experimental data. Although the computer-simulated $V_{simulnted}$ values showed R_2 values of 0.8517 for CRL-2.0 NK and 0.8416 for CRL-2.0 MK, the discrepancy between $V_{exprimental}$ and $V_{simulnted}$ appeared to be significant at several substrate concentrations. This could be due to (i) the constraints employed in the iteration (curve fitting), which limits the flexibility required to examine a real system in solution, (ii) the error in the experimental such as differences in the volume of catalyse added due to accidental overflow of the enzyme while put into the reaction vessel.

The comparison between plots for the experimental and simulated rates versus the concentration of hexanoic acid for lipases can be seen in [Figures 4.42 (a), (b), and (c)] and the coefficient of determination (R^2) were listed in Table 4.16. These findings show that the predicted model fitted the estimated data, which is more fitted for free-CRL than immobilized lipases due to the effects that arise from the immobilization.

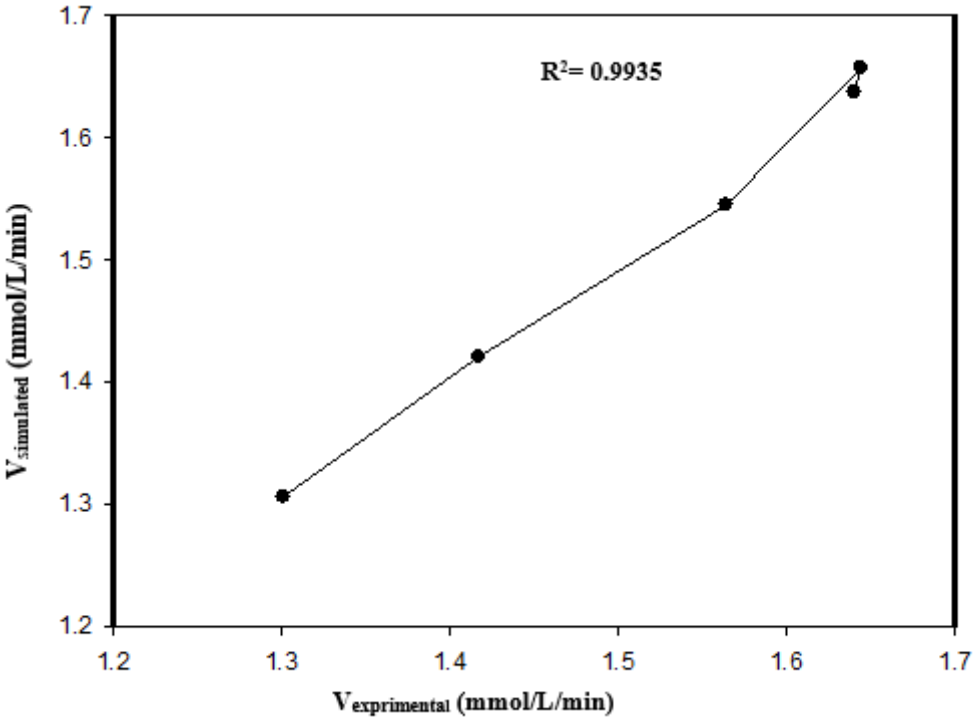
R²= 0.9935
V simulated (mmol/L/min)
V exprimental (mmol/L/min)
1.7
1.6
1.5
1.4
1.3
1.2
1.2
1.3
1.4
1.5
1.6
1.7

(a)

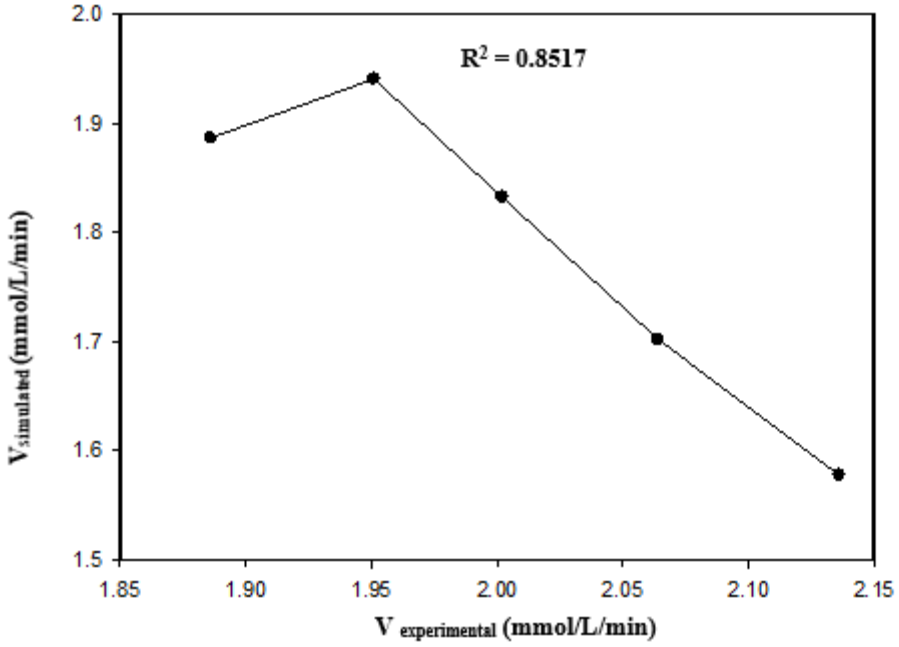
R² = 0.8517
V simulated (mmol/L/min)
V experimental (mmol/L/min)
2.0
1.9
1.8
1.7
1.6
1.5
1.85
1.90
1.95
2.00
2.05
2.10
2.15

(b)

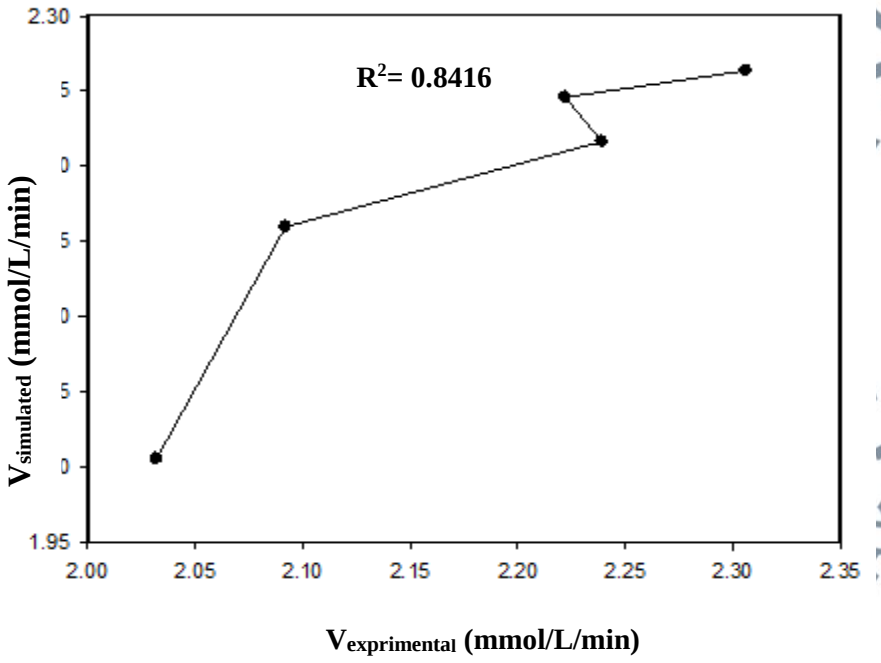

(c)

Figure 4.41: Parity Plots of the Experimental and Simulated Rates for the Ping-Pong Bi-Bi Mechanism for (a) Free-CRL, (b) CRL-2.0 NK and (c) CRL-2.0 MK

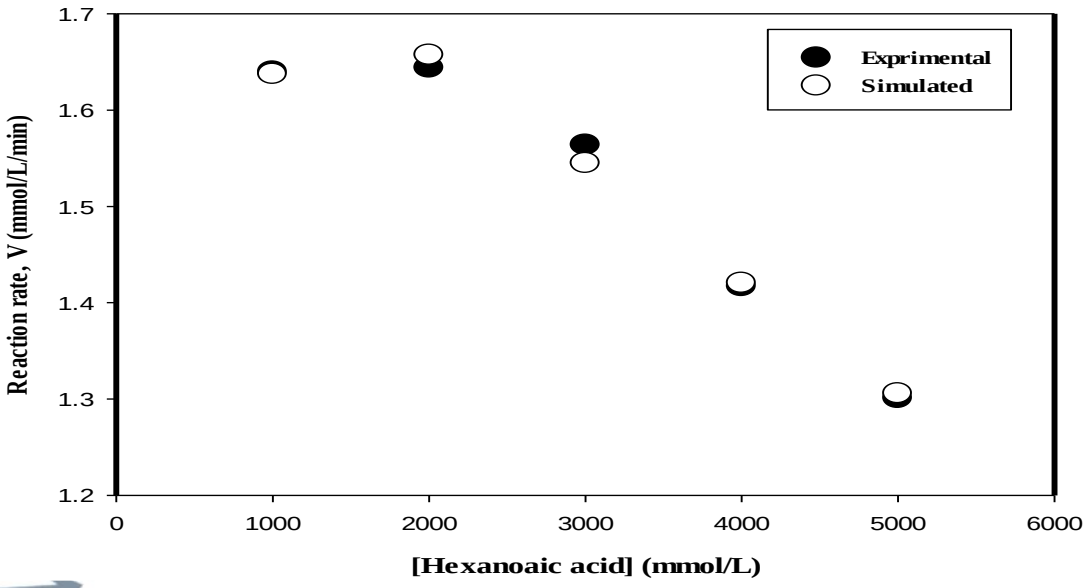

(a)

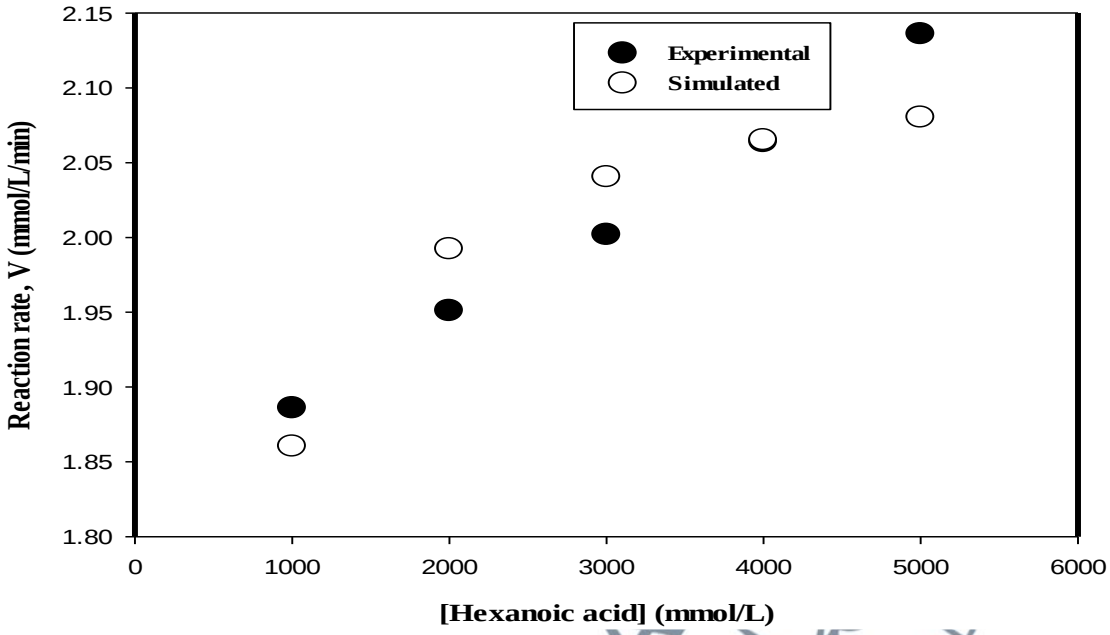
Experimental
Simulated
Reaction rate, V (mmol/L/min)
[Hexanoic acid] (mmol/L)
2.15
2.10
2.05
2.00
1.95
1.90
1.85
1.80
0
1000
2000
3000
4000
5000
6000

(b)

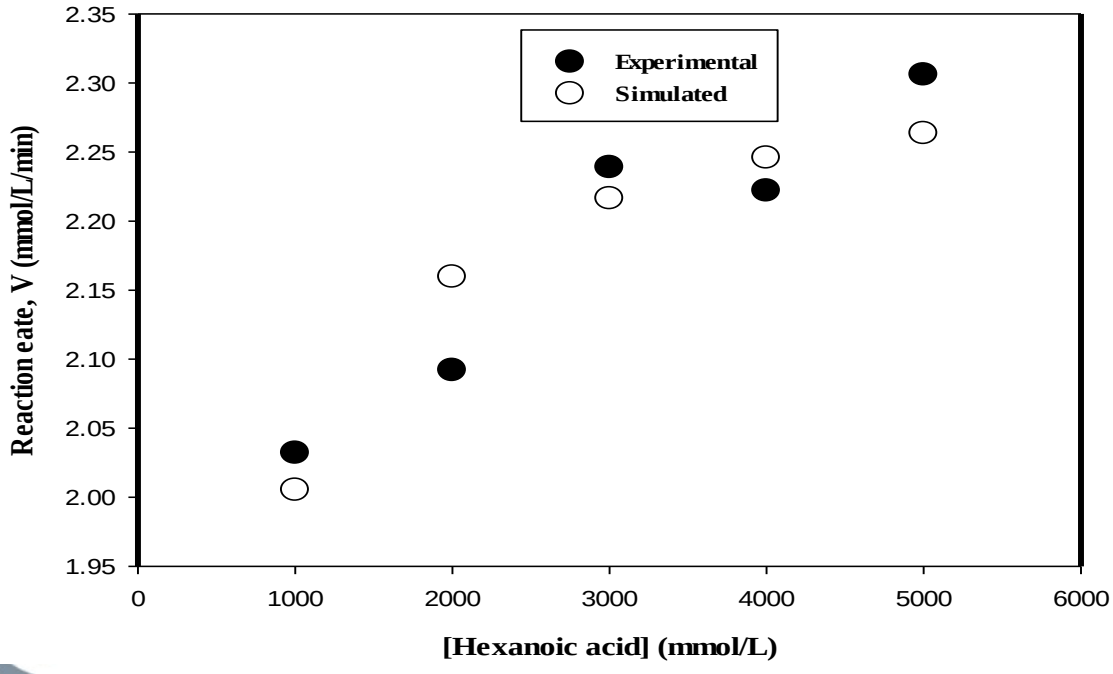
Experimental
Simulated
Reaction eate, V (mmol/L/min)
[Hexanoic acid] (mmol/L)
2.35
2.30
2.25
2.20
2.15
2.10
2.05
2.00
1.95
0
1000
2000
3000
4000
5000
6000

(c)

Figure 4.42: Comparison between Plots of Simulated (Theoratical) and Experimental Rates of a) Free-CRL, b) CRL-2.0 NK, c) CRL-2.0 MK.

Table 4.16: R^2 of Simulated and Experimental Plots for Free and Immobilized Lipases

Selected Lipases	Coefficient of Determination (R^2)	
	Simulated	**Experimental**
Free-CRL	0.9121	0.9095
CRL-2.0 NK	0.8519	0.997
CRL-2.0 MK	0.8453	0.9057